SYNTHESIS, CHARACTERIZATION AND INVESTIGATION OF THERMOLUMINESCENCE PROPERTIES OF STRONTIUM PYROPHOSPHATE DOPED WITH METALS

A THESIS SUBMITTED TO
THE GRADUATE SCHOOL OF NATURAL AND APPLIED SCIENCES
OF
MIDDLE EAST TECHNICAL UNIVERSITY

BY
LEVENT SAİT İLKAY

IN PARTIAL FULFILLMENT OF THE REQUIREMENTS
FOR
THE DEGREE OF MASTER OF SCIENCE
IN
MINING ENGINEERING

SEPTEMBER 2009

Approval of the thesis:

SYNTHESIS, CHARACTERIZATION AND INVESTIGATION OF THERMOLUINESCENCE PROPERTIES OF STRONTIUM PYROPHOSPHATE DOPED WITH METALS

submitted by **LEVENT SAİT İLKAY** in partial fulfillment of the requirements for the degree of **Master of Science in Mining Engineering Department, Middle East Technical University** by,

Prof. Dr. Canan Özgen _____
Dean, Graduate School of **Natural and Applied Sciences**

Prof. Dr. Celal Karpuz _____
Head of Department, **Mining Engineering**

Prof. Dr. Gülhan Özbayoğlu _____
Supervisor, **Mining Engineering Dept., METU**

Assoc. Prof. Dr. Ayşen Yılmaz _____
Co-Supervisor, **Chemistry Dept., METU**

Examining Committee Members:

Prof. Dr. Ümit Atalay _____
Mining Engineering Dept., METU

Prof. Dr. Gülhan Özbayoğlu _____
Mining Engineering Dept., METU

Assoc. Prof. Dr. Ayşen Yılmaz _____
Chemistry Dept., METU

Prof. Dr. Ali İhsan Arol _____
Mining Engineering Dept., METU

Prof. Dr. Asuman Türkmenoğlu _____
Geological Engineering Dept., METU

Date: 25.09.2009

I hereby declare that all information in this document has been obtained and presented in accordance with academic rules and ethical conduct. I also declare that, as required by these rules and conduct, I have fully cited and referenced all material and results that are not original to this work.

Name, Last name: Levent Sait İLKAY

Signature:

ABSTRACT

SYNTHESIS, CHARACTERIZATION AND INVESTIGATION OF THERMOLUMINESCENCE PROPERTIES OF STRONTIUM PYROPHOSPHATE DOPED WITH METALS

İlkay, Levent Sait

M.Sc., Department of Mining Engineering

Supervisor : Prof. Dr. Gülhan Özbayoğlu

Co-Supervisor : Assoc. Prof. Dr. Ayşen Yılmaz

September 2009, 92 pages

Strontium pyrophosphate is a promising phosphate that is used widely in the industry as a result of its luminescent, fluorescent, dielectric, semi-conductor, catalyst, magnetic and ion exchange properties. Thermoluminescent dosimetry (TLD) is one of such areas. Recent researches in METU on thermoluminescence property of strontium pyrophosphate showed that strontium pyrophosphate could give enough intensity for radiation dosimetry when doped with oxides of some rare-earth elements. In this study strontium pyrophosphate was synthesized and the product was doped with copper-silver, copper-indium and manganese-praseodymium ions by solid-state reaction. In addition to these processes, characterization and the investigation of thermoluminescence properties of strontium pyrophosphate with and without dopants was conducted.

Stoichiometric quantities of strontium carbonate and ammonium dihydrogen phosphate were weighed, mixed and ground by agate mortar. Afterwards, the mixture was heated at 900˚C for 14.5 hours. For doping process, synthesized strontium pyrophosphate and different amounts of copper oxide, indium oxide, silver nitrate, manganese oxide and praseodymium oxide were weighed and powdered together. Then, mixture was heated at 950˚C for 11 hours.

For characterization of strontium pyrophosphate samples with and without dopants; X-ray Diffraction (XRD) was implemented. Fourier Transform Infrared Spectroscopy (FTIR) was used to determine whether the bond structures were affected from doping or not. Thermal properties of the samples were investigated with the help of Differential Thermal Analysis (DTA). Morphology of compounds was observed by Scanning Electron Microscope (SEM). Afterwards thermoluminescence (TLD) studies were carried out.

XRD pattern of samples showed that the intensity of hkl-310 peak of strontium pyrophosphate increased with the inclusion of metal oxides, however none of the characteristic peaks of metal oxides was observed. Addition of metal oxides caused no change in FTIR meaning that the anionic part of matrix compound, which is strontium pyrophosphate, has structural stability. Thermal analysis and morphological investigation of this material were performed. TLD results were different for each sample, which has different content. The most significant peak, which is suitable for radiation dosimetry was observed at 160˚C in the glow curve with the sample doped with 7% manganese oxide and 1% praseodymium oxide.

Keywords: Strontium pyrophosphate, solid state synthesis methods, material characterization techniques, thermoluminescence

ÖZ

METAL KATKILI STRONSİYUM PİROFOSFAT SENTEZİ, KARAKTERİZASYONU VE ISISAL IŞIMA ÖZELLİKLERİNİN İNCELENMESİ

İlkay, Levent Sait
Yüksek Lisans, Maden Mühendisliği Bölümü
Tez Yöneticisi : Prof. Dr. Gülhan Özbayoğlu
Ortak Tez Yöneticisi : Doç. Dr. Ayşen Yılmaz

Eylül 2009, 92 sayfa

Stronsiyum pirofosfat, ışıma, floresan, dielektrik, yarı-iletken, katalizör, manyetik ve iyon değişim özelliklerinin bir sonucu olarak endüstride geniş bir kullanım alanına sahiptir. Isısal ışıma dozimetrisi de bu alanlardan birisidir. Araştırma grubumuzun stronsiyum pirofosfatın ısısal ışıma özellikleri üzerine yakın zamanda yaptığı çalışmalar sonucunda, stronsiyum pirofosfatın bazı nadir toprak elementleri ile katkılandığında radyasyon dozimetrisinde kullanmaya yetecek ölçüde ısısal ışıma özelliği gösterdiği bulunmuştur. Bu araştırmada stronsiyum pirofosfat sentezlenmiş ve elde edilen ürün bakır-gümüş, bakır-indiyum ve mangan-praseodim iyonları ile katı hal reaksiyonu kullanılarak katkılandırılmıştır. Bu işlemlerin ardından katkılı ve katkısız stronsiyum pirofosfatın karakterizasyonu ve ısısal ışıma özelliklerinin incelenmesi gerçekleştirilmiştir.

Belirli miktarlarda tartılan stronsiyum karbonat ve amonyum dihidrojen fosfat karıştırılmış ve agat havan yardımıyla toz haline getirilmiştir. Bu işlemin ardından elde edilen karışım 14,5 saat boyunca 900˚C'de ısıtılmıştır. Katkı işlemi için sentezlenmiş stronsiyum pirofosfat ve farklı miktarlarda bakır oksit, indiyum oksit, gümüş nitrat, mangan oksit ve praseodim oksit ile karıştırılarak bir arada öğütülmüştür. Karışım daha sonra 11 saat boyunca 950˚C'de ısıtılmıştır.

Katkılı ve katkısız stronsiyum pirofosfat numunelerinin karakterizasyonu için XRD uygulanmıştır. FTIR ile bağ yapılarının katkılama işleminden etkilenip etkilenmediği incelenmiştir. Numunelerin ısıl özellikleri DTA yardımıyla incelenmiştir. Bileşiklerin morfolojisi ise SEM yardımıyla incelenmiştir. Bu işlemlerin ardından ısısal ışıma çalışmaları gerçekleştirilmiştir.

Numunelerin XRD grafikleri, metal oksitlerin eklenmesi ile stronsiyum pirofosfatın hkl-310 pikinin şiddetinin arttığını göstermiş; fakat metal oksitlerin kendi piklerinin hiçbiri gözlenmemiştir. Metal oksitlerin eklenmesi FTIR sonuçlarında herhangi bir değişikliğe yol açmamıştır; bu durum da matris yapısındaki anyonik kısım olan stronsiyum pirofosfatın yapısal kararlılığa sahip olduğunu göstermektedir. Buna ek olarak malzemenin ısıl analizi ile morfolojik incelenmesi de yapılmıştır. Kimyasal içeriği farklı olan her numune için TLD sonuçlarının farklı olduğu bulunmuştur. TLD ölçümleri sonucunda elde edilen ısl ışıma eğrisine göre; en belirgin ve radyasyon dozimetrisi için en uygun pik olan 160˚C'deki pik, %7 mangan oksit ve %1 praseodim oksit katkılı numunede gözlenmiştir.

Anahtar Sözcükler: Stronsiyum pirofosfat, katı hal sentez yöntemleri, malzeme karakterizasyonu, ısısal ışıma

To My Bandi

ACKNOWLEDGMENTS

I would like to express my sincere thanks to the following people:

Prof. Dr. Gülhan Özbayoğlu and Assoc. Prof. Dr. Ayşen Yılmaz not only for sharing their precious information with me but also for their patience;

My parents, Çiğdem and Mehmet, my aunt, Nuray and my brother, Bülent for giving a lot from their hearts and for supporting me at every step;

Neriman, for always being there and making me the person I am now;

Murat Erderen, Esin Pekpak and Kutay Kazbek for making life bearable, for their moral supports and everlasting helps;

Pınar Genç, Emine Kazbek, Selin Yoncacı and Pınar Dündar for being there at any time and for being so dependable;

Semih Seyyidoğlu, Tolga Depci and Mehmet Kayhan for sharing a peaceful and efficient working environment in the laboratory and sharing experience during the experimental stages of the thesis;

Prof. Dr. Necmeddin Yazıcı and Dr. Vural Emir Kafadar for their valuable contributions, guidance and support;

Müge Aksoyoğlu for encouraging me with her negative comments and sarcastic attitude; yet with her secret support…

TABLE OF CONTENTS

LIST OF TABLES

LIST OF FIGURES

CHAPTER 1

INTRODUCTION

1.1 GENERAL REMARKS

It has been more than 400 years since Boyle incidentally discovered the thermoluminescence of the diamonds. All through those years, it piqued scientist interest and curiosity and numerous studies were done for this phenomenon. Thermoluminescence had many different explanations during these years but in simplest and modern form, *thermoluminescence* (*TL*) can be defined as the emission of light from a semiconductor or an insulator when it is heated, due to the previous absorption of energy from irradiation [1]. Because of numerous efforts of the scientists, thermoluminescence now has various application areas such as radiation dosimetry, age determination and geological researches.

In today's evolving world, pyrophosphates are becoming more and more important for many industrial areas including radiation dosimetry, which is the most common and the most important application area of thermoluminescence. Strontium pyrophosphate is a kind of pyrophosphate, which has various application areas as, fluorescence lamps and color display. According to literature survey, strontium pyrophosphate had promising results for its thermoluminescence property. Especially, when some rare earth element ions were doped, it gave required thermoluminescence intensity for radiation dosimetry [2,3]. On the other hand, there was not enough research for strontium pyrophosphate on its thermoluminescence properties. In light of the foregoing, the purpose of this thesis was drawn.

1.2 THE PURPOSE OF THE THESIS

Pure and doped pyrophosphates have variety of applications, such as lamp industry, color display, radiation dosimetry and X-ray imaging because of their luminescent, dielectric, semi-conductive, catalyst, magnetic, fluorescent, and ion-exchange properties. When literature was checked, it was found that so far there were no detailed investigations on thermoluminescent properties of doped strontium pyrophosphate compounds. Thus, in this study it was aimed to synthesize strontium pyrophosphate and to investigate the thermoluminescence properties of strontium pyrophosphate doped with copper-silver, copper-indium and manganese-praseodymium ions. In this respect, different amounts of these ions were doped into the solid state synthesized strontium pyrophosphate. At the end of the study, the results of the characterization analysis and thermoluminescence readings were discussed.

1.3 METHODOLOGY OF THE THESIS

Strontium pyrophosphate was synthesized by solid-state reaction at high temperatures. Strontium pyrophosphate was then doped with copper-silver, copper-indium and manganese-praseodymium ions in several different concentrations. Moreover, strontium pyrophosphate and the new products were characterized by X-Ray Diffraction (XRD) and Fourier Transform Infrared Spectrometry (FTIR) analysis. Differential Thermal Analysis (DTA) was used for examination of the thermal properties of the compounds and the morphology of new compounds was observed by using Scanning Electron Microscopy (SEM). Dosimetric properties of the compounds were investigated by Thermoluminescence (TL) technique. At the end, changes in the properties of strontium pyrophosphate with the addition of previously mentioned ions were examined by comparing the results obtained from the XRD, FTIR, DTA, SEM and TL studies carried out both for the synthesized strontium pyrophosphate and doped strontium pyrophosphate.

1.4 ORGANIZATION OF THESIS

Chapter 1 covers the general remarks about the subject studied. In this part, the purpose and the methodology of the study are presented.

Chapter 2 is dedicated to the literature survey about strontium pyrophosphate and thermoluminescence phenomena. The first part devoted to strontium pyrophosphate embodies sound information about the some properties of the material, utilization of strontium pyrophosphate in different areas, and synthesis. In the second part of this chapter, developments in thermoluminescence between seventeenth and nineteenth century and detailed information about thermoluminescence are discussed. In addition, this part includes the application areas of thermoluminescence. At the end, some of the up until now researches parallel to this study and characterization results in the literature are covered.

Chapter 3 includes the materials and methods for the experimental studies. The materials, the details of synthesis and doping procedures as well as the analysis methods and conditions employed for characterization and determination of thermoluminescence response are included at this part.

Chapter 4 embraces the results of the experiments stated in Chapter 3. These results include the outputs from characterization analysis as well as thermoluminescence measurements.

Finally, Chapter 5 is dedicated to the conclusions to be drawn from this study and recommendations.

CHAPTER 2

LITERATURE SURVEY

2.1 STRONTIUM PYROPHOSPHATE

2.1.1 Overview

The pyrophosphate ion $P_2O_7^{4-}$, which is also called diphosphate, can be obtained from acid orthophosphates. When acid orthophosphates are heated, the water is removed by condensation and the simplest condensed phosphate, $P_2O_7^{4-}$, is formed.

An oxygen atom is shared at the center of the molecule in pyrophosphate. The angle at this particular oxygen atom and the relative orientation of the involved tetrahedras are important.

Structure determinations of a number of pyrophosphate salts have shown that both linear (straight) and non-linear (bent) ions can exist, with a value of P/O/P in the range 130-180˚ [4]. Different divalent metal pyrophosphates can be found, both in low temperature and in high temperature form. The oxygen atoms in these forms are in distorted octahedral arrangements around the cations. At least two forms of $Sr_2P_2O_7$ exist, one of which is isomorphous with $Ba_2P_2O_7$ [4,5,6]. The bond data for strontium pyrophosphate are given in Table 2.1.

Table 2.1 Bond data for strontium pyrophosphate

α-$Sr_2P_2O_7$		
P-O-(P) (Å)		1.60
P/O/P (degrees)		131
O/P/O (degrees)		107
PO_3 group	P-O (Å)	1.50
	O/P/O (degrees)	111

$Sr_2P_2O_7$ has a dimorphic crystalline structure. If the material is treated with high temperature, a α-phase crystal forms while at low temperatures a β-phase crystal structure is formed. The practical phosphorus belongs to an alpha type [6]. In high temperature form of $Sr_2P_2O_7$, there is a plane containing the oxygen and phosphorus atoms. The $P_2O_7^{4-}$ ion in this form is in an eclipsed form with the plane and the SrO_9 group. The structure of the strontium pyrophosphate is illustrated in Figure 2.1.

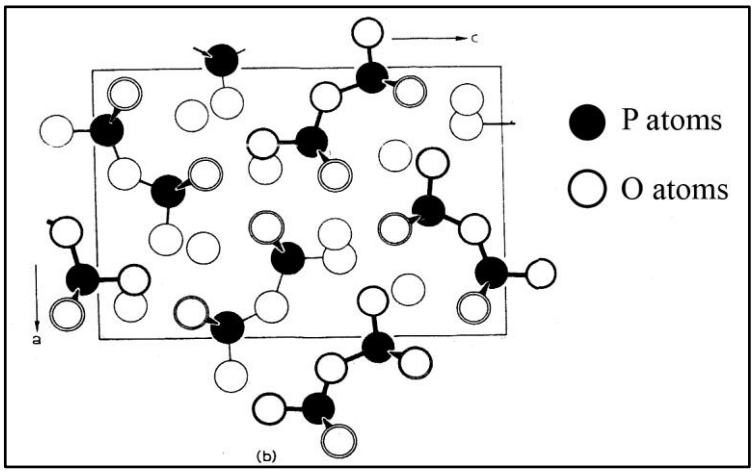

Figure 2.1 Strontium pyrophosphate structure in [b] projection

Usually the raw materials for preparation of strontium pyrophosphate is $SrHPO_4$, $SrCO_3$, $(NH_4)_2HPO_4$. Preferable firing temperatures are between 900 to 1000^oC [6].

2.1.2 Uses of pyrophosphate

Pyrophosphates are used in ceramics, fluorescent lamps, catalysts, ion exchange and optical materials. Typical phosphate phosphorus activated with the rare-earth ions are $Sr_2P_2O_7:Eu^{2+}$ (used for diazo photocopy lamps), $2SrO{\cdot}0.84P_2O_5{\cdot}0.16B_2O_3:Eu^{2+}$ (employed as the blue green emitting component in extremely high color rendering fluorescent lamps), and $LaPO_4:Ce^{3+},Tb^{3+}$ (which is most commonly used in three band lamps as the green emitting component in Japan) [6]. $Sr_2P_2O_7:Sn^{2+}$ has a blue green light with a peak wavelength of 464 nm and is used as a high color rendering.

2.1.3 Synthesis

After literature survey, two synthesis methods were found for strontium pyrophosphate. First one was studied by Natarajan and his colleagues. In this method, strontium hydrogen phosphate was precipitated from strontium nitrate solution containing Eu^{3+} by adding diammonium hydrogen phosphate. Then the pH of the solution was adjusted to be around 7-8. Analytical grade strontium nitrate, diammonium hydrogen phosphate and very pure Eu_2O_3 were used for the preparation. The precipitate was filtered and dried with alcohol. Later, it was ground thoroughly and heated at 1173 K for 3-4 h in nitrogen atmosphere. Undoped $Sr_2P_2O_7$ sample was also prepared in a similar way. [7]

Seyyidoğlu and his colleagues provided the second method in their study on investigation of solid solution of ZrP_2O_7-$Sr_2P_2O_7$ [3]. Strontium pyrophosphate was produced by using the $SrCO_3$ and $NH_4H_2PO_4$ with solid-state reaction. Also Shi Ye and his research group synthesized strontium pyrophosphate by solid-state reaction [8]. The raw materials were prepared according to the stoichiometric amounts, and then mixture was homogenously ground in an agate mortar. Then, mixture was transferred to furnace in alumina ceramic crucibles and heated at 950˚C for 10 hours in muffle furnaces [2].

2.1.4 Properties of Strontium Pyrophosphate

Strontium pyrophosphate was synthesized by Seyyidoğlu et al. and they investigated the thermoluminescence properties of strontium pyrophosphate doped with 5% of CuO and some rare earth minerals (Y_2O_3, La_2O_3, CeO_2, Pr_6O_{11}, Nd_2O_3, Sm_2O_3, Eu_2O_3, Gd_2O_3, Tb_2O_3, Dy_2O_3, Ho_2O_3, Er_2O_3, Tm_2O_3, Yb_2O_3, Lu_2O_3). Appendix A shows the effect of praseodymium oxide amount effects on the XRD pattern of the strontium pyrophosphate. Observation of Seyyidoğlu and et al. were that the doped patterns were similar to those of undoped orthorombic strontium pyrophosphate and only the 10% and 15% Pr_6O_{11} doping had small effects on the XRD patterns by lowering the intensities of two most intense peaks [2].

In order to examine the structural properties of strontium pyrophosphate, Seyyidoğlu et al. have used FTIR [3]. They have examined the peaks resulting from P_2O_7 ion, therefore the PO_3 and P-O-P vibrations and observed bands between 609 and 455 cm^{-1}. The FTIR results, obtained by Seyyidoğlu and his colleagues are given in Appendix B. Both Guler et al. [9]and Khay [10,11]has obtained similar FTIR analysis. For a FTIR analysis of strontium pyrophosphate the bands that are expected are given in Table 2.2.

Table 2.2 Table of the expected bands for strontium pyrophosphate after FTIR analysis

450 – 500 cm^{-1}	δ-symmetrical PO_3 bands
550 – 600 cm^{-1}	δ-asymmetrical PO_3 bands
700 – 720 cm^{-1}	ν-symmetrical P-O-P bridge bands
890 – 920 cm^{-1}	ν-asymmetrical P-O-P bridge bands
1040 – 1080 cm^{-1}	ν-symmetrical PO_3 bands
980 – 1150 cm^{-1}	ν-asymmetrical PO_3 bands

In addition, the SEM Micrograph of the undoped strontium pyrophosphate that was investigated in the study of Seyyidoğlu and his colleagues is demonstrated in Appendix B [3]. They found the difference of the particle size between $Zr_2P_2O_7$ doped with $Sr_2P_2O_7$ and $Sr_2P_2O_7$ doped with $Zr_2P_2O_7$.

Natarajan and his colleagues researched the photoluminescence, thermally stimulated luminescence and electron paramagnetic resonance of europium-ion doped strontium pyrophosphate [7]. Appendix C includes the thermoluminescence glow curve of europium doped strontium pyrophosphate with different heating rates. It can be easily observed that it has significant peaks between 550 and 600K (277 and 327°C).

Seyyidoğlu and et al. examined the thermoluminescence of strontium pyrophosphate doped with 5% copper and different amounts of praseodymium [2]. The thermoluminescence glow curve of $Sr_2P_2O_7$ doped with 5% CuO and 5% Pr_6O_{11}, which is also given in Appendix C, had the highest intensity observed. First peak was seen around 100°C and the second one is around 180°C with an intensity of approximately 75 million arbitrary units.

2.2 THERMOLUMINESCENCE

Thermoluminescence as mentioned by McKever and et al., is one of the processes in Thermally Stimulated Phenomena [12]. In a general view, *thermoluminescence* is a temperature stimulated light emission from a crystal after removal of excitation. Nevertheless, microscopically, it is much more complicated. In this chapter, the thermoluminescence mechanism will be discussed in detail. With the developing technology, thermoluminescence has various application areas such as, radiation dosimetry, age determination and geology.

2.2.1 History of Thermoluminescence

The studies on thermoluminescence go back to the seventeenth century, when scholars like Johann Sigismund Elsholtz, Robert Boyle and Henry Oldenburg conducted experiments on minerals to see their radiation due to heating. George Kaspar Kirchmaier, who regarded the phosphorus as a green stone powdered and mixed with water and glows when heated, and Nathaniel Grew, who used the name Phosphorus metallorum [13], are other scientists who showed interest in the concept.

Among the eighteenth century researchers, Dufay is the first to be acknowledged for his findings on thermoluminescence. He referred to lighting as a kind of burning. He worked on many materials, primarily chlorophane, and found out that too much heating would lead to loss of thermoluminescence of the material.

A famous scientist, Canton brought Dufay's studies to a new level, by raising the temperature of phosphorus even further and discovering a new type of light, which he referred to as the thermoluminescence of artificial phosphorus [13].

Leading scientists, De Saussure and Thomas Wedgwood need to be mentioned in the thermoluminescence studied of the eighteenth century. The former recognized three types of stones which luminesced on heating: (1) those containing sulphur or a hepar (fois) , a compound of sulphur, which burned in the free air, (2) those which absorb the light and then emit it, like the diamond, and (3) those which do not require air and will luminesce under hot water, like dolomite and fluorspar [13]. He declared that the intensity of the color of the fluorspar is an indicator for the level of thermoluminescence. The latter conducted a study on the thermoluminescence and triboluminescence, lighting as a result of friction. His findings showed that it was not possible to claim a solid relation between the patterns of two types of luminescence.

Studies on thermoluminescence continued in the nineteenth century. Researcher, Heinrich claimed that almost all substances could emit light, provided that they are in powder form and subject to moderate heating. Another researcher

Theodor von Grotthus dealt specifically with the fluorspar, and showed resemblance between thermoluminescence and essence; both are made of positive and negative parts. Later, scientist David Brewster opposed to Grotthus, arguing that the luminescence property cannot always be regained on exposing the minerals to light.

Other researchers who studied thermoluminescence in the nineteenth century are Pearsall, who tried to find a relation between color and thermoluminescence; Specia, who invalidated Pearsall's findings; Napier, who experimented on the chalks; Wiedmann and Schmitt, who attributed the thermoluminescence characteristic to cathode rays.

2.2.2 Thermoluminescence Mechanism

In sum, thermoluminescence can be described by two stages. First stage is the change of the system from equilibrium to metastable state by absorption of energy from UV or ionizing radiation. Then the second stage is relaxation of the system back to the equilibrium by energy release such as light with the help of thermal stimulation [12]. Thus, thermoluminescence (TL) is the thermally stimulated emission of light following the previous absorption of energy from radiation [14]. In this chapter, these stages and output of this light emission will be discussed briefly.

A-Energy Storage

There are two ways for the stabilization of this absorbed energy: *electronic excitation* and *displacement damage*. At the end of both processes, radiation-induced defects are formed in the material structure. *Radiation-induced defects* are localized electronic states occupied by non-equilibrium concentration of electrons. [15]. Alias, before irradiation, materials have localized electronic energy states and after irradiation, some of these states are occupied by a non-equilibrium concentration of electrons. Therefore, these occupied states are called radiation-induced defects. According to McKeever, when investigations are taken into consideration, they show

that the cause of defect creation is electronic excitation rather than non-ionizing displacement damage [12].

Energy storage caused by electronic excitation takes place by the electron-hole pair production and excitation creation. *Electron-hole pair production* is the formation of mobile holes and electrons in the crystal structure of the material after radiation.

In addition, there exists a *mid gap state* caused by defects which may be created by pre-existing impurities or radiation induced defects. This gap is found between the two energy bands; called *conduction band* and *valence band*. The valence band is the outer most energy level and contains electron-hole pairs in ground state of the solid. On the other hand; in the conduction band, electrons are free to move and have ability to produce electric current [16].

According to thermoluminescence phenomena it is assumed that there are two kinds of imperfections called *electron trap* and *hole trap* in the crystal which are localized at mid gap states [12,14,16]. In the mid gap, the electron trap is believed close to the conduction band and the hole trap is far from the valence band.

Figure 2.2 illustrates the energy storage mechanism. After irradiation, the electrons pass from valence band to conduction band and hole becomes positively charged area in the valence band. When electron reaches the conduction band, electron find its way into an electron trap and hole occupies its associated trap. Hole traps are called *luminescence center* in this process [12,14,16,17].

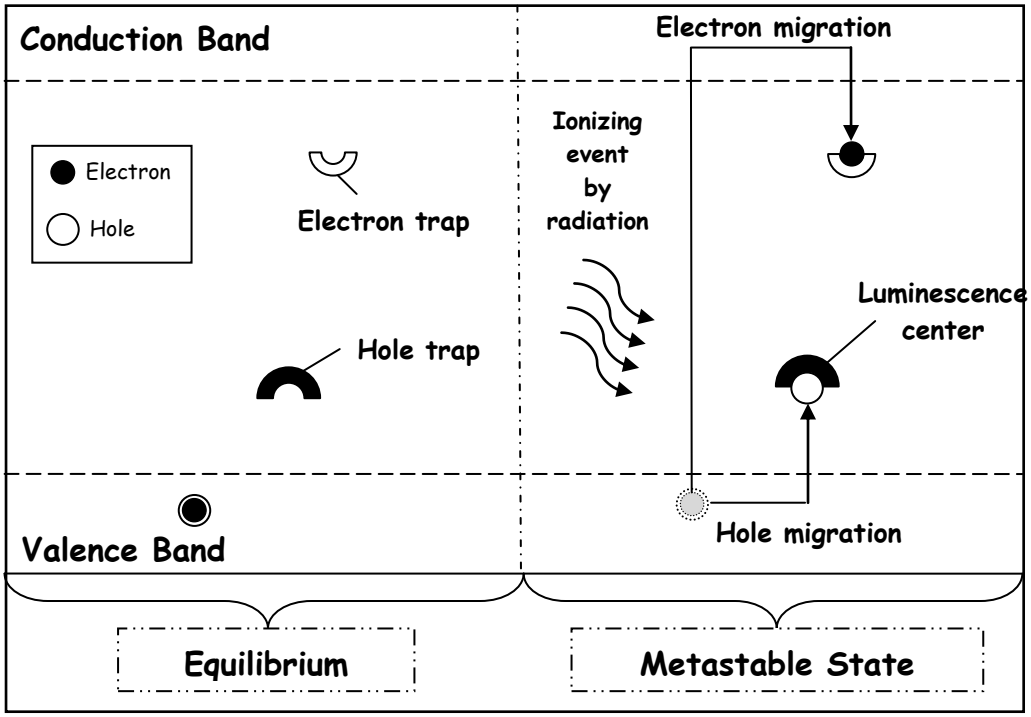

Figure 2.2 Energy-level diagram of the energy storage stage for thermoluminescence processes

B-Energy Release

Excitation with an increase in temperature or giving light, results in release of the stored energy. Furthermore, state of the material changes from metastable to ground. When heat is increased, the electron trapped in the electron trap is released to conduction band. After that electron is free to retrap or recombine with the hole found in the hole trap. The recombination of the electron with the hole in hole trap results in the emission of photons. In this case hole trap is called as *recombination center* [14]. This process is illustrated in the Figure 2.3.

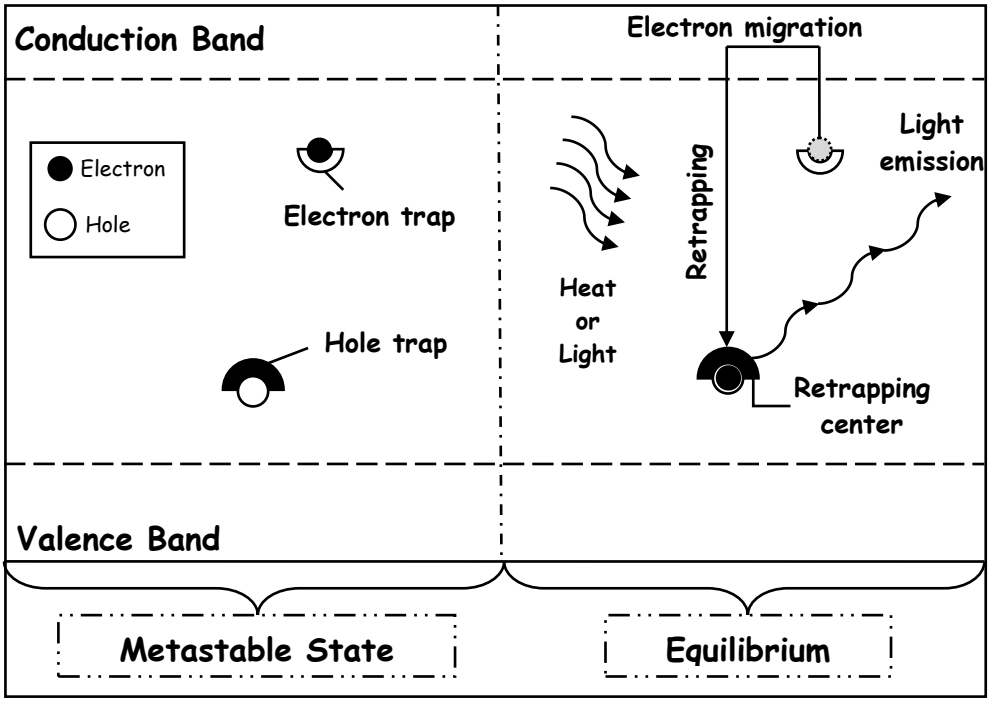

Figure 2.3 Energy-level diagram of the energy release stage for thermoluminescence processes

C-Glow Curve

After the energy release, the output of the emitted light as a function of temperature is called *thermoluminescence glow curve* [14]. Shape of the glow curves is one or more peaks of emitted light and some of them may overlap. Magnitudes and looks of the glow curves may change depending on the spectral response of the light sensitive device, different filter usage between the sample and the detector and heating rate. In addition, when the sample is irradiated it has only one shot effect. A second thermoluminescence emission cannot be recorded by cooling and reheating it unless it is not irradiated again [14]. Figure 2.4 shows some glow curve examples of some thermoluminescent materials.

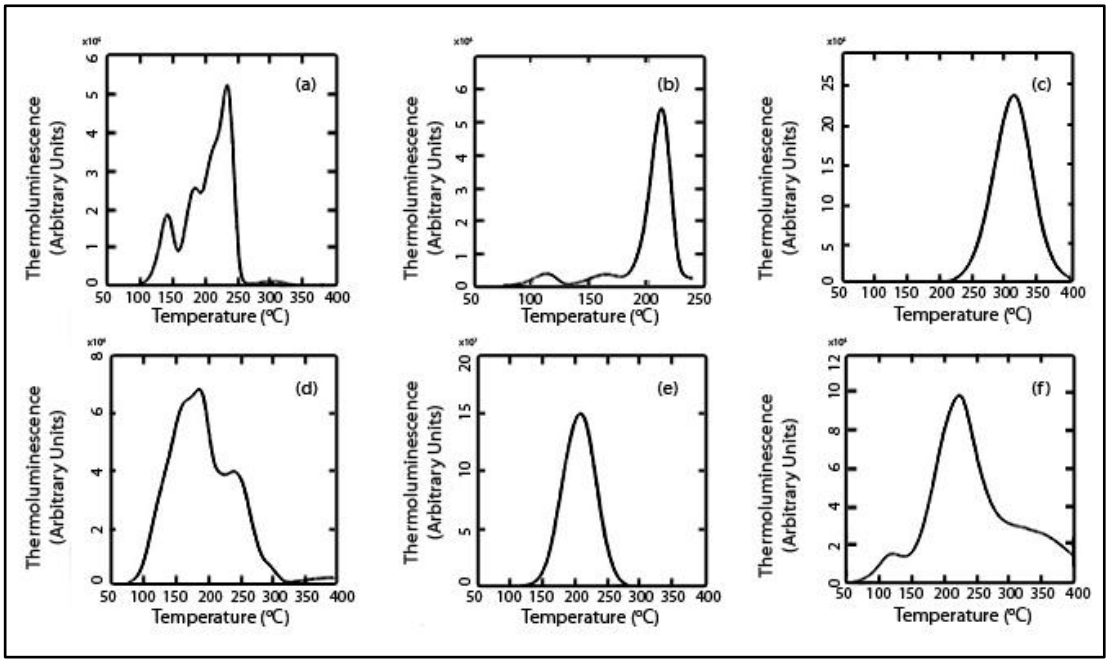

Figure 2.4 Some representative examples of glow curves of some of the main TLD materials. (a) LiF:Mg,Ti; (b) LiF:Mg,Cu,P; (c) CaF_2:Mn; (d) CaF_2:Dy; (e) AI_2O_3:C; (f) $CaSO_4$: Dy. [14]

2.2.3 Applications of Thermoluminescence

The thermoluminescent materials used in the industry have three major areas; *radiation dosimetry*, *age determining* and *geology*.

The radiation dosimetry measures the dose that is absorbed by the sample that is exposed to irradiation. Radiation dosimetry has three subgroups; *personnel dosimetry*, *medical dosimetry* and *environmental dosimetry*. Personnel dosimetry is used in areas where the personnel are exposed to radiation; nuclear reactors, radiotherapy wings in hospitals and nuclear powered submarines or such. Therefore, the purpose of using personnel dosimetry is to keep track of the radiation exposure level of the individual to avoid avert radiation based effects. The safe limits are determined by organizations such as International Commission on Radiological Protection (IRCP). Besides, from the constant radiation exposure, there are

accidental or incidental radiation exposures, which are also measured by personnel dosimetry.

Personnel dosimetry has three sub categories; extremity dosimetry, whole-body dosimetry and tissue dosimetry. The first one focuses on body parts that are exposed to radiation such as hands, arms or feet while the whole-body focuses on the tissue below the surface of the body or the critical organs. It measures the dose absorbed in these parts of the body by dealing with gamma and X rays (greater than 15 keV) and neutrons which are penetrating rays. Tissue dosimetry, which is also called skin dose, measures the dose absorbed by skin. However rather than dealing with penetrating radiation, it focuses on non-penetrating radiation such as beta particles or <15 keV X rays.

In order for these measurements to be done, a thermoluminescence dosimetry (TLD) material that is equivalent to the human tissue is needed. The TLD material should absorb the same dose or amount of radiation as the human tissue would do in the same area within the same radiation levels.

Medical dosimetry intends to measure the effects of a TLD that is placed into the appropriate places within human body. By doing so, before exposing the patient, to ionizing radiations for treatment procedures or diagnosis, measurements can be made upon these TLD. From the data obtained, possible additional treatments or dose control can be implemented. It is impossible to do so by means of other than radiation dosimeter. The major variables that determine patient doses include imaging modality, technical factors and in the case of fluoroscopy, beam time [17]. In addition to these factors, the size of the patient is also a determining factor.

Medical dosimetry has two categories; diagnostic radiology and radiotherapy. The radiation used here may be X-rays (near 10 keV level), gamma rays, beta particles, protons and other heavy particles and neutrons [12].

Again, the TLD material needs to be tissue equivalent and highly sensitive. The latter is needed for measurements done in laboratory conditions that require the possible smallest size of TLD material. Other than these properties, the TLD should not be toxic. Recommended diagnostic reference levels for medical imaging modalities have been published by the ICRP [17].

Environmental dosimetry deals with the radiation present in the environment due to humankind. Due to applications like nuclear power stations, waste disposals, usage or processing of nuclear fuels and disastrous nuclear power plant malfunctions introduce high levels of radiation into the environment. Therefore, it become essential to monitor the radiation released to the environment continuously.

TLD's are used for environmental dosimetry applications. However, the performance criteria for TLDs in this application are different from those required for personnel monitoring [17]. They are still needed to be highly sensitive, more preferably extremely sensitive and this time it is not essential for TLDs to be tissue equivalent. Because the environment is exposed to radiation for a long time continuously, environmental dosimetry measures the values within a long period. Therefore, the TLDs should be structurally intact and stable in long term.

In recent years, with the help of cutting edge technological innovations, space flight with astronauts has been possible. Radiation exists in space and since there is no more an atmosphere to protect from galactic cosmic rays, it is important to measure the radiation at these space flights. Besides, from the astronauts on board, the radiation is also harmful for the digital equipment of the vehicles. The radiation sources are galactic cosmic rays of which the main component is high-energy protons and heavy charged particles from the solar wind [17]. In order to measure the effects of these radiation sources, TLDs are used.

Thermoluminescence is used in age determining processes of materials, as it became an established method of age determination. A famous scientist, Daniels and his coworkers are the first to suggest the use of thermoluminescence for this purpose.

They argued that there are already radioactive elements within the rocks, such as uranium, thorium and potassium and these elements assigned a natural thermoluminescence to the rocks. From this radioactivity an accumulation, which is called ‘geological’ dose, takes place in the material. If the rate of irradiation from the radioactive minerals is established, and if the rate of thermal release of the thermoluminescence during the rock’s irradiation can be shown to be negligible, then the length of time over which the rock has been irradiated (i.e., its ‘geological age’) can be determined from the ratio of absorbed dose over dose rate [7,18].

Thermoluminescence was used for age determination of rock formations however; it was not used for archeological dating until natural thermoluminescence was found in ancient samples. Due to the effects of heat on thermoluminescence, thermoluminescence of the pots diminished to zero during its bakery. Nevertheless, the surroundings of the pot does not change and is naturally radioactive itself with elements like uranium, thorium and potassium. Therefore, the pot continues to be exposed to radioactivity and will absorb a certain amount of it, which will be measured to get the archeological age of the pottery. Thermoluminescence is now an established way of age determination.

Minerals tend to give off different glow-curves according to their location of extraction. Since thermoluminescence is a finer way of radiation trace detection, this enables to identify the source of these minerals by using thermoluminescence in geology. Another aspect of geology that uses thermoluminescence is in examining meteorites and materials originating from the moon. It is possible to tell the distance of meteorite to the sun while it was travelling in the space as well as how long the meteorite was on earth.

2.2.4 Commercially Used Thermoluminescent Materials

Thermoluinescent properties of materials enable them to be used in dosimeters, which are used in measuring doses of radiation. Since characteristics of materials differ from each other, different materials with different thermoluminescent properties are preferred for different purposes. LiF and CaF_2 are the most common thermoluminescence materials, which are followed by sulfates [19]. Some of the key thermoluminescent materials used in dosimeters are given in Table 2.3.

Table 2.3 Characteristics of thermoluminescent materials used in commercial dosimeters [19]

Thermoluminescent Materials	Dosimeter Type
LiF:Mg, Ti	TLD-100
LiF:Mg, Cu, P	TLD-100H
LiF:Mg, Ti	TLD-600
LiF:Mg, Cu, P	TLD-100H
CaF_2:Dy	TLD-200
CaF_2:Mn	TLD-400
$CaSO_4$:Dy	TLD-900

The first thermoluminescent material used in dosimeters is TLD-100. The most popular form is the hot pressed chip and many commercial manufacturers of TLD dosimeter badges use chips of this size as the central element of their badge design [12]. Since they are not suitable for automating routine handling procedures, powders are rarely used in personnel dosimetry. It is also possible to design LiF-based dosimeters sensitive to neutrons by enriching them in the ^{6}Li isotope [19]. However LiF based dosimeters does not have a simple glow curve. LiF:Ti, Mg, for instance, has a glow curve that consists of minimum seven peaks which makes it

harder to implement the material. The number of curves makes it harder to heat dosimeters. The heating process should include preheating for the depletion of shallow traps and additional high-temperature annealing for the depletion of deep traps [19]. The simplest curves belong to CaF_2:Mn and Al_2O_3:C. Both of these materials are extremely sensitive to radiation yet they have a simple TL curve.

CaF_2:Mn dosimeters may be obtained as single crystals, extruded rods and hot pressed chips [12]. They come in sizes same with LiF dosimeters. There is a single maximum in the glow curve and it is observed around 313^oC at a heating rate of 10$^oC.s^{-1}$. Further studies have shown that the glow curve actually consists of several tightly placed separate peaks which seem to be on glow curve; however this does not affect the use of these dosimeters commercially.

Calcium fluoride doped with Dy is available as single crystals, as polycrystalline chips or as powders [12]. The procedure for this material does not differ from CaF_2:Mn. The commercial name for CaF_2:Dy is TLD-200. CaF_2:Dy does not have a single peak, instead there are minimum four peaks in the glow curve and these curves are known as I-IV. They occur around 160^oC, 185^oC, 245^oC and 290^oC. Peaks also appear in higher temperatures between 350^oC and 400^oC.

2.3 RELATED STUDIES

In Middle East Technical University (METU), thermoluminescence properties of different materials have been conducted since 2001. Özdemir et al. have studied thermoluminescence properties of metal oxide doped lithium triborate, LiB_3O_5 [20,21]. They have used solid state reaction method and concluded that lithium triborate samples that are doped with CuO and Al_2O_3 exhibited very significant thermoluminescence glow curves and they are good candidates for being a dosimetric material. Ardıçoğlu et al. have also produced rare earth doped lithium triborates using Gd, La, Y as dopants [22,23]. They investigated the thermal, morphological and thermoluminescence properties of the samples. They found that

addition of the rare earth elements made no observable changes to the compounds, structurally; while according to SEM images, rare earth elements and lithium borate particles were observed, separately. Depci et al. examined thermoluminescent properties of aluminum activated lithium triborate, LiB_3O_5 [24]. They observed that both undoped and doped samples showed different glow curve structures and concluded that the Al-doped LiB_3O_5 sample can be used in dosimetric applications because of its promising characteristics. Seyyidoğlu et al. have investigated the solid solution of ZrP_2O_7, $Sr_2P_2O_7$ and $Sr_2P_2O_7$ doped ZrP_2O_7 [3]. They have analyzed surface morphology and thermoluminescence properties of these samples. Seyyidoğlu have also reported the synthesis and characterization of novel rare earth phosphates and rietveld structural analysis of rare earth orthoborates [2]. Pekpak [16] and Kayhan [25] have investigated the effects of synthesis and doping methods on thermoluminescence glow curves of manganese and copper doped lithium tetraborate, $Li_2B_4O_7$ and found that added dopants did not change any structural or bonding properties of lithium tetraborate, however they did change the thermoluminescence glow curves.

Férid and coworkers have conducted studies on the structure of pyrophosphates and have synthesized a new form of diphosphate $NaLaP_2O_7$. They examined its complete structural characterization by X-ray diffraction [26]. They also produced $NaEuP_2O_7$ and analyzed its structure and infrared spectrum [27]. Hamady, Faouzi Zid and Jouni has determined the structure of KYP_2O_7 and found that the structure consists of pyrophosphate groups and YO_6 octahedra sharing corners to form a three-dimensional framework having intersecting tunnels where the K^+ ions are located [28]. Trunov, Oboznenko, Sirotinkin and Tskhelashvili has synthesized $K_2SrP_2O_7$ [29], $CsSrP_2O_7$ and $Rb_2SrP_2O_7$ in single crystal form [30]. Ledain, Leclaire, Borel and Raveau have synthesized monoclinic $LiMoP_2O_7$ single crystals using controlled cooling method [31]. They used a structure built up from MoP_2O_{11} units, which were composed of a MoO_6 octahedron that shared corners with a bidentate P_2O_7 group. Boutfessi, Boukhari and Holt have synthesized triclinic lead diironpyrophosphate, monoclinic barium diiron pyrophosphate [32]and monoclinic copper diiron pyrophospate using the same technique [33]. Khay,

Ennaciri and Harcharras have studied rubidium double diphosphates $RbLnP_2O_7$ (Ln=Dy, Ho, Y, Er, Tm, Yb) by using X-ray diffraction and vibrational spectroscopy [10] and $CsLnP_2O_7$ (Ln=Gd, Tb, Dy, Ho, Y, Er, Tm, Yb) double diphosphates by using raman and infrared absorption spectra [11].

İdrissi et al. have synthesized the monoclinic pyrophosphates with the formula of MP_2O_7 where M was Ca_2, CaCu, SrCu, SrCd, BaMg and studied the IR and Raman spectra of the samples [34]. Stock and co-workers have synthesized hydrothermally $Na_2CrP_2O_7{\cdot}0.5H_2O$ using chromium (II) acetate and tetrasodium pyrophosphate [35]. They found that chromium pyrophosphate, which had one-dimensional chains of alternating Cr^{2+} and $P_2O_7^{4-}$ ions, exhibited Curie–Weiss paramagnetism between 6 and 300 K. Assaaoudi, Butler, Kozinski and Bélanger-Gariépy have synthesized a new, dicationic, hydropyrophosphate dihydrate salt, $KHMgP_2O_7{\cdot}2H_2O$ by using a mixture of aqueous equimolar solutions of $MgCl_2{\cdot}4H_2O$ and $K_4P_2O_7$ [36]. They have analyzed the characteristics of this compound using XRD, IR, Raman Spectra and DSC-TGA and found that there were alternating layers of $[HP_2O_7]^{3-}$ groups and MgO_6 octahedra in the structure of this pyrophosphate with K^+ ions and bridging hydrogen bonds. Varga et al. have prepared $(M^{III}_{0.5}\ M'^{V}_{0.5})\ P_2O_7$ compounds where $M^{III}M'^{V}$ are AlTa, FeTa, GaTa, InNb, YNb, NdTa, and BiTa respectively and have close structural relatives of cubic ZrP_2O_7 structure [37]

Chernaya et al. have synthesized Tin(II) Pyrophosphate ($Sn_2P_2O_7$) and investigated its structure by using single crystal and powder X-ray diffraction [38]. Güler and Kurtuluş have developed a new method for preparing lead pyrophosphate $Pb_2P_2O_7$ [9]. By using microwave heating as synthesis technique, they were able to produce the compound as a pure phase. Gover and co workers have examined the structure and phase transitions of SnP_2O_7 using X-ray and neutron powder diffraction [39]. These analyses showed that SnP_2O_7 had two phase transitions, one with a pseudo-cubic 3×3×3 superstructure at room temperature. Withers, Tabira, Evans, King and Sleight found a new three-dimensional incommensurately modulated cubic phase in ZrP_2O_7 and studied its characteristics using Temperature Dependent

Electron Diffraction [40]. The crystal structure of a novel pyrophosphate WP_2O_7 was studied by Lisnyak and co-workers using X-ray powder diffraction [41]. Using solid state reaction Tie, Li and Yang have synthesized a new phosphate with formula $NaDyP_2O_7$ and characterized this new pseudo-pyrophosphate with XRD, infrared and Raman spectra [42].

In addition to structural properties, the electrical and conductivity characteristics of pyrophosphates were also examined. Marcu et al. have measured the semiconductive and redox properties of Ti and Zr pyrophosphate catalysts (TiP_2O_7 and ZrP_2O_7) [43] while the effect of tetravalent metal on dielectric property in ZrP_2O_7 and TiP_2O_7 was investigated by Kim and Yim [44]. Amezawa et al. have analyzed protonic conduction in LaP_3O_9 doped with 1 mol percentage of divalent metals (Ca, Sr, and Ba) [45].

Luminescent properties of pyrophosphate were also of researchers interest. Doat, Pellé and Lebugle have examined europium doped calcium pyrophosphates and their photoluminescent properties [46]. They concluded that in alternating excitation wavelengths the luminescence occurs either in blue or red regions and this outcome discriminates it from parasitic signals that come off from other dyes or organelles in living cells. Another work on luminescence of pyrophosphates was conducted by Schipper et al. who examined luminescence of hafnium compounds [47]. They found that Li_2HfO_3 and HfP_2O_7 emit in the UV spectral range while HfO_2 and $BaHfO_3$ do not. In a different study, Assaaoudi and his co-workers have investigated crystal structure and luminescence spectra of a new erbium potassium pryophosphate dihydrate $ErKP_2O_7.2H_2O$ [48]. They have measured and interpreted UV-visible and flourescence spectra of $ErKP_2O_7.2H_2O$, which they synthesized. In their work on lutetium diphosphate $NH_4LuP_2O_7$, Li and colleagues have analyzed the Ce doped luminescence of the compound and concluded that the measurements of their samples showed interesting scintillation properties with a short decay time of 16ns at room temperature [49]. Pang, Li, Shi and Su have successfully prepared a kind of new phosphorus with blue and long lasting phosphorescence by introducing the Y^{3+} into $Sr_2P_2O_7:Eu^{2+}$ [50]. They have used the high temperature solid state

reaction method in this work and observed that the phosphorus emitted blue light which was related to the transition of Eu ion. They also added that the bright blue phosphorescence could be observed by naked eyes even 8 h after the excitation source was removed.

Pang and Li, this time with Jiang and Su have prepared long lasting phosphorescence (LLP) phosphorus with composition of $(Zn_{1-x}Tm_x)_2P_2O_7$ using the high-temperature solid state method [51]. They have observed a blue long lasting phosphorescence can be observed which could last for more than 1 h in the limit of light perception of dark-adapted human eyes (0.32 mcd/m^2). In their work with Zhang and Su, Pang and Li have also examined the luminescent properties of a new blue long lasting phosphorus $Ca_2P_2O_7$:Eu^{2+}, Y^{3+} and investigated its properties by XRD, photoluminescence, phosphorescence and thermoluminescence (TL) spectra [52]. They observed that the TL spectra show that the doping of Y^{3+} ions enhanced intensity of 335 K peak to a great extent and created new TL peak at about 373 K which is also responsible for the blue LLP. They concluded that Y^{3+} ions are suggested to act as electron traps to improve the performance of the blue phosphorescence of Eu^{2+}. Natarajan and et al. have worked on europium-ion doped strontium pyrophosphate to study its photoluminescence, thermally stimulated luminescence and electron paramagnetic resonance [7]. They have observed signals originating from PO_2^{2-}, PO_3^{2-} and O_2^- radical ions upon gamma irradiation in the undoped and doped samples. For the gamma irradiated europium-ion doped samples, additional low-field EPR signals which are attributed to Eu^{2+} ions, were observed in this analysis.

There is relatively less amount of research upon thermoluminescence of pyrophosphates. Miyoshi and Yoshino have prepared calcium pyrophosphate, $Ca_2P_2O_7$, which exhibited thermoluminescence with X-ray and γ-ray irradiation [53]. They used 7 wt % Tm as dopant and observed that there were shallow hole and electron traps on Tm-doped $Ca_2P_2O_7$ powder surface. Kundua, Massanda, Marathea and Venkataramana have synthesized sodium pyrophosphate doped with dysprosium oxide aiming to develop a thermoluminescent detector [54]. They investigated the

gamma ray response characteristics of the prepared phosphorus along with the thermal and fast neutron responses and reported that the compound three glow peaks at 90°C, 181°C and 228°C. They concluded that the glow peak at 181°C was stable and useful for dosimetry purposes.

CHAPTER 3

MATERIALS AND METHODS

3.1 MATERIALS

During the synthesis and doping procedure of strontium pyrophosphate, the materials listed in Table 3.1 were used. All the materials used were in solid state and they were ground by agate mortar before synthesis.

Table 3.1 Materials used for the synthesis and doping of strontium pyrophosphate

Chemical Formula of the Material	Procedure Used
$SrCO_3$	Synthesis of Strontium Pyrophosphate
$NH_4H_2PO_4$	Synthesis of Strontium Pyrophosphate
CuO	Doping
$AgNO_3$	Doping
In_2O_3	Doping
MnO	Doping
Pr_6O_{11}	Doping

3.2 INSTRUMENTATION

3.2.1 Furnace

Protherm trademarked furnace with maximum 1300˚C heating capacity and control options was used to perform solid-state reactions for synthesis of strontium pyrophosphate and doping procedures.

3.2.2 Powder X-Ray Diffractometer

To characterize the crystal structure of synthesized strontium pyrophosphate and the doped samples, the powder X-ray diffraction (XRD) measurements were established. For these measurements, Rigaku MiniFlex X-ray Diffractometer with a radiation source of CuKα was used.

According to previous studies, 2θ ranges are set as between 5˚ and 70˚ where the characteristic peaks were observed [3] and 2 degree/minute was adopted as scan speed. Then, obtained XRD patterns and d-values of these examinations, were discussed based on Joint Committee on Powder Diffraction Standards (JCPDS) card numbered 24-1011 [55].

3.2.3 Fourier Transform Infrared Spectrometer

Fourier Transform Infrared Spectroscopy (FTIR) identifies chemical bonds in a molecule by producing an infrared absorption spectrum. Thus, the presence of specific functional groups can be monitored.

The pellet samples for Fourier Transform Infrared Spectrometer (FTIR) measurements prepared based on 100mg: 2mg sample to KBr ratio. The produced samples were studied by VARIAN 1000 FTIR spectrometer and the wave numbers were set between 400 and 4000cm^{-1} [56].

3.2.4 Differential Thermal Analyzer

For differential thermal analysis of the samples, Setaram Simultaneous TG/DTA equipment was employed. The temperature range adopted was between room temperature 25^{o}C and 1200^{o}C. The heating rate employed was 10^{o}C/min and measurements were performed under normal atmosphere.

3.2.5 Scanning Electron Microscope

To analyze the morphology of the strontium pyrophosphate and to investigate the effect of doping on morphology, Scanning Electron Microscope (SEM) was employed. The SEM analyses were performed using Zeiss SUPRA 50 VP with has magnification between 12-900000, variable pressure between 2-133Pa, acceleration voltage of 0.1-30 kV.

3.2.6 Thermoluminescence Reader

Harshaw TLD Reader Model 3500 was employed for the thermoluminescence property analysis of the samples. The heating rate was set as 1°C/sec and samples were heated from room temperature to 400°C. Before TL procedure, 10 mg sample was exposed to β radiations at room temperature for 5 minutes. After 1-minute retention period, sample was put into TLD reader.

3.3 EXPERIMENTAL PROCEDURE

The main goal of this study was to synthesis $Sr_2P_2O_7$ and dope copper oxide-silver nitrate (CuO-$AgNO_3$), copper oxide-indium oxide (CuO-In_2O_3) and manganese oxide-praseodymium oxide (MnO-Pr_6O_{11}) into $Sr_2P_2O_7$. These processes were done by using an earlier reported solid-state heating method [3].

3.3.1 Synthesis of Strontium Pyrophosphate

During the production of $Sr_2P_2O_7$, solid powders of strontium carbonate ($SrCO_3$) and ammonium dihydrogen phosphate ($NH_4H_2PO_4$) were used. Stoichiometric amounts of the reactants were calculated with the help of the following formula:

$2SrCO_3(s) + 2NH_4H_2PO_4(s) \rightarrow Sr_2P_2O_7(s) + 3H_2O(g) + 2NH_3(g) + 2CO_2(g)$ ***(Hata! Burada görünmesini istediğiniz metne Heading 1 uygulamak için Giriş sekmesini kullanın.****-1)*

Required amounts of $SrCO_3$ and $NH_4H_2PO_4$ were weighed and ground in agate mortar separately. Two materials were then mixed homogeneously in a porcelain mortar. The mixture was put into furnace and was heated to 900˚C with a heating rate of 700˚C/hr. Retention time was set as 14.5 hr.

At the end of this process, when the temperature reduced to room temperature, the product was reground nicely in an agate mortar. The product synthesized was controlled by X-ray powder diffraction analysis.

3.3.2 Doping Procedure

The solid-state doping technique was used in doping process. In this study, experiments were divided into four groups. In the first group, 3%, 5% and 7% by weight CuO and 0.5%, 1%, 2%, 3%, 4%, 5%, 10% and 15% by weight In_2O_3 for each percentage rate of CuO were doped into previously synthesized $Sr_2P_2O_7$. In addition, in the second group, same percentages of CuO by weight were doped but rather than In_2O_3, $AgNO_3$ was used with the same percentages by weight for doping. In the third group 3%,5%, 7% and 9% by weight MnO was doped in $Sr_2P_2O_7$. In the last group 3%, 5%, 7% and 9% by weight MnO was doped into $Sr_2P_2O_7$ with 0,5%, 1%, 3%, 7% and 9% of Pr_6O_{11} respectively for each MnO percentage. The amounts and other details of these groups are given in Tables 3.2 to 3.5.

Table 3.2 Amounts of the group doped with CuO and In_2O_3

Sample Name	$Sr_2P_2O_7$ (gr)	CuO %	CuO (gr)	In_2O_3 %	In_2O_3 (gr)
I0	1	0	0.000	0	0
I1	2	3	0.060	0.5	0.010
I2	2	3	0.060	1	0.020
I3	2	3	0.060	2	0.040
I4	2	3	0.060	3	0.060
I5	2	3	0.060	4	0.080
I6	2	3	0.060	5	0.100
I7	2	3	0.060	10	0.200
I8	2	3	0.060	15	0.300
I9	2	5	0.100	0.5	0.010
I10	2	5	0.100	1	0.020
I11	2	5	0.100	2	0.040
I12	2	5	0.100	3	0.060
I13	2	5	0.100	4	0.080
I14	2	5	0.100	5	0.100
I15	2	5	0.100	10	0.200
I16	2	5	0.100	15	0.300
I17	2	7	0.140	0.5	0.010
I18	2	7	0.140	1	0.020
I19	2	7	0.140	2	0.040
I20	2	7	0.140	3	0.060
I21	2	7	0.140	4	0.080
I22	2	7	0.140	5	0.100
I23	2	7	0.140	10	0.200
I24	2	7	0.140	15	0.300
Total	49		2.400		2.430

Table 3.3 Amounts of the group doped with CuO and $AgNO_3$

Sample Name	$Sr_2P_2O_7$ (gr)	CuO %	CuO (gr)	$AgNO_3$ %	$AgNO_3$ (gr)
A0	1	0	0.000	0	0.0000
A1	2	3	0.060	0.5	0.0147
A2	2	3	0.060	1	0.0293
A3	2	3	0.060	2	0.0586
A4	2	3	0.060	3	0.0880
A5	2	3	0.060	4	0.1173
A6	2	3	0.060	5	0.1466
A7	2	3	0.060	10	0.2932
A8	2	3	0.060	15	0.4398
A9	2	5	0.100	0.5	0.0147
A10	2	5	0.100	1	0.0293
A11	2	5	0.100	2	0.0586
A12	2	5	0.100	3	0.0880
A13	2	5	0.100	4	0.1173
A14	2	5	0.100	5	0.1466
A15	2	5	0.100	10	0.2932
A16	2	5	0.100	15	0.4398
A17	2	7	0.140	0.5	0.0147
A18	2	7	0.140	1	0.0293
A19	2	7	0.140	2	0.0586
A20	2	7	0.140	3	0.0880
A21	2	7	0.140	4	0.1173
A22	2	7	0.140	5	0.1466
A23	2	7	0.140	10	0.2932
A24	2	7	0.140	15	0.4398
Total	49		2.400		3.5626

Table 3.4 Amounts of the group doped with MnO

Sample Name	$Sr_2P_2O_7$ (gr)	MnO %	MnO (gr)
LM1	2	3	0.060
LM2	2	5	0.100
LM3	2	7	0.140
LM4	2	9	0.180
Total	8		0.480

Table 3.5 Amounts of the group doped with MnO and Pr_6O_{11}

Sample Name	$Sr_2P_2O_7$ (gr)	MnO %	MnO (gr)	Pr_6O_{11} %	Pr_6O_{11} (gr)
L3-1	2	3	0.060	7	0.140
L3-2	2	3	0.060	5	0.100
L3-3	2	3	0.060	3	0.060
L3-4	2	3	0.060	1	0.020
L3-5	2	3	0.060	0.5	0.010
L5-1	2	5	0.100	7	0.140
L5-2	2	5	0.100	5	0.100
L5-3	2	5	0.100	3	0.060
L5-4	2	5	0.100	1	0.020
L5-5	2	5	0.100	0.5	0.010
L7-1	2	7	0.140	7	0.140
L7-2	2	7	0.140	5	0.100
L7-3	2	7	0.140	3	0.060
L7-4	2	7	0.140	1	0.020
L7-5	2	7	0.140	0.5	0.010
L9-1	2	9	0.180	7	0.140
L9-2	2	9	0.180	5	0.100
L9-3	2	9	0.180	3	0.060
L9-4	2	9	0.180	1	0.020
L9-5	2	9	0.180	0.5	0.010
Total	40		2.400		1.320

For doping, all amounts of the materials were weighed and afterwards they were mixed and ground in agate mortar. The samples were transferred to porcelain crucibles and were put into furnace and heated to 950˚C with a heating rate of 700˚C/hr. Retention time was set as 11 hr according to the studies of Seyyidoğlu et al. [3]. At the end of this procedure, when the furnace was cooled to the room temperature, each mixture was ground with the help of agate mortar, and then characterization analyzes were carried out.

CHAPTER 4

RESULTS AND DISCUSSION

4.1 POWDER X-RAY DIFFRACTION

The crystal structure of the synthesized $Sr_2P_2O_7$ materials with and without dopant was determined by powder X-ray diffraction (XRD). The JCPDS Card No: 24-1011 taken as a reference for the original XRD peaks of strontium pyrophosphate is shown in Figure 4.1 [55]. Also to check the effect of the metal oxides on the structure, JCPDS Cards Numbered 80-1917, 84-1108, 88-2160, 78-0424 and 42-1121 were taken as reference. (Appendix L) [57,58,59,60,61].

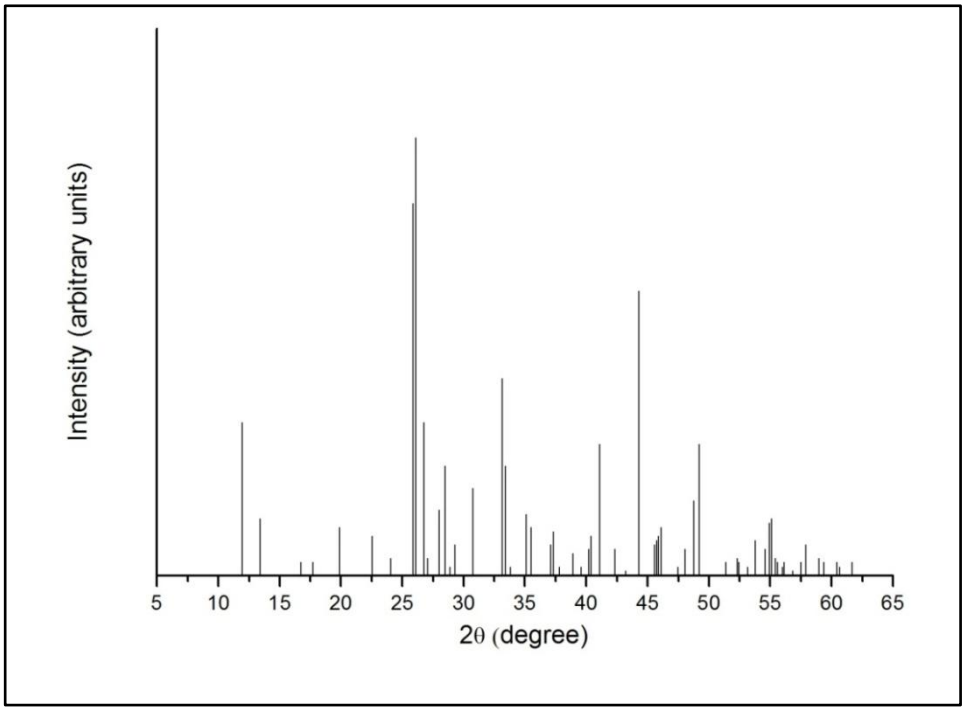

Figure 4.1 XRD pattern of strontium pyrophosphate (JCPDS Card No: 24-1011) [55]

Following Figures 4.2 to 4.11 represent the X-ray patterns of the strontium pyrophosphate samples doped with CuO-$AgNO_3$, CuO-In_2O_3 and MnO-Pr_6O_{11} and they were grouped according to their CuO and MnO amounts. Figure 4.12 represents the X-ray data of the strontium pyrophosphate doped with MnO. In all figures, to ease the comparison, the undoped sample of strontium pyrophosphate was given at the bottom in bold.

As seen from the illustrations in Figures 4.2 to 4.12, the XRD patterns of undoped strontium pyrophosphate samples synthesized by solid state reaction almost fit with the peaks in JCPDS card 24-1011 [55]. This compliance can be observed from table of the X-ray powder data for orthorhombic strontium pyrophosphate and synthesized strontium pyrophosphate with and without dopant, which are given in Appendix D-K.

Although decrease in two of the most intense peaks of the orthorhombic strontium pyrophosphate at 2θ value of around 26 and 45 degrees can be seen from Figures 4.2 to 4.7, the effect of doping was not so appreciable in lower concentrations. Moreover, an increase in a peak was observed at the value of 2θ of around 30 degree (hkl-310) with the increase in the amount of the $AgNO_3$ and In_2O_3; especially with the 10 and 15% of $AgNO_3$ and In_2O_3 by weight. The results are similar with the studies of Seyyidoğlu and his colleagues [2].

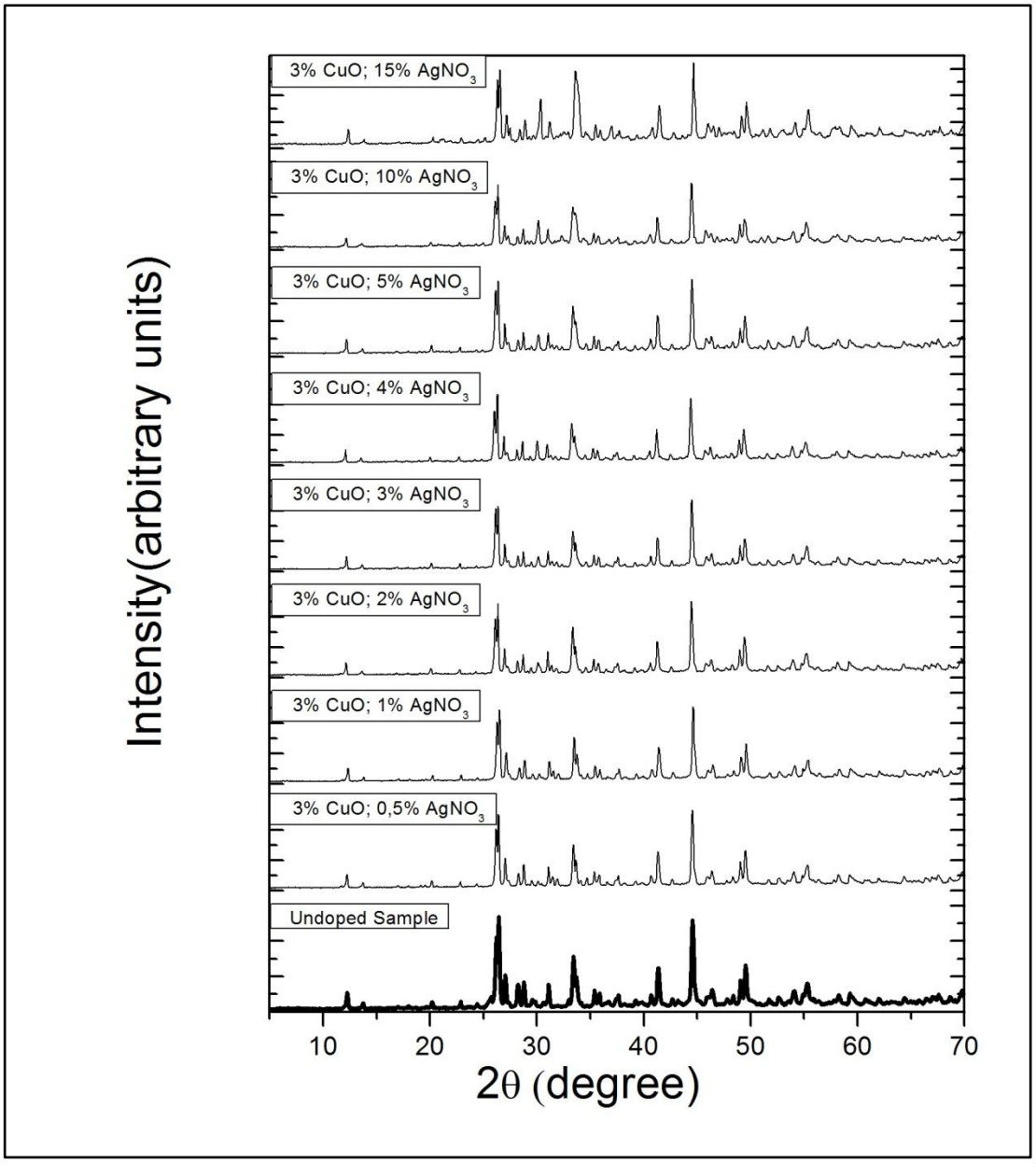

Figure 4.2 XRD pattern of 3% CuO and 0.5-15% $AgNO_3$ doped $Sr_2P_2O_7$ samples

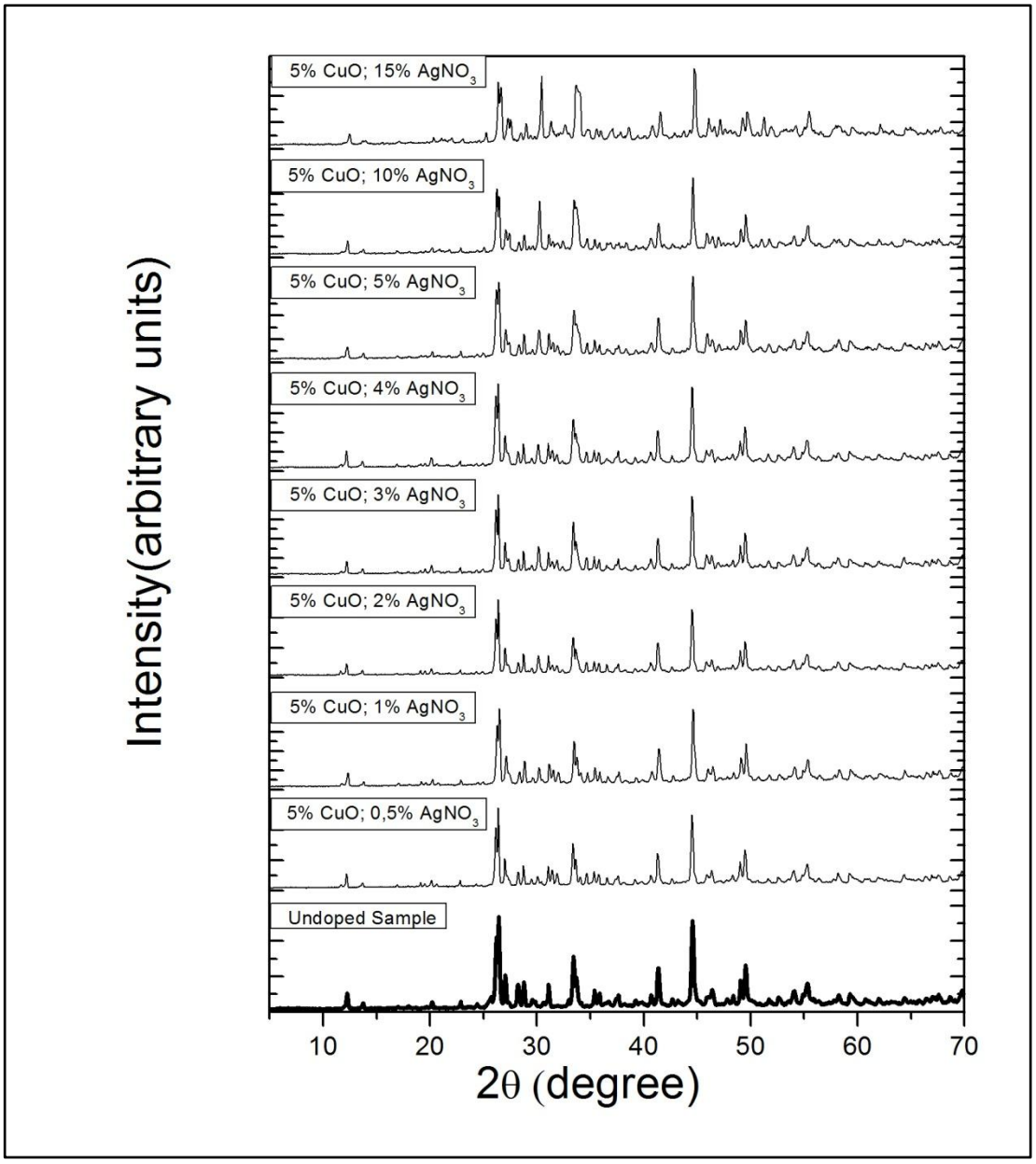

Figure 4.3 XRD pattern of 5% CuO and 0.5-15% $AgNO_3$ doped $Sr_2P_2O_7$ samples

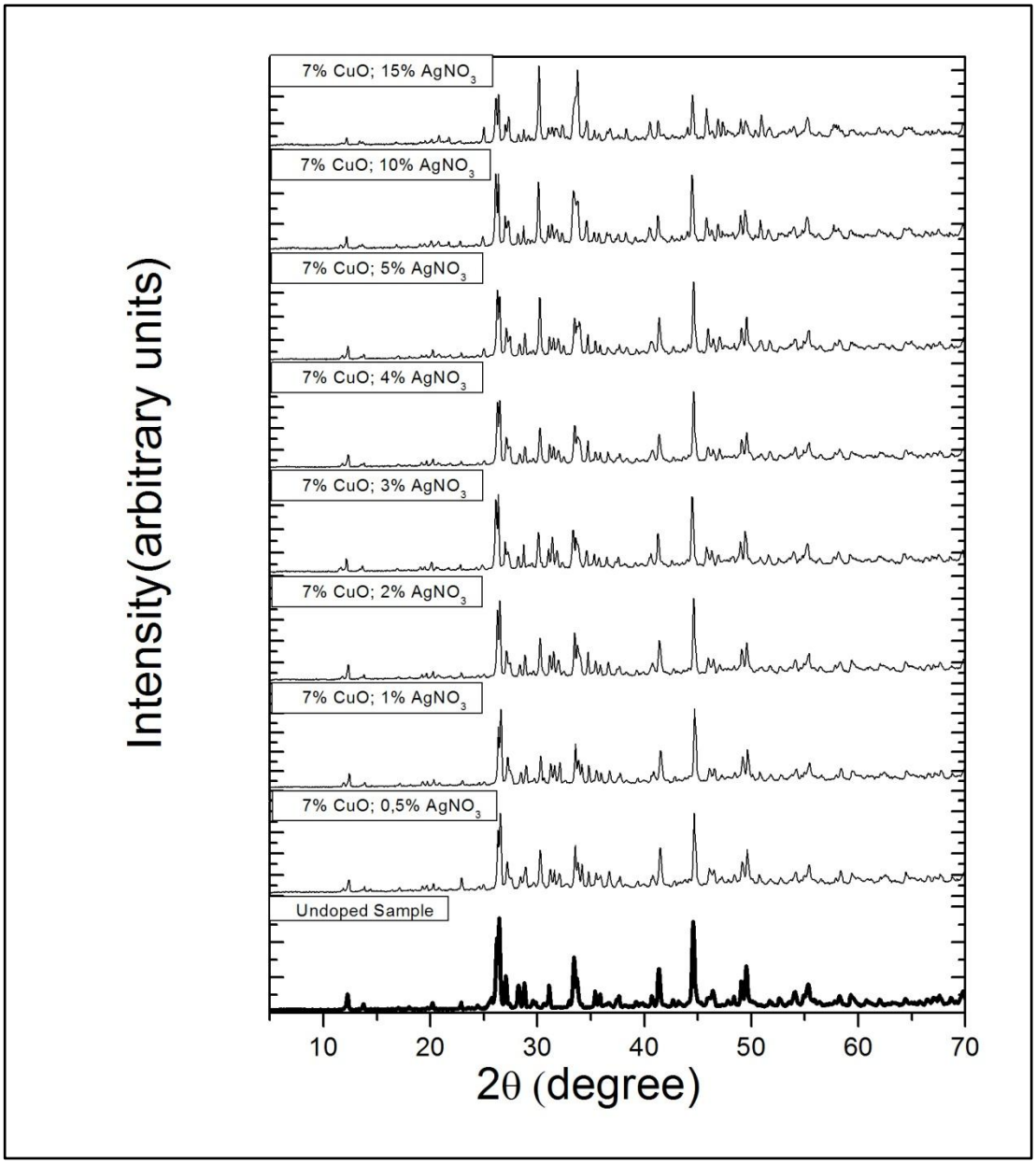

Figure 4.4 XRD pattern of 7% CuO and 0.5-15% $AgNO_3$ doped $Sr_2P_2O_7$ samples

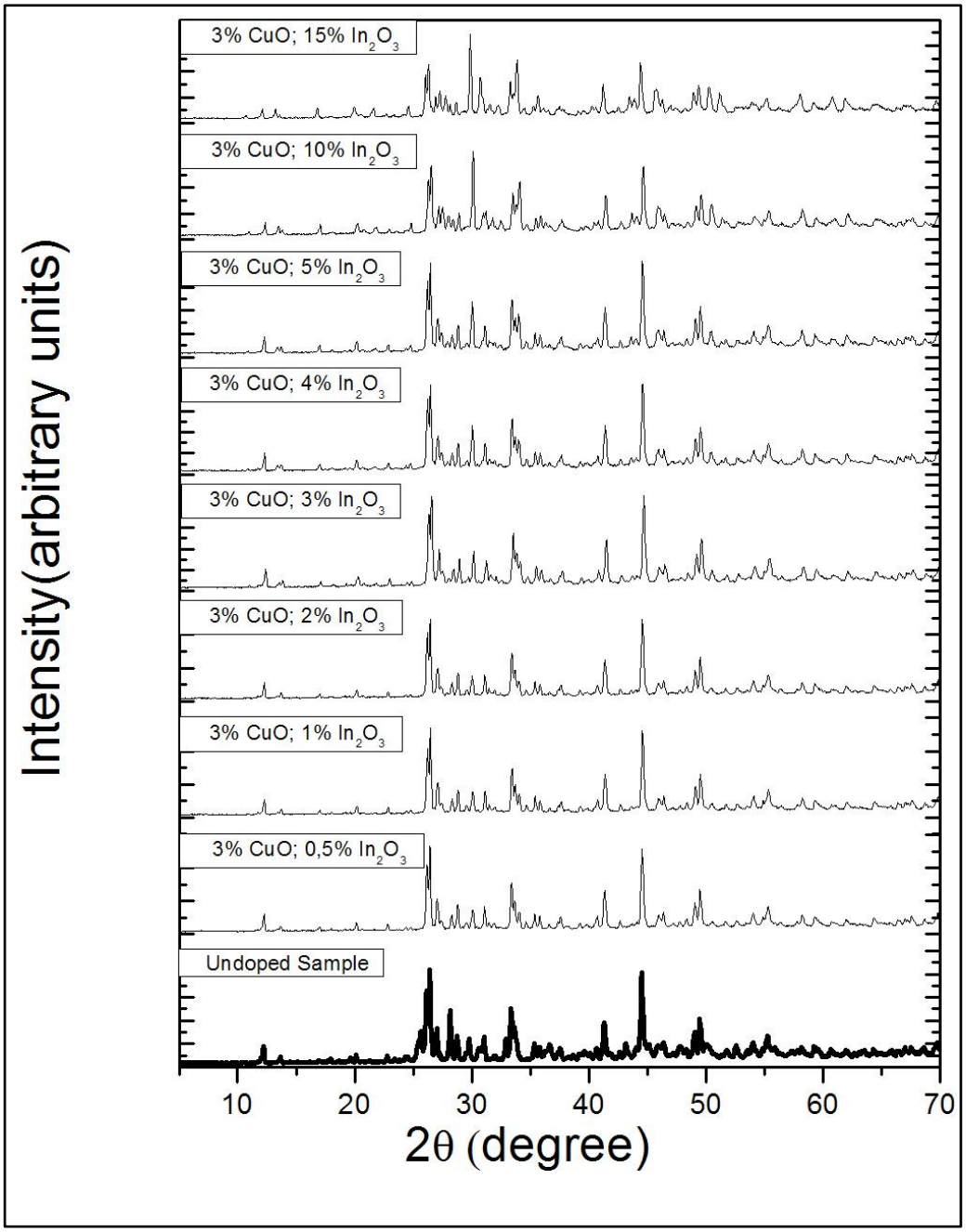

Figure 4.5 XRD pattern of 3% CuO and 0.5-15% In_2O_3 doped $Sr_2P_2O_7$ samples

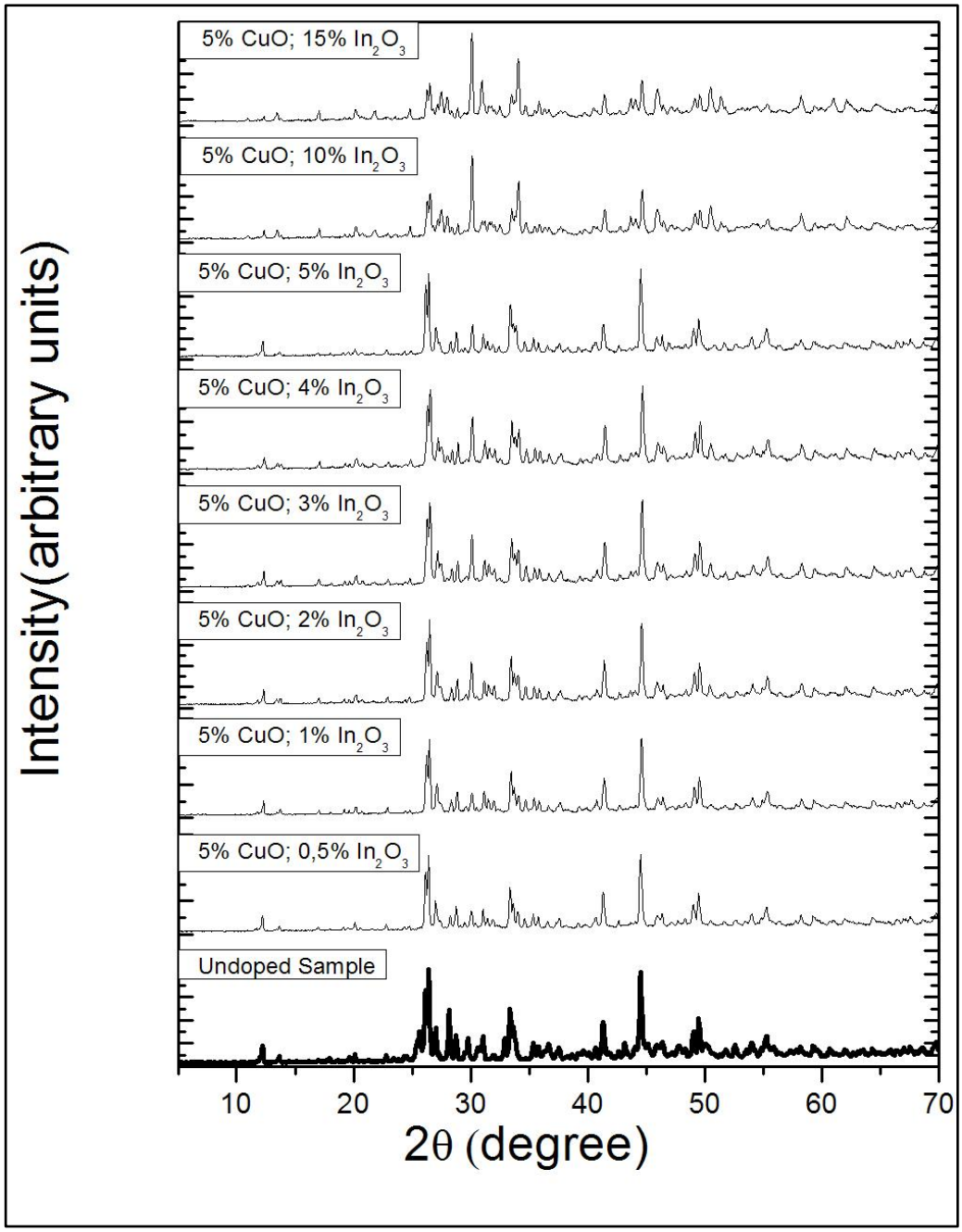

Figure 4.6 XRD pattern of 5% CuO and and 0.5-15% In_2O_3 doped $Sr_2P_2O_7$ samples

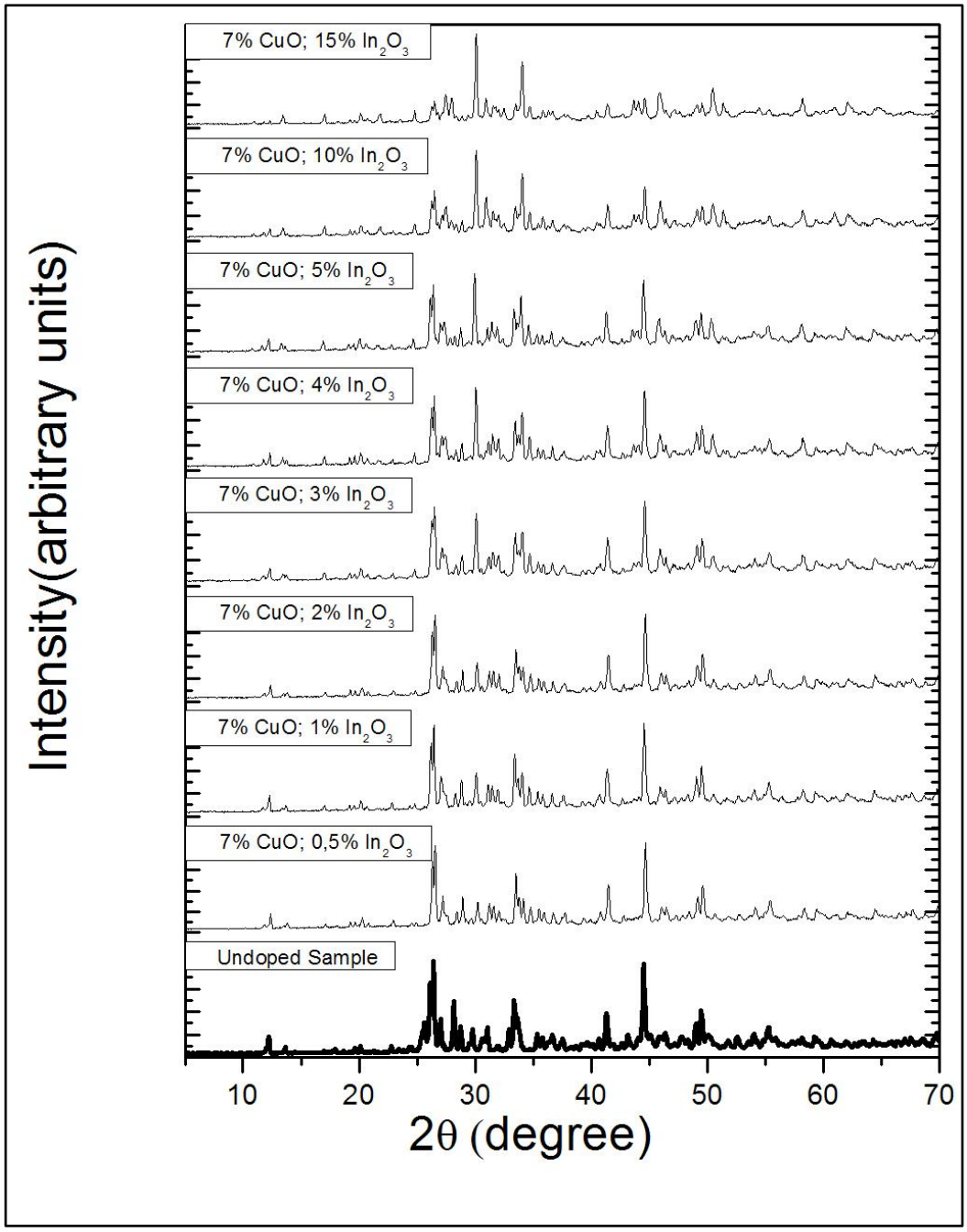

Figure 4.7 XRD pattern of 7% CuO and and 0.5-15% In_2O_3 doped $Sr_2P_2O_7$ samples

Figure 4.8, 4.9, 4.10 and 4.11 show XRD patterns of $Sr_2P_2O_7$ doped with MnO. It was seen that by increasing Pr_6O_{11} percentage by weight, little lowering in the two of the most highest peaks (around 26 and 45 degrees of 2θ value) and an increase in the peak at 30 degree (hkl-310) were observed.

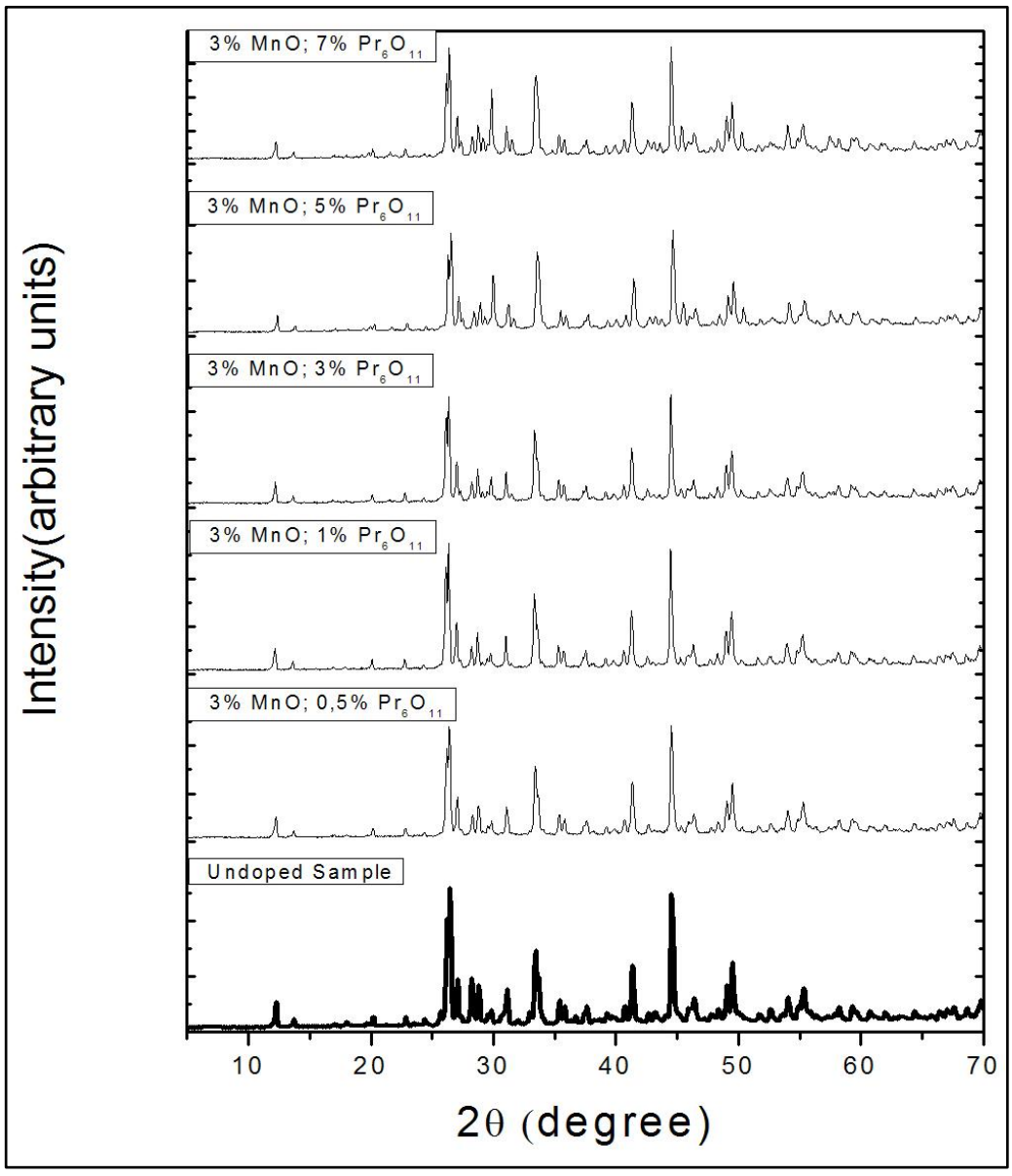

Figure 4.8 XRD pattern of 3% MnO and 0.5, 1, 3, 5 & 7% Pr_6O_{11} doped $Sr_2P_2O_7$ samples

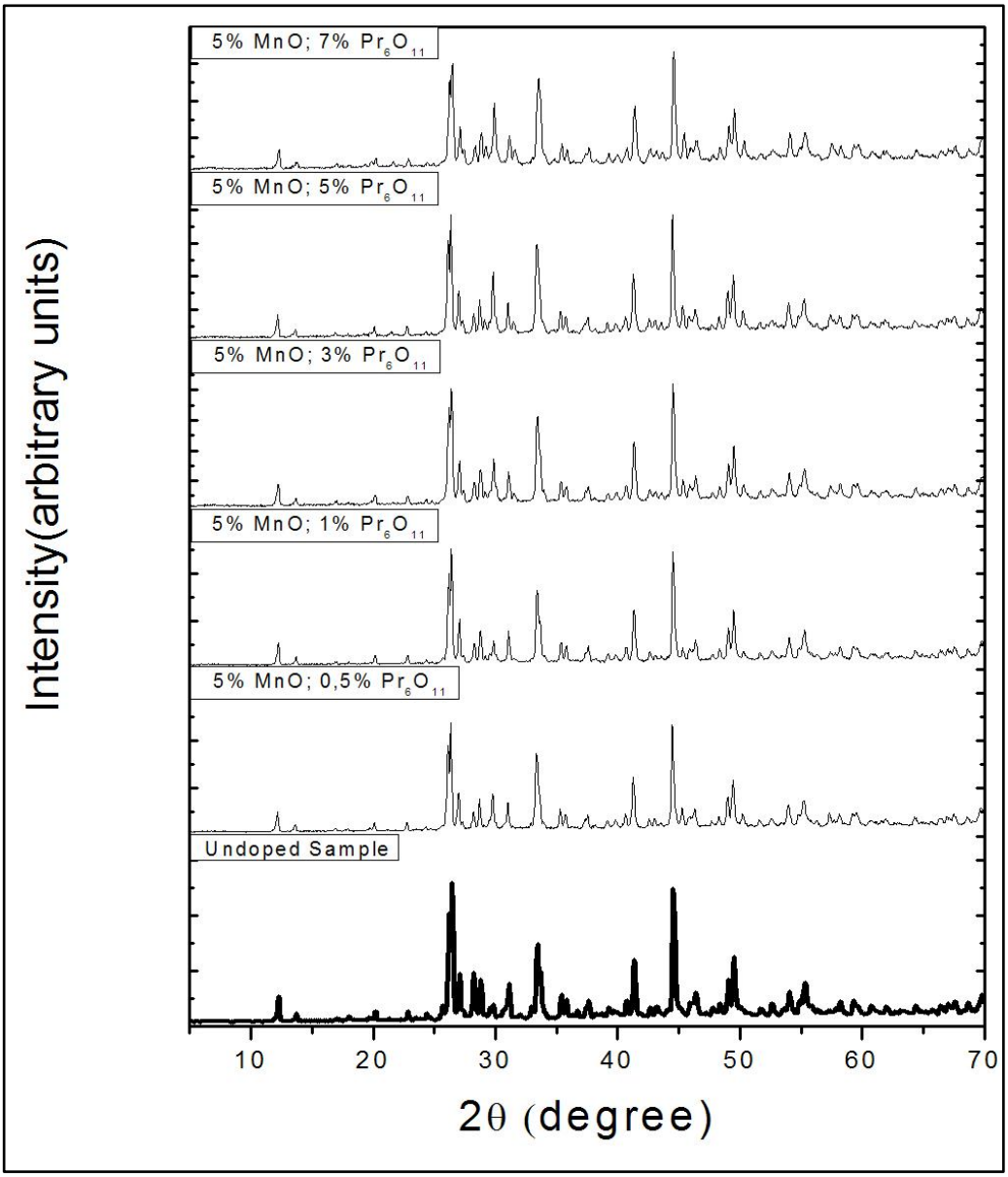

Figure 4.9 XRD pattern of 5% MnO and 0.5, 1, 3, 5 & 7% Pr_6O_{11} doped $Sr_2P_2O_7$ samples

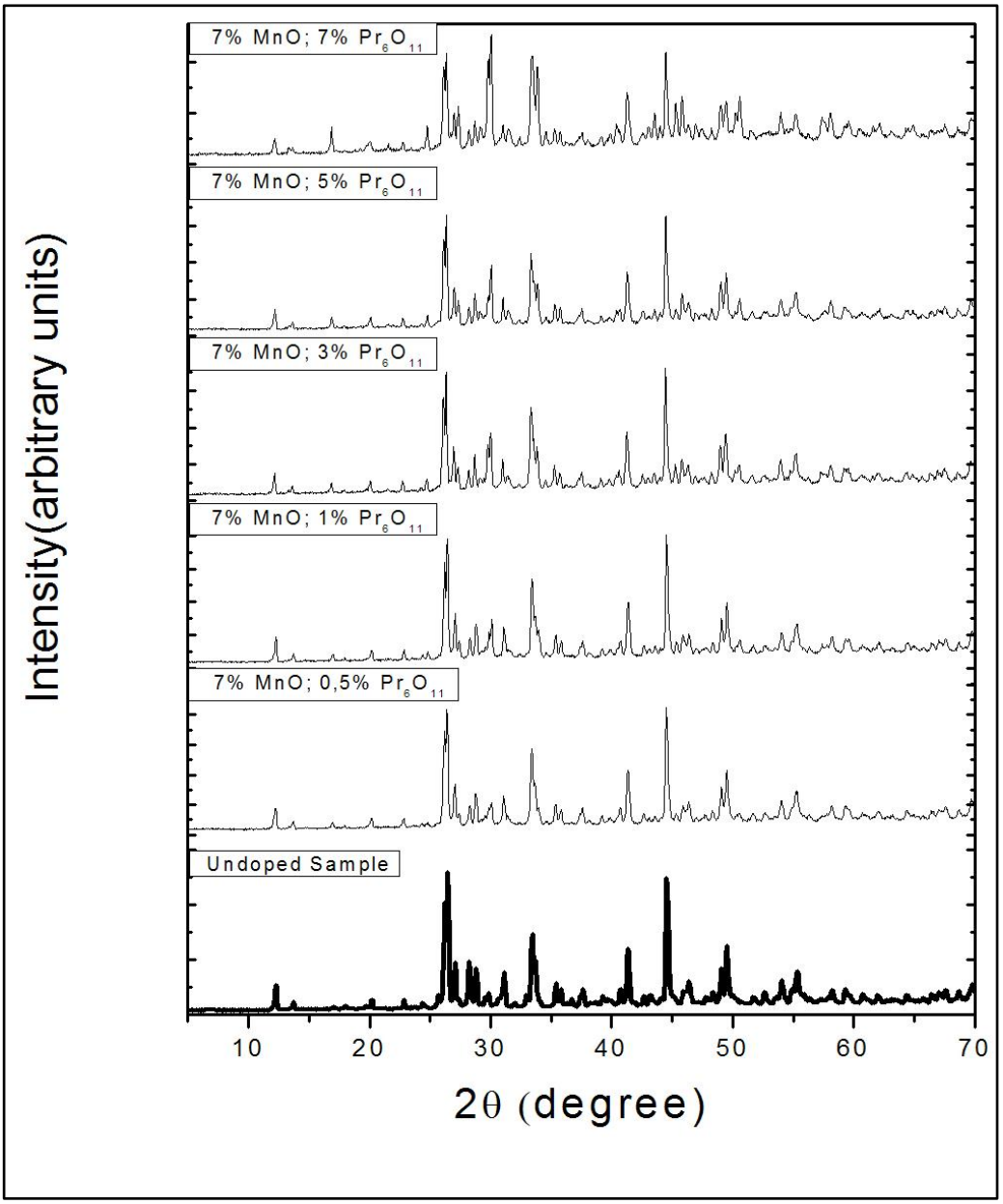

Figure 4.10 XRD pattern of 7% MnO and 0.5, 1, 3, 5 & 7% Pr_6O_{11} doped $Sr_2P_2O_7$ samples

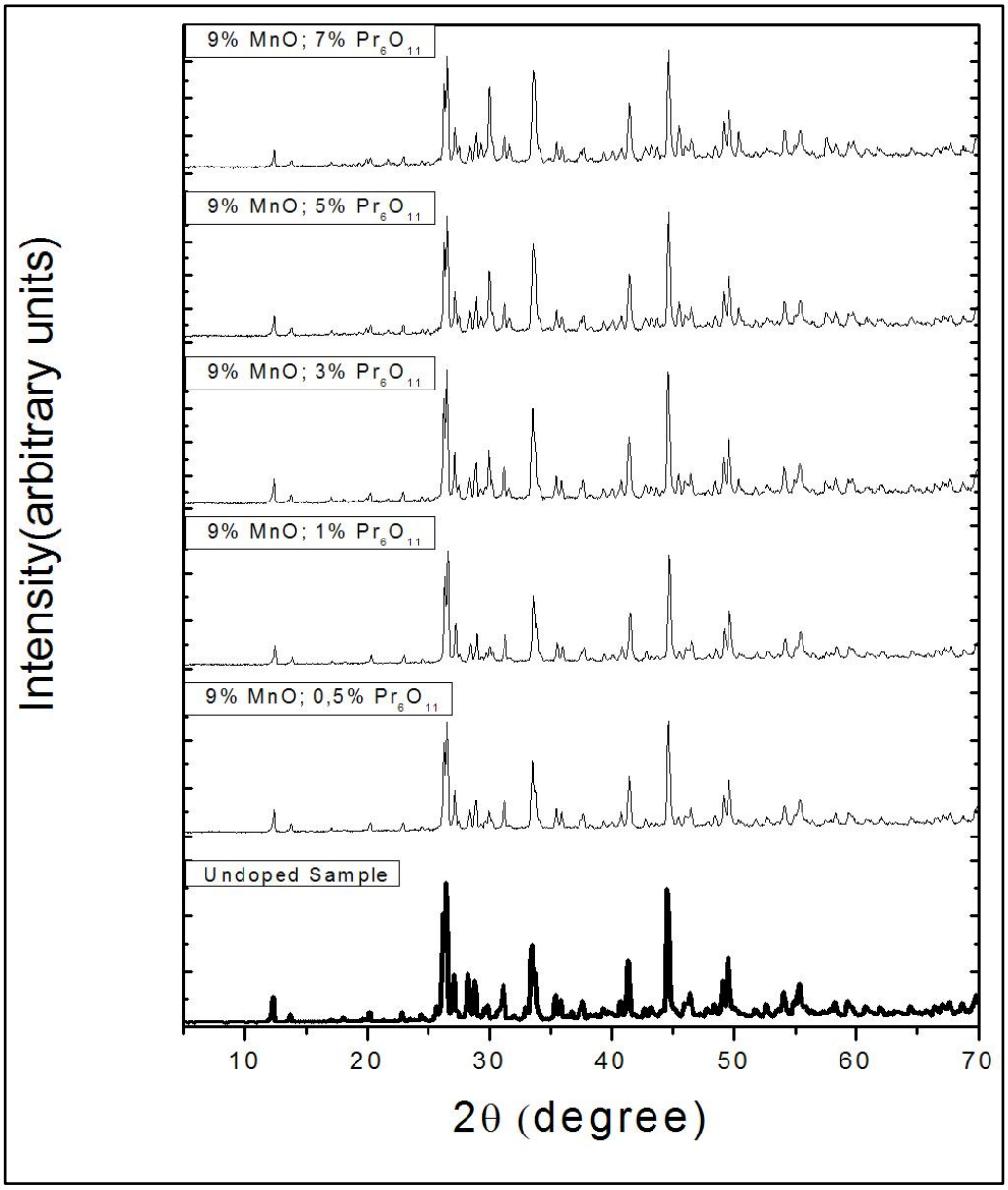

Figure 4.11 XRD pattern of 9% MnO and 0.5, 1, 3, 5 & 7% Pr_6O_{11} doped $Sr_2P_2O_7$ samples

In the Figure 4.12, no change in the peak distribution was observed. So the increasing rate in the MnO% by weight did not affect the crystal structure of orthorhombic strontium pyrophosphate, which means that there is no change in 2θ values of lines.

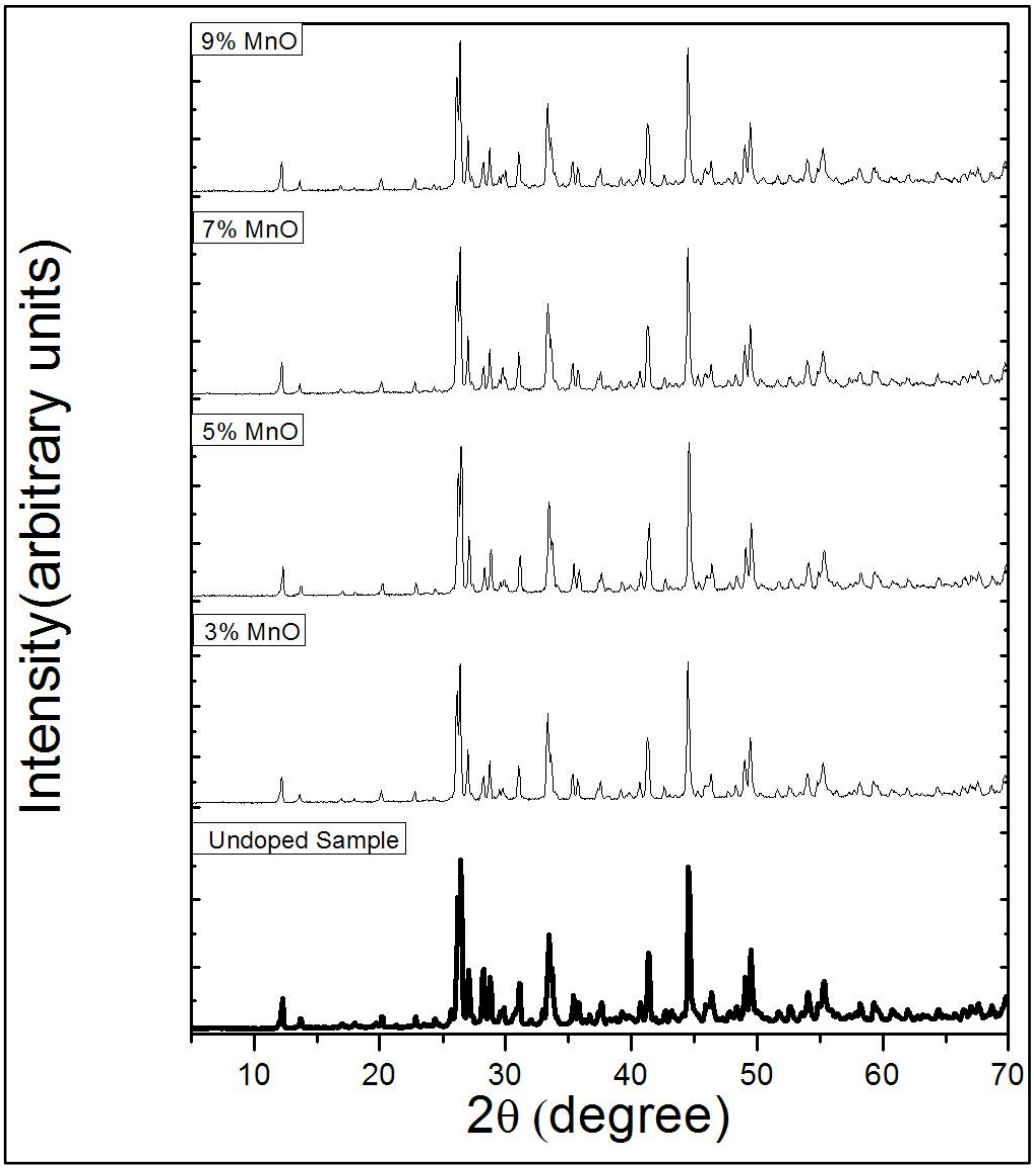

Figure 4.12 XRD pattern of 3, 5, 7 and 9% MnO doped $Sr_2P_2O_7$ samples

To sum up, X-ray powder diffraction patterns for the doped strontium pyrophosphates were in fair agreement with the pattern of JCPDS Card No: 24-1011 [55], indicating the phase purity of the synthesized samples of the $Sr_2P_2O_7$.

4.2 FOURIER TRANSFORM INFRARED SPECTROMETRY

Vibrational modes of anionic group of the strontium pyrophosphate with or without dopant were examined by Fourier Transform Infrared Spectrometry (FTIR). $P_2O_7^{4-}$ vibrational modes were observed within the range of 1400 – 400 cm^{-1} which were consistent with the literature [62]. The anion $P_2O_7^{4-}$ contains the PO_3^{2-} radical and the P-O-P bridge. For the symmetrical and asymmetrical stretching, frequencies are expected within 900-1000 and 1000-1100 cm^{-1} [63]. In Figure 4.13 which is the FTIR of strontium pyrophosphate sample, peaks of asymmetrical PO_3^{2-} radical bending mode was seen around 1000 and 1060 cm^{-1}. The P-O-P bridge peaks were observed around 700 – 825 cm^{-1}. These peaks proved the presence of pyrophosphate within the structure. The overall peak structure in Figure 4.13 was consistent with the undoped strontium pyrophosphate structural peaks [3]. Starting from Fig. 4.14, the following figures given are FTIR analysis of samples doped with CuO, In_2O_3, $AgNO_3$, MnO and Pr_6O_{11}.

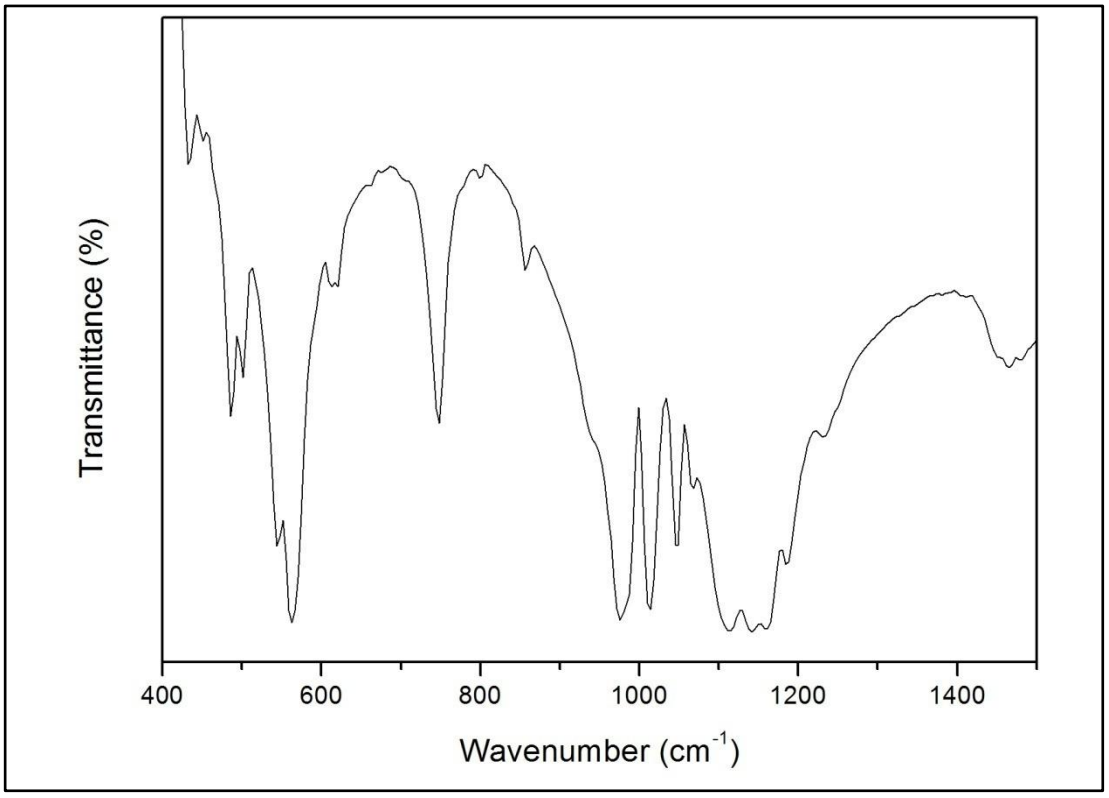

Figure 4.13 FTIR of undoped $Sr_2P_2O_7$ sample

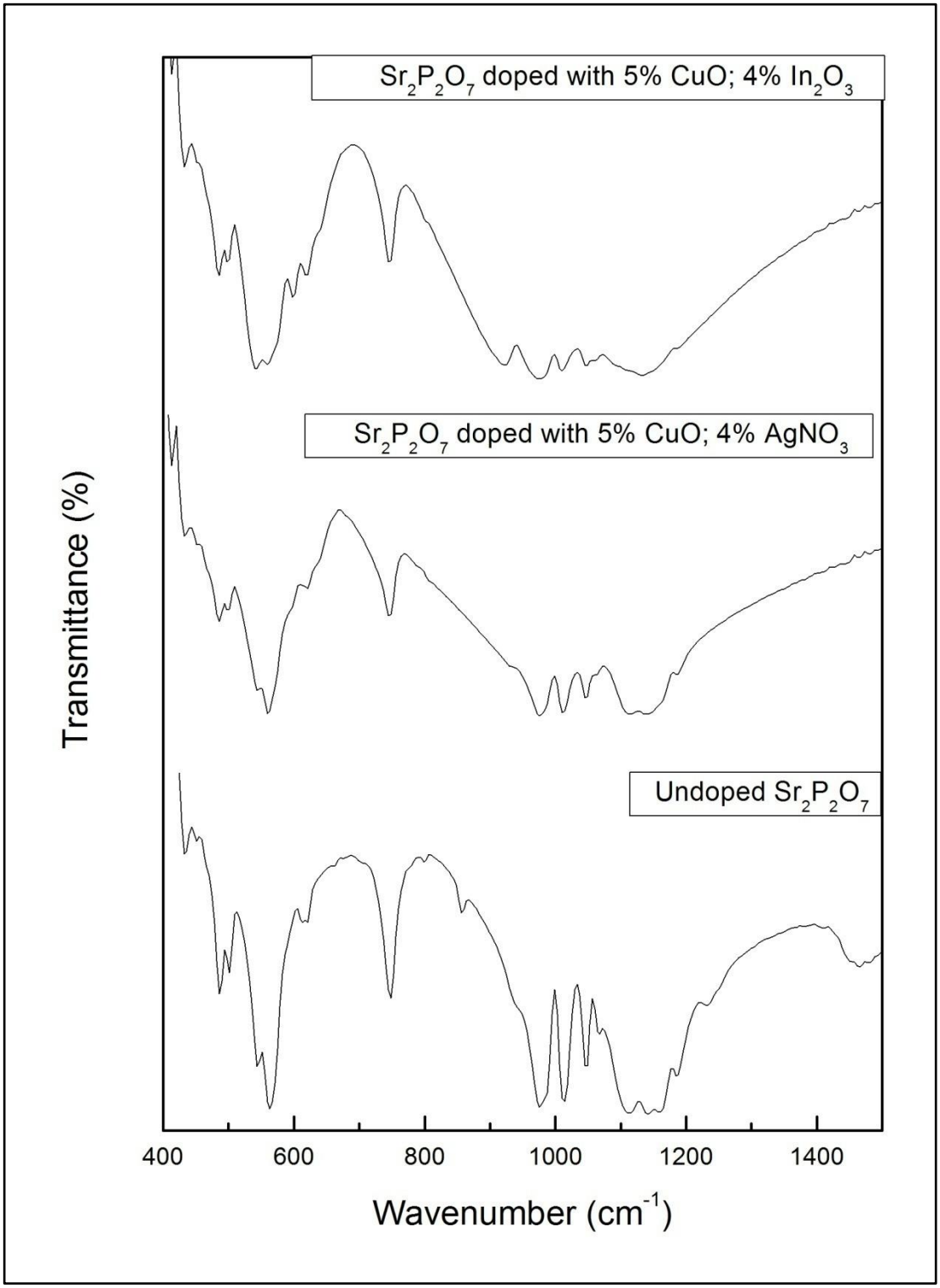

Figure 4.14 FTIR analysis of undoped, CuO-In_2O_3 and CuO-$AgNO_3$ doped $Sr_2P_2O_7$ samples

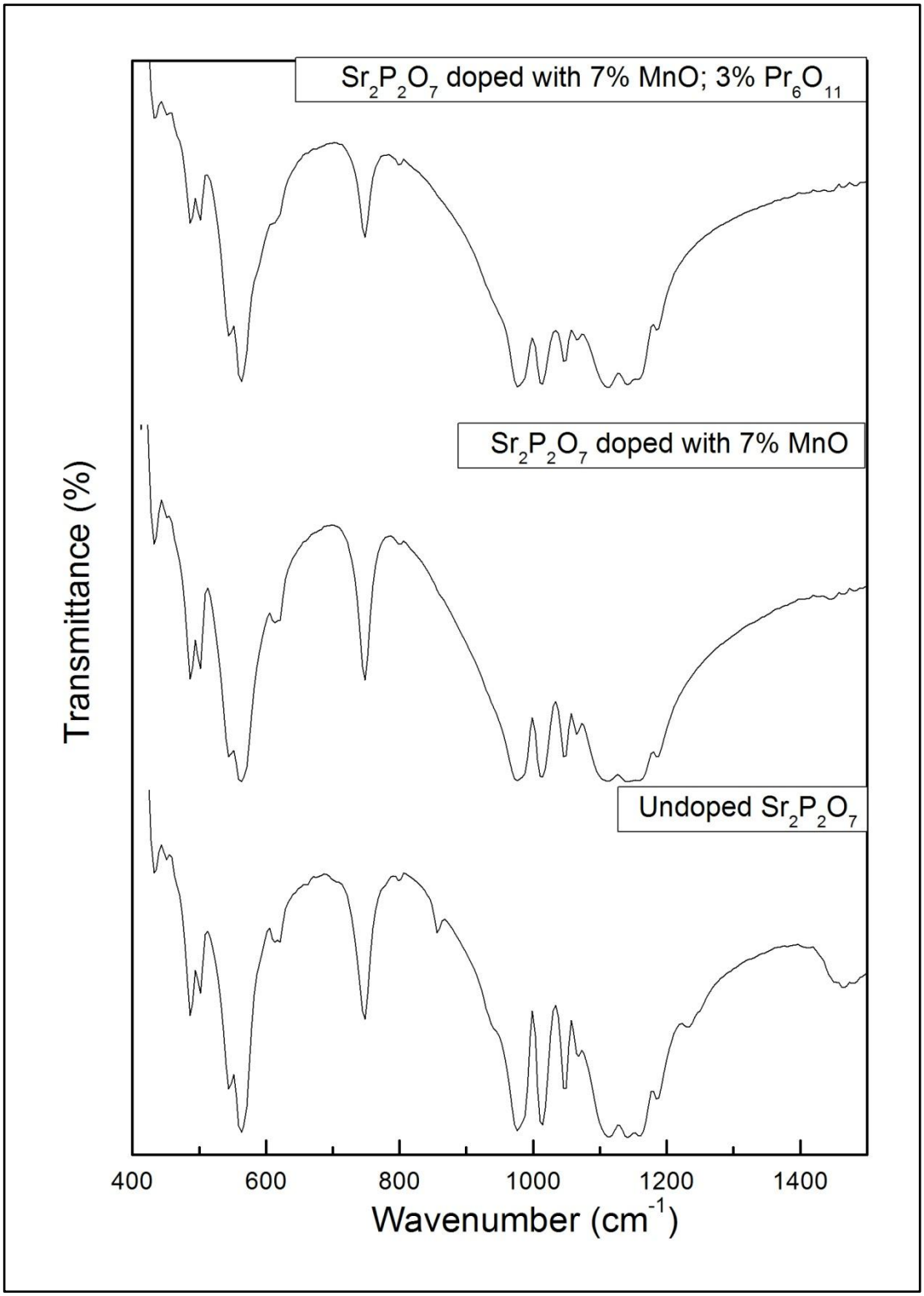

Figure 4.15 FTIR analysis of undoped, MnO and MnO-Pr_6O_{11} doped $Sr_2P_2O_7$ samples

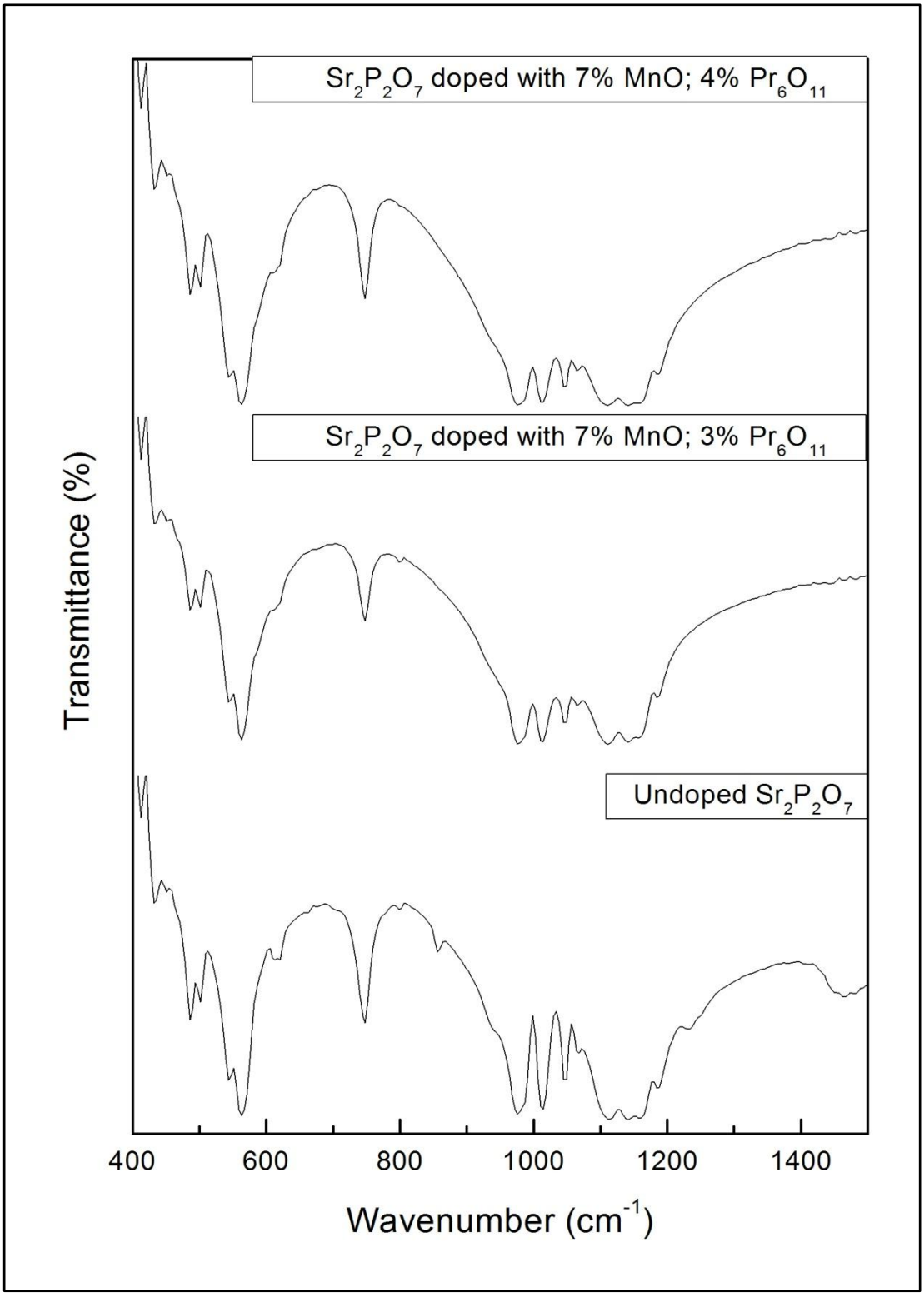

Figure 4.16 FTIR analysis of undoped and MnO-Pr_6O_{11} doped $Sr_2P_2O_7$ samples

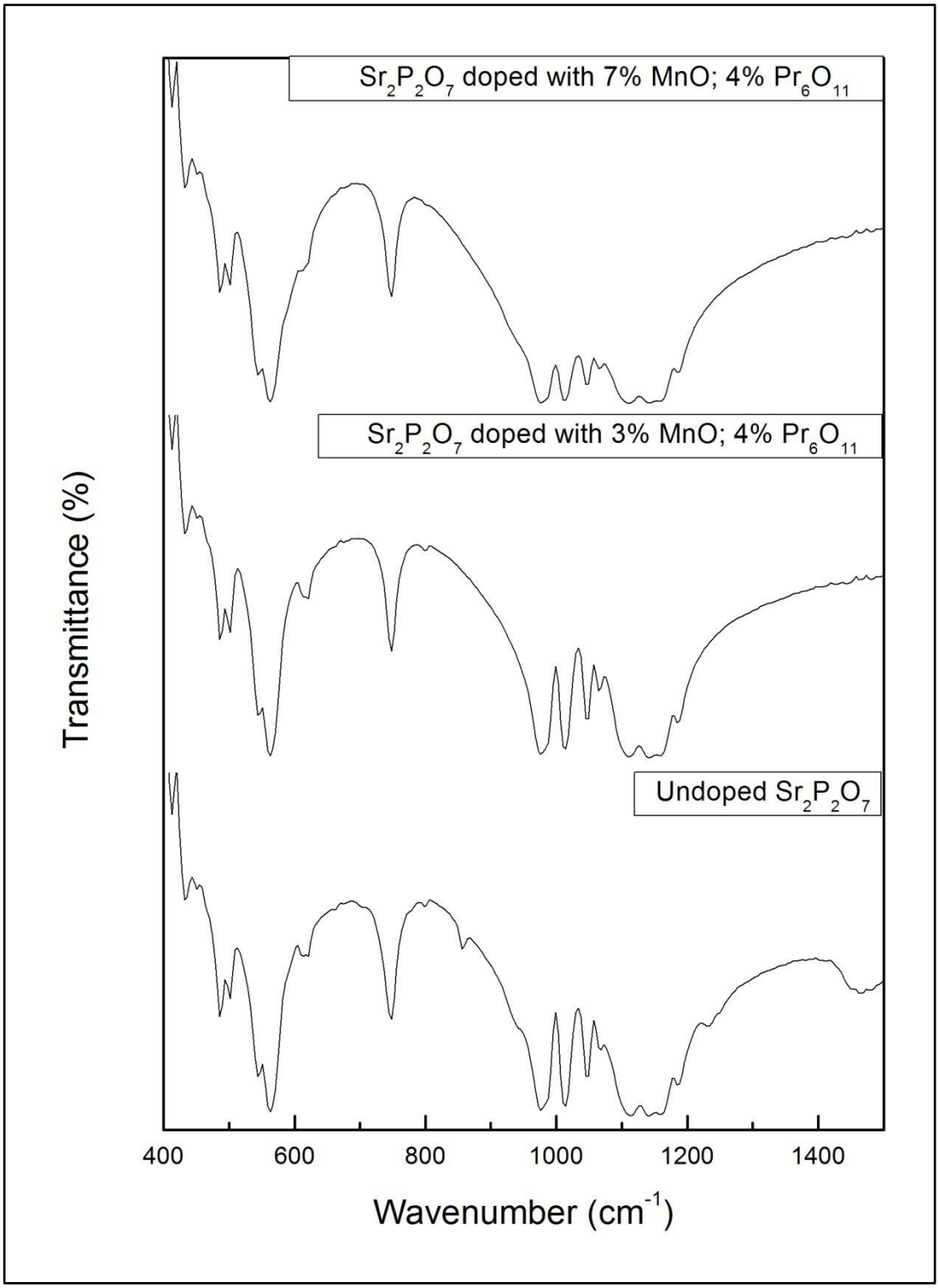

Figure 4.17 FTIR analysis of undoped and MnO-Pr_6O_{11} doped $Sr_2P_2O_7$ samples

4.3 DIFFERENTIAL THERMAL ANALYSIS

Differential Thermal Anlaysis (DTA) was carried out to obtain the thermal behaviour of the produced new materials. DTA results of strontium pyrophosphate without dopant and strontium pyrophosphate doped with 7% MnO and 1% Pr_6O_{11} are illustrated in Figures 4.18 and 4.19. In both figures, no peaks were observed so it was concluded that the samples were thermally stable.

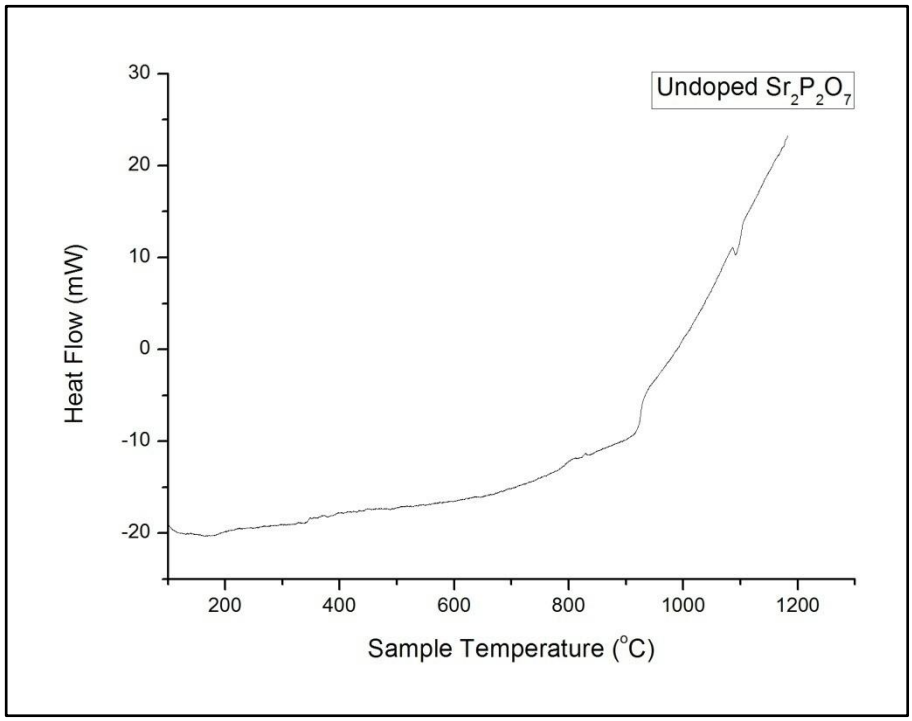

Figure 4.18 DTA result for $Sr_2P_2O_7$ produced by solid state synthesis

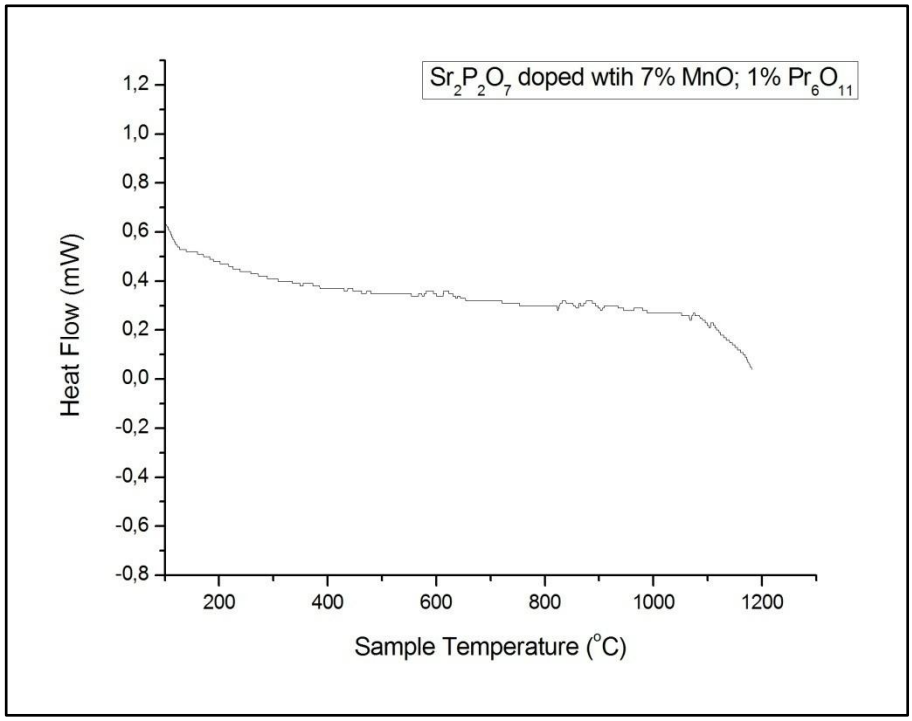

Figure 4.19 DTA result for $Sr_2P_2O_7$ doped with 7% MnO & 1% Pr_6O_{11}

4.4 SCANNING ELECTRON MICROSCOPY

To determine the morphology of the samples Scanning Electron Microscope (SEM) was employed. SEM of strontium pyrophosphate without dopant and with dopant; 7% MnO and 1% Pr_6O_{11}, are illustrated in Figures 4.20 and 4.21. The comparison of these figures showed that the particle size distribution of doped and undoped strontium pyrophosphate was not homogeneous. In addition, from the SEM results it was observed that particles of $Sr_2P_2O_7$ with and without dopant had smooth surface.

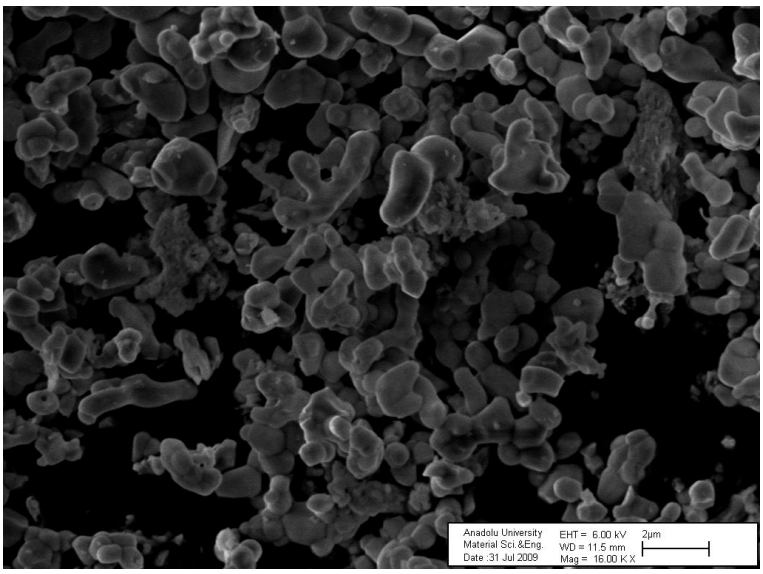

Figure 4.20 SEM of $Sr_2P_2O_7$ without dopant-magnification=16.00 K X

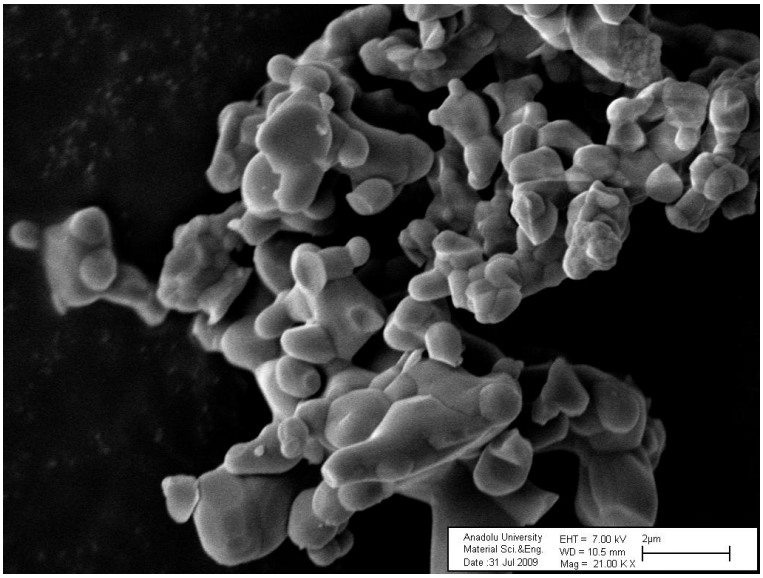

Figure 4.21 SEM of $Sr_2P_2O_7$ with 7% MnO and 1% Pr_6O_{11} dopant-magnification=21.00 K X

4.5 THERMOLUMINESCENCE STUDIES

As mentioned in Chapter 2, thermoluminescence properties of strontium pyrophosphate were not reported in details in literature. In this research, emphasis was given to determine the effect of dopant on TL properties of strontium pyrophosphate.

Figure 4.22 shows the glow peaks of undoped strontium pyrophosphates that have different waiting periods after irradiation in order to check the stabilities of peak positions. Figures 4.23 to 4.38 show the glow peaks of strontium pyrophosphate doped with Cu-Ag, Cu-In and Mn-Pr ions with different amounts.

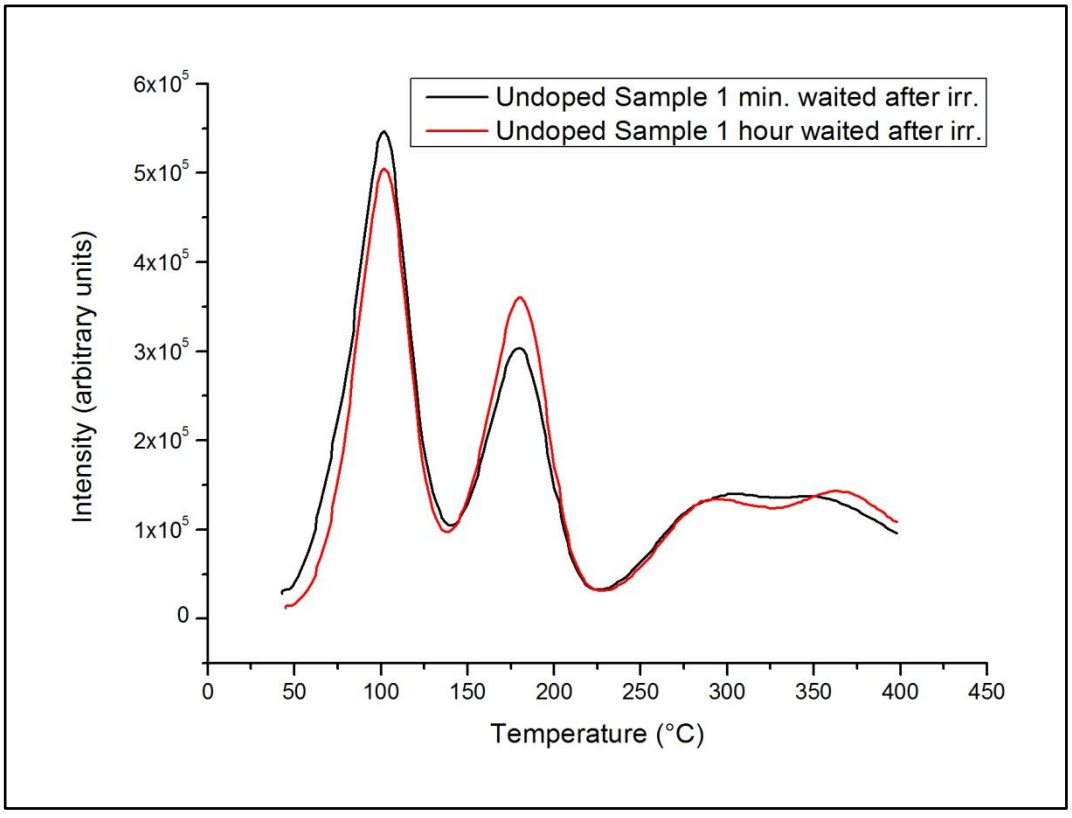

Figure 4.22 Glow curves of undoped $Sr_2P_2O_7$ waited for 1 minute and for 1 hour after irradiation

Figure 4.22 represents the glow peaks of two strontium pyrophosphate samples. One of them was left to rest for 1 minute after irradiation and the other was left to rest for 1 hour after irradiation. Then their thermoluminescence studies were done. From the Figure 4.22 it was observed that there was no effect of residence time on intensities. These evaluations show that the 1 minute residence time was enough for further thermoluminescence measurements.

In the Figure 4.23 the glow peaks for strontium pyrophosphates doped with 3% CuO and 0.5, 1, 2, 3, 4, 5, 10 and 15% by weight of $AgNO_3$ are illustrated. It could be easily seen that the desired peaks for thermoluminescence between 150 and 200˚C could not be achieved. In addition, the peak around 100°C was observed and increase in the amount of $AgNO_3$ decreased the intensity of that peak. Thus, the high amount $AgNO_3$ doped samples showed the lowest intensities.

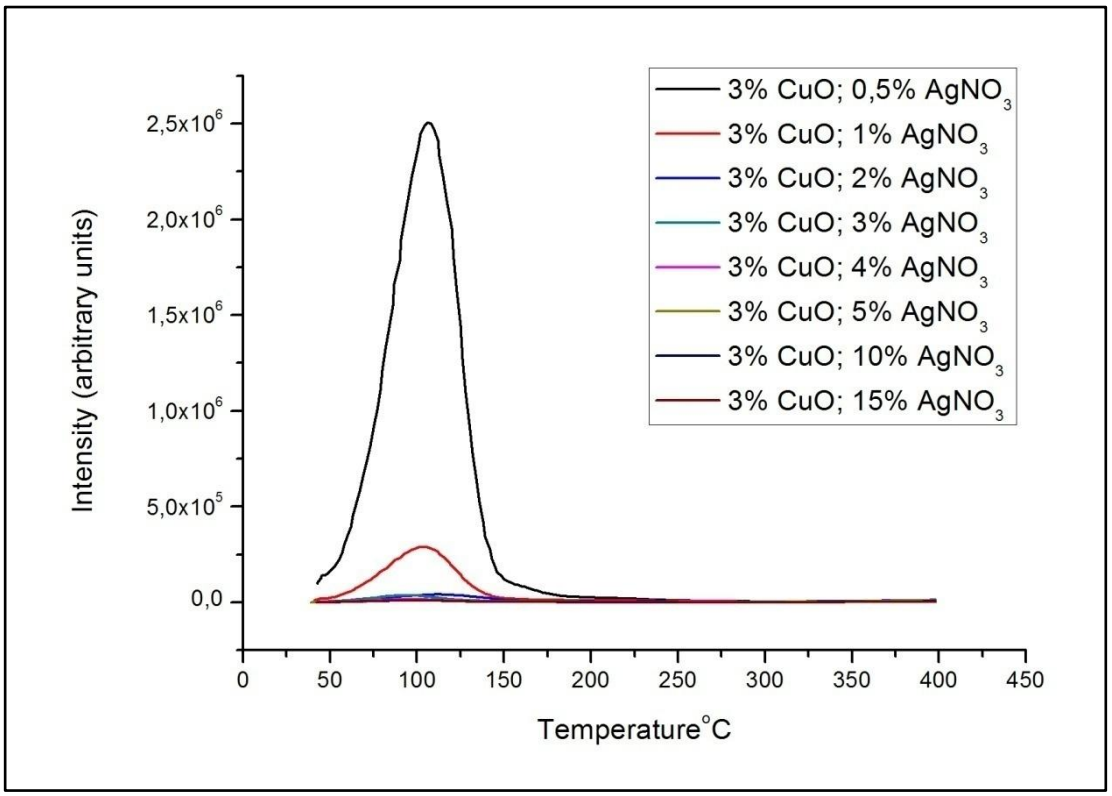

Figure 4.23 Glow curves of $Sr_2P_2O_7$ doped with 3% CuO and 0.5-15% $AgNO_3$

Figure 4.24 illustrates the glow peaks for 5% CuO and 0.5, 1, 2, 3, 4, 5, 10 and 15% by weight of $AgNO_3$ doped samples. Like the previous samples, there was no desired peak for thermoluminescence dosimetry, which must be between 150 and 200°C, which was. The peak around 100°C had a trend of decrease with increasing percentage of $AgNO_3$.

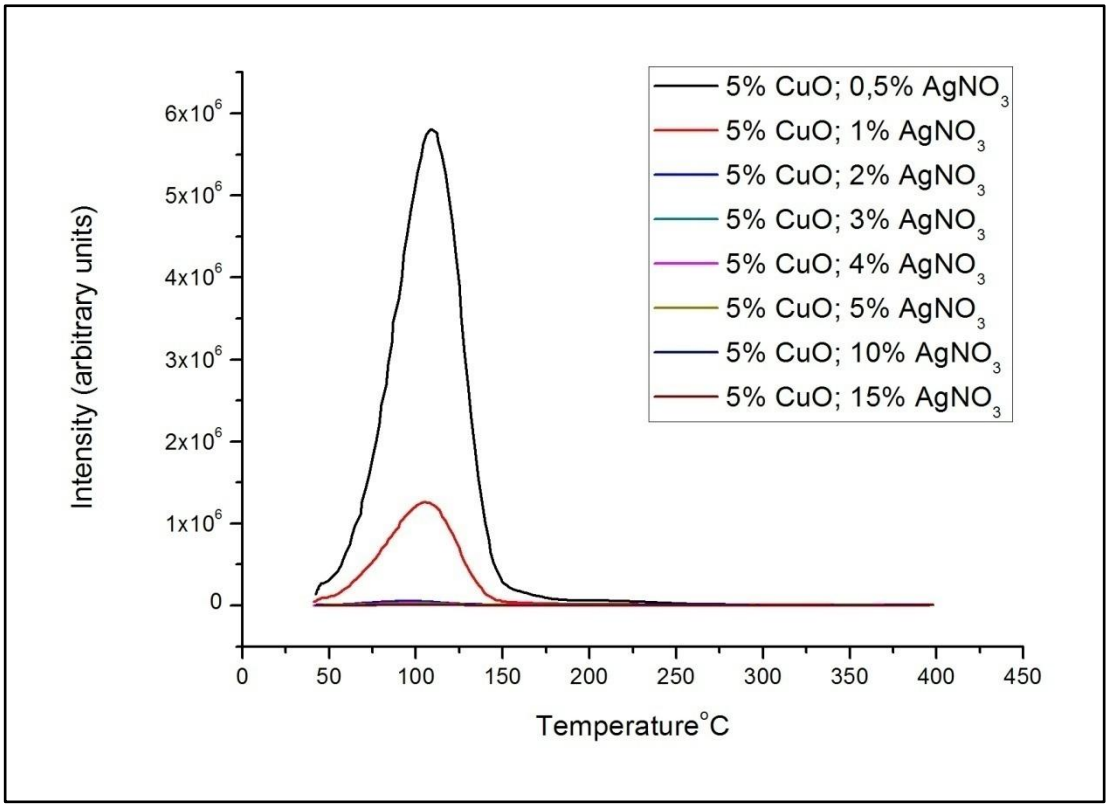

Figure 4.24 Glow curves of $Sr_2P_2O_7$ doped with 5% CuO and 0.5-15% $AgNO_3$

In Figure 4.25 same observations in previous figure were monitored. Further, there was no increase or decrease in the peak around 100°C with the increase in the percentage of $AgNO_3$. On the other hand, the highest peaks were observed at the lowest percentages of $AgNO_3$ and the lowest peaks at the highest percentages. When Figures 4.23, 4.24 and 4.25 were taken to consideration, an increase at the intensity of the peak at 100°C was monitored with increasing CuO percentage.

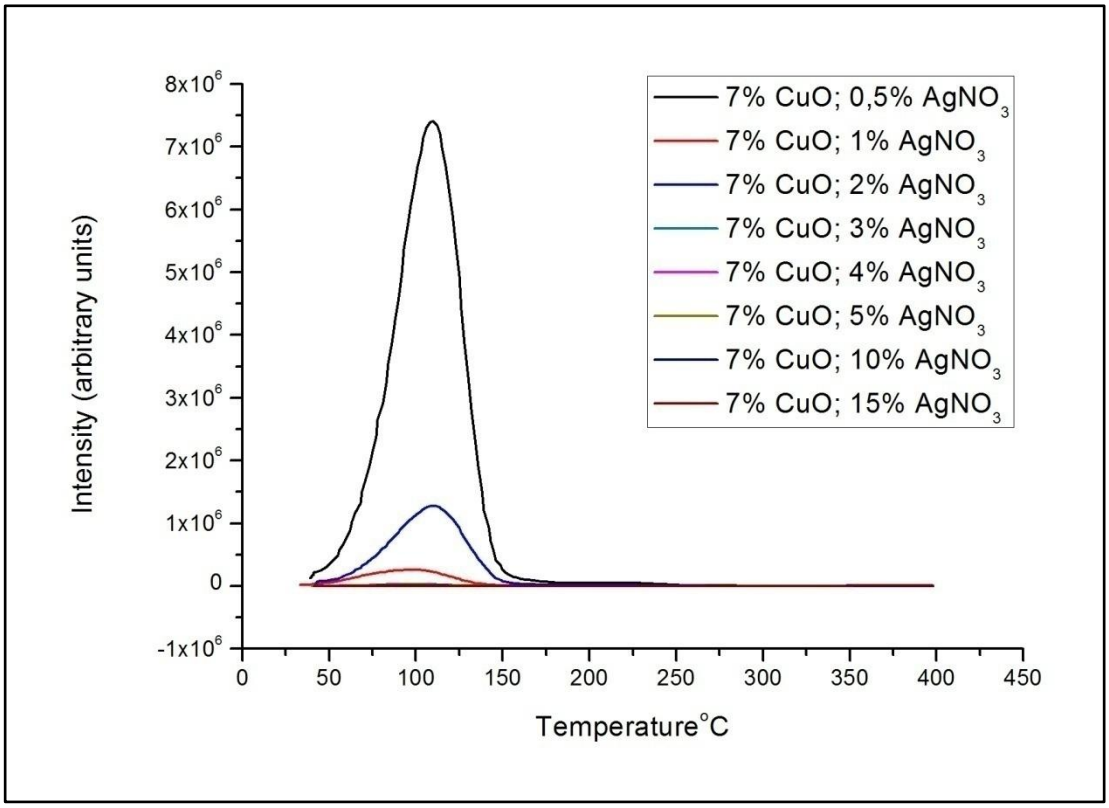

Figure 4.25 Glow curves of $Sr_2P_2O_7$ doped with 7% CuO and 0.5-15% $AgNO_3$

In Figure 4.26, glow peaks of strontium pyrophosphates doped with 3% CuO and 0.5, 1, 2, 3, 4, 5, 10 and 15% In_2O_3 were plotted. Desired peak for thermoluminescence dosimetry between 150 and 200˚C were not observed. On the other hand the peak at 100°C was again observed. Any decrease or increase was not observed with the change in In_2O_3 amount, but the highest In_2O_3 concentration showed lowest intensities in the glow curve.

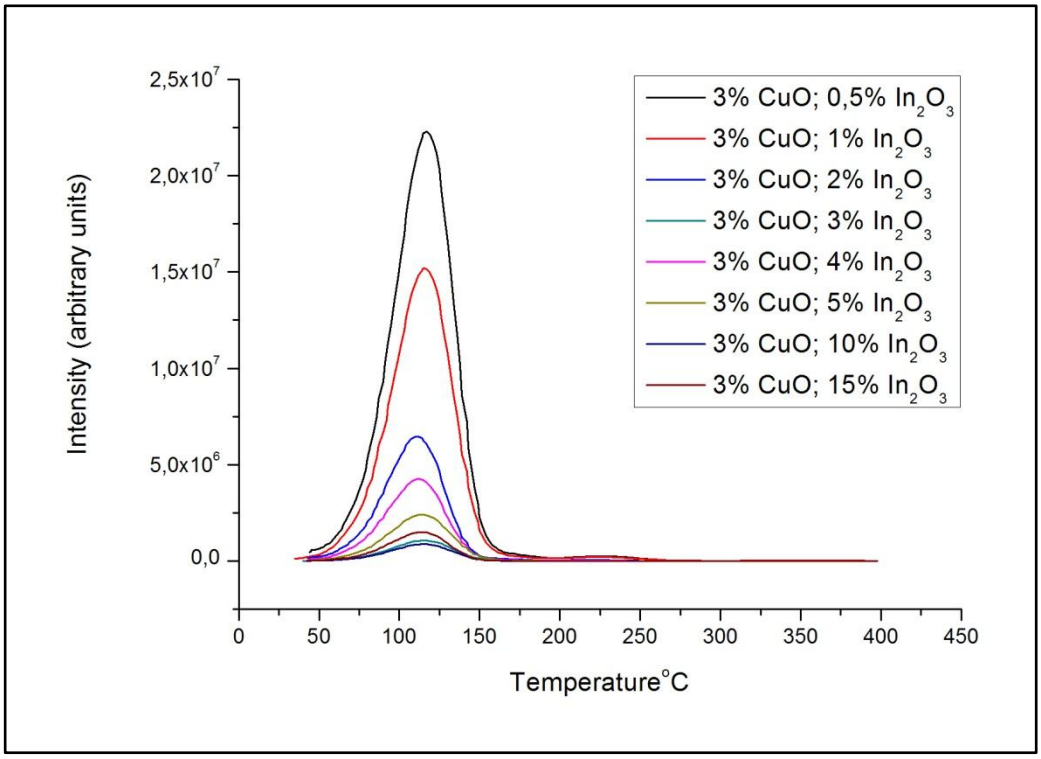

Figure 4.26 Glow curves of $Sr_2P_2O_7$ doped with 3% CuO and 0.5-15% In_2O_3

Figure 4.27 shows samples doped with 5% CuO and different percentages of In_2O_3 and Figure 4.28 illustrates the samples doped with 7% CuO and different percentages of In_2O_3. Like the previous figures, in both illustrations the intended peak of each sample between 150 and 200°C were not observed. In addition, the peak at 100°C did not show any regular change in intensity with the increase in In_2O_3. Moreover, the lowest peak were obtained with the highest In_2O_3 percentages. From Figures 4.26, 4.27 and 4.28, an increase in the amount of intensity peaks around 100°C was observed.

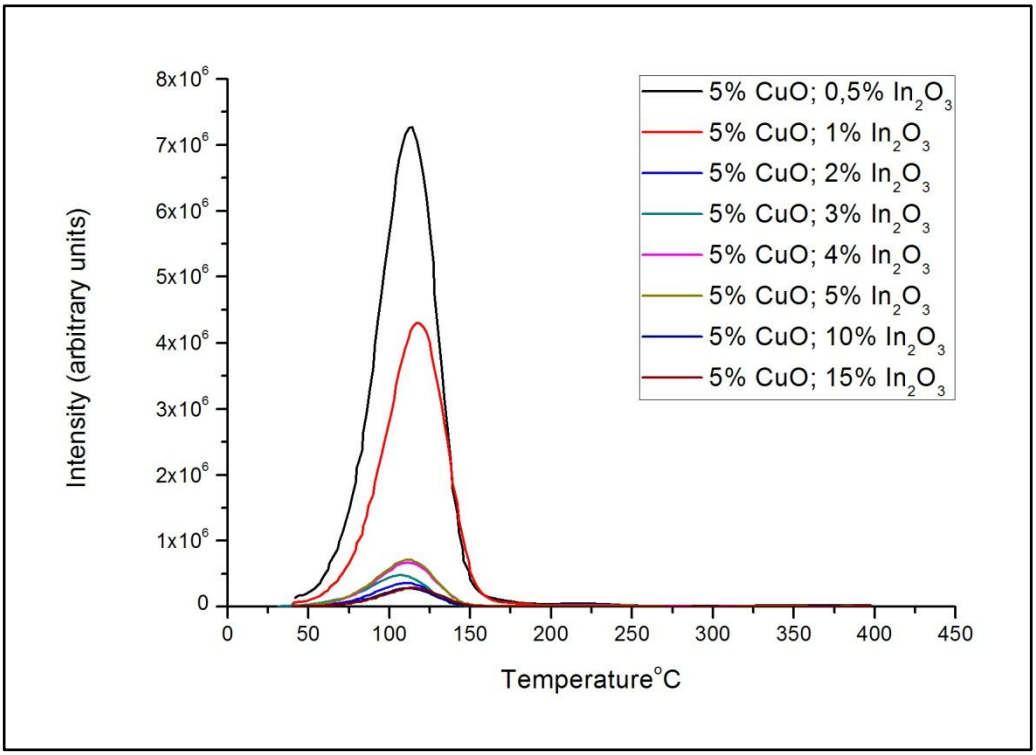

Figure 4.27 Glow curves of $Sr_2P_2O_7$ doped with 5% CuO and 0.5-15% In_2O_3

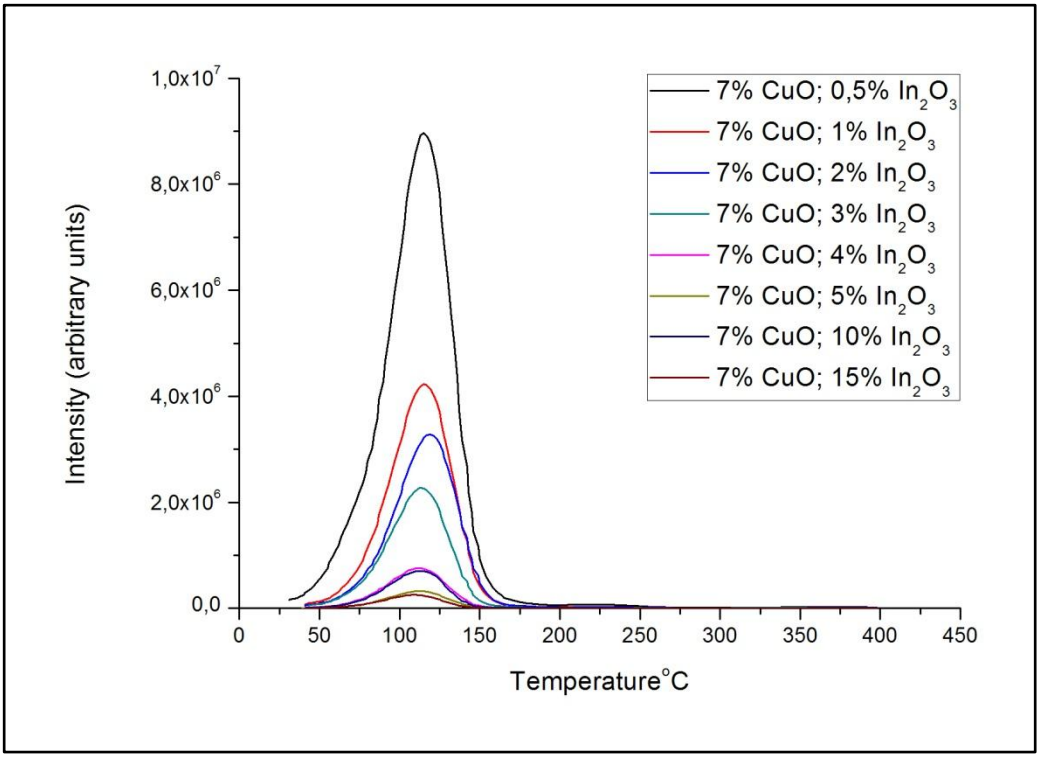

Figure 4.28 Glow curves of $Sr_2P_2O_7$ doped with 7% CuO and 0.5-15% In_2O_3

Figure 4.29 displays the glow curve of the strontium pyrophosphate doped with 3, 5, 7 and 9% MnO. The first peak was observed at 100°C and the intensity of that peak decreased with the increase in MnO%. Another peak around 135°C was detected. No regular change with the increasing MnO amount was detected for this peak. Nevertheless, the highest intensity for this peak was recorded with 7% MnO.

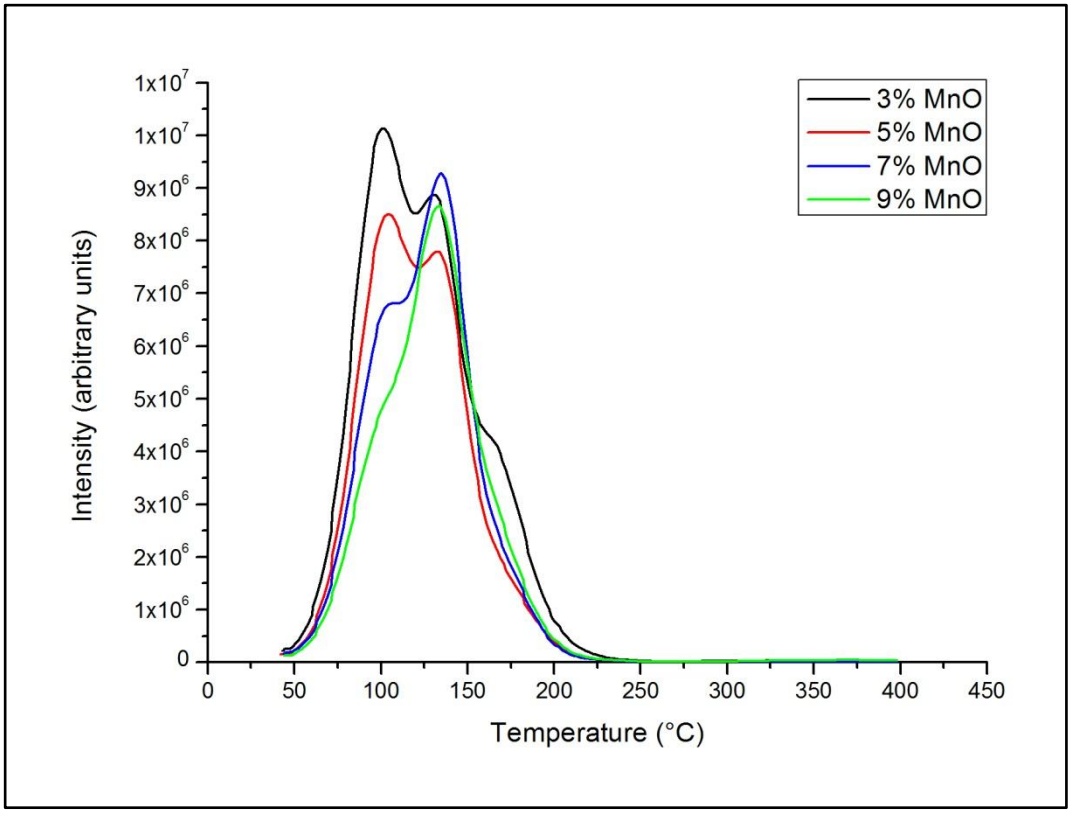

Figure 4.29 Glow curves of $Sr_2P_2O_7$ doped with 3-9% MnO

In the Figure 4.30 illustrates the glow peaks of the strontium pyrophosphate doped with 3% MnO and 0.5, 1, 3, 5 and 7% Pr_6O_{11} by weight. The first peak observed at 100°C changed with increasing the amount of Pr_6O_{11}. So the lowest intensities for the first peak were seen with 5 and 7% of Pr_6O_{11}. Second peak was seen at 175°C, which was close to the desired temperature for thermoluminescence dosimetry. Intensity of that peak increases with the decreasing amount of Pr_6O_{11} and reached the highest value with 1% of Pr_6O_{11}. When the Pr_6O_{11} amount decreased to 0.5%, intensity started to decrease.

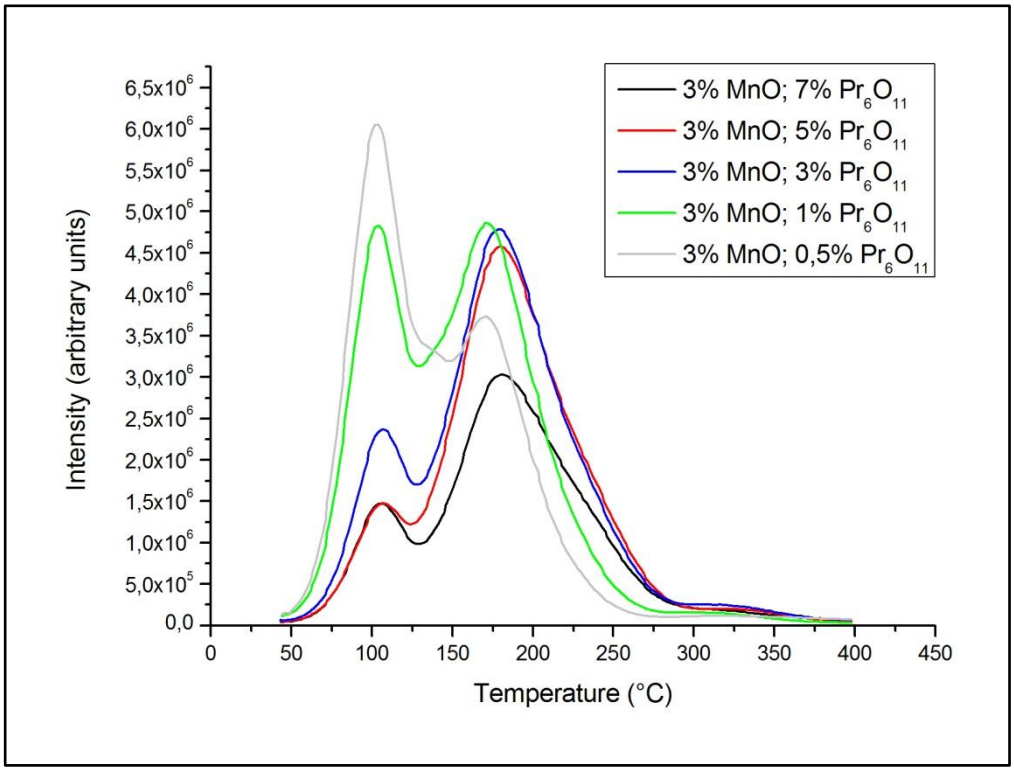

Figure 4.30 Glow curves of $Sr_2P_2O_7$ doped with 3% MnO and 0.5-7% Pr_6O_{11}

From the Figure 4.31, it was seen that the increase in the amount of Pr_6O_{11} decreased the intensity of glow curves at 100°C, which is the requested behavior for thermoluminescence dosimetry. The second peak, which was around 170°C, increased with the decrease in amount of Pr_6O_{11} except 0.5% Pr_6O_{11}. The highest intensity for the second peak was observed, when the Pr_6O_{11} amount was 1% by weight.

The Figure 4.32 shows the thermoluminescence glow curves of the strontium pyrophosphate doped with 7% MnO and 0.5-7% Pr_6O_{11}. From the graph, it could be observed that the second and desired peak reached the highest value and shadowed the first peak. The general trend with the 7% MnO was an increase in the intensity with decreasing Pr_6O_{11} percentage from 7% to 1%. The highest intensity value of this study was observed around $1.5x10^7$ arbitrary units at around 160°C with 1% Pr_6O_{11} 7% MnO.

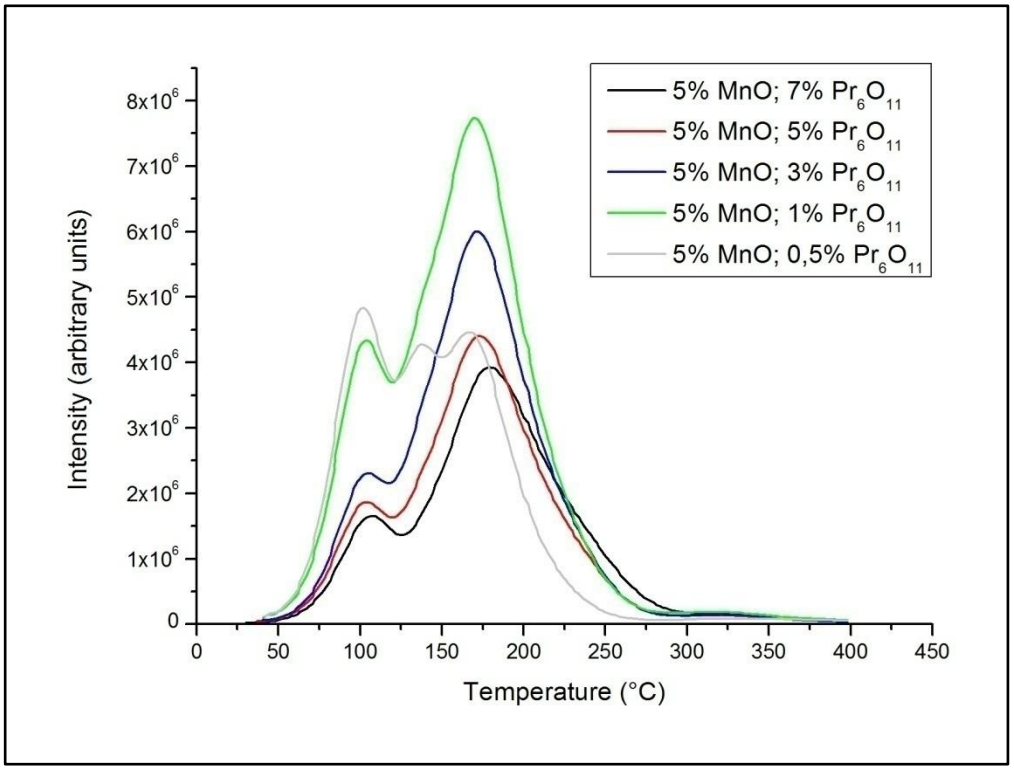

Figure 4.31 Glow curves of $Sr_2P_2O_7$ doped with 5% MnO and 0.5-7% Pr_6O_{11}

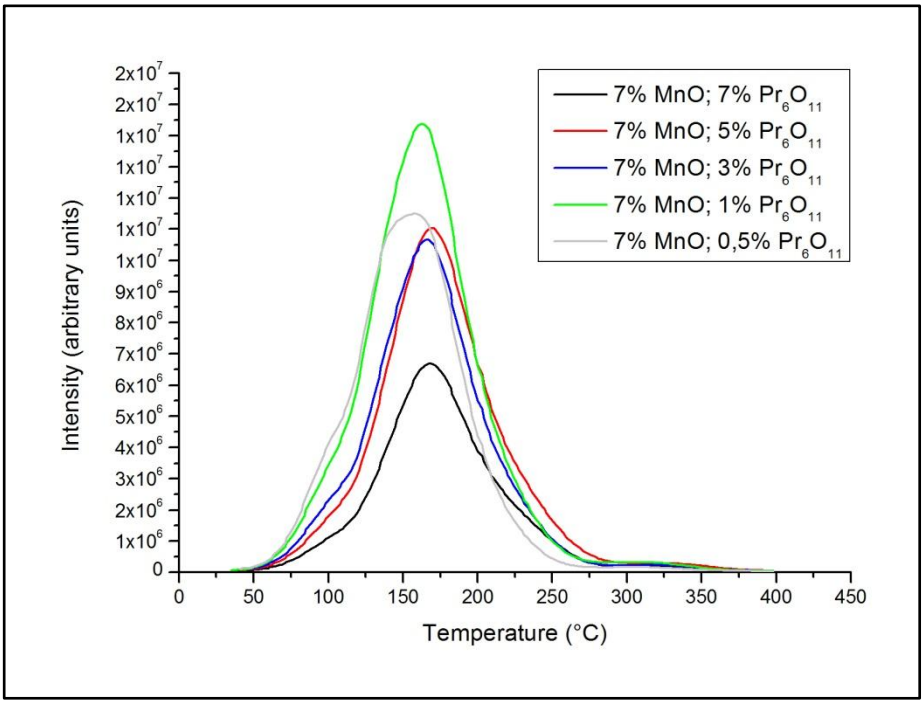

Figure 4.32 Glow curves of $Sr_2P_2O_7$ doped with 7% MnO and 0.5-7% Pr_6O_{11}

Figure 4.33 shows the intensities for 9% MnO and 0.5-7% Pr_6O_{11} .Similar with the Figures 4.31 and 4.32; the increase in amount of Pr_6O_{11} decreased the first peak intensity and after 1% Pr_6O_{11}, it decreased the second peak intensity. In addition, the highest peak was observed with value 1% Pr_6O_{11}.

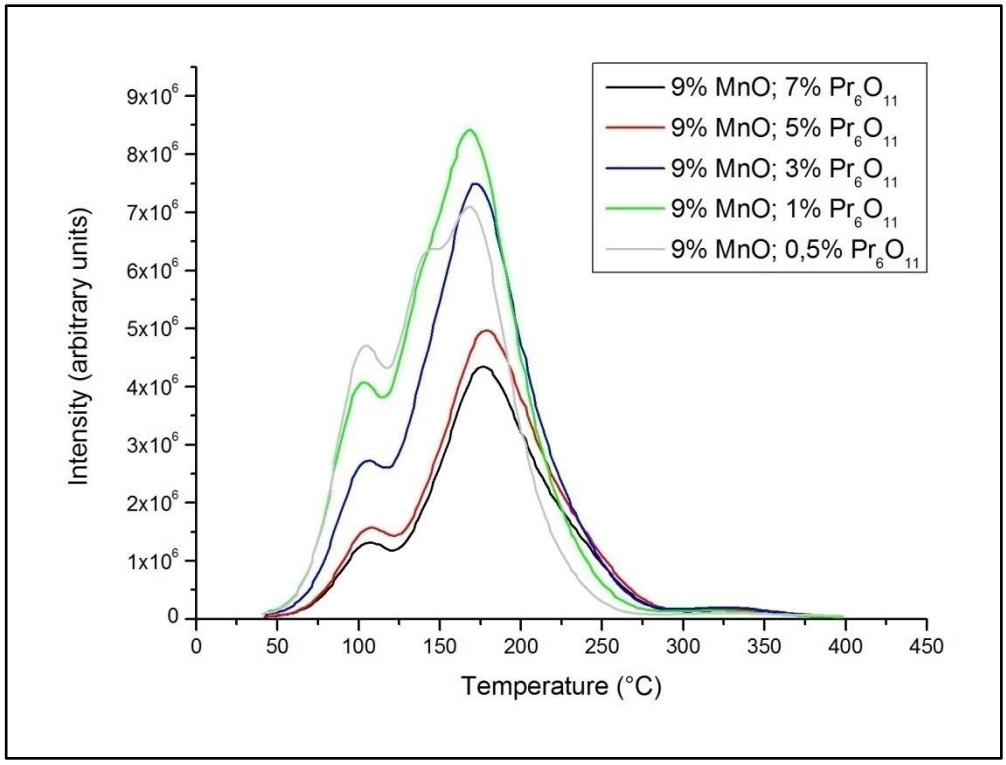

Figure 4.33 $Sr_2P_2O_7$ doped with 9% MnO and 0.5-7% Pr_6O_{11}

In the following Figures 4.34-4.38, the effect of MnO was shown. By increasing the amount of MnO from 3% to 7%, the intensity around 170°C increased but when the MnO amount reached to 9%, the intensity decreased. When the first peak around 100°C was examined, any considerable effect was not found but when the percentage reached 7%, first peaks were shadowed by the second peak.

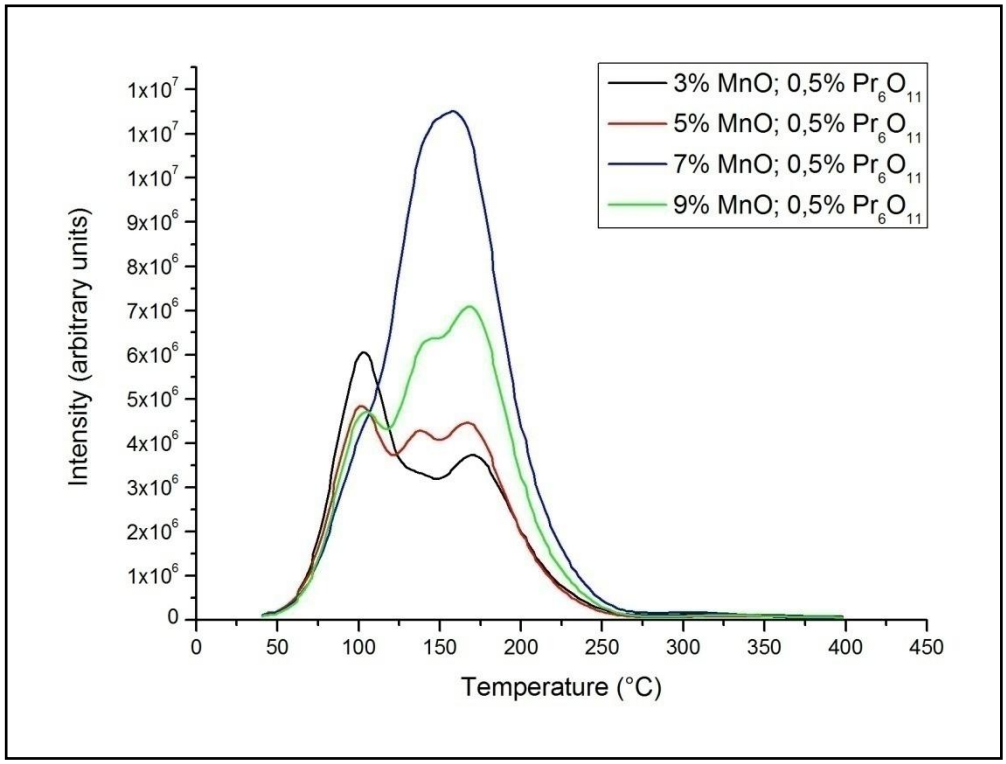

Figure 4.34 Glow curves of $Sr_2P_2O_7$ doped with 0.5% Pr_6O_{11} and 3-5% MnO

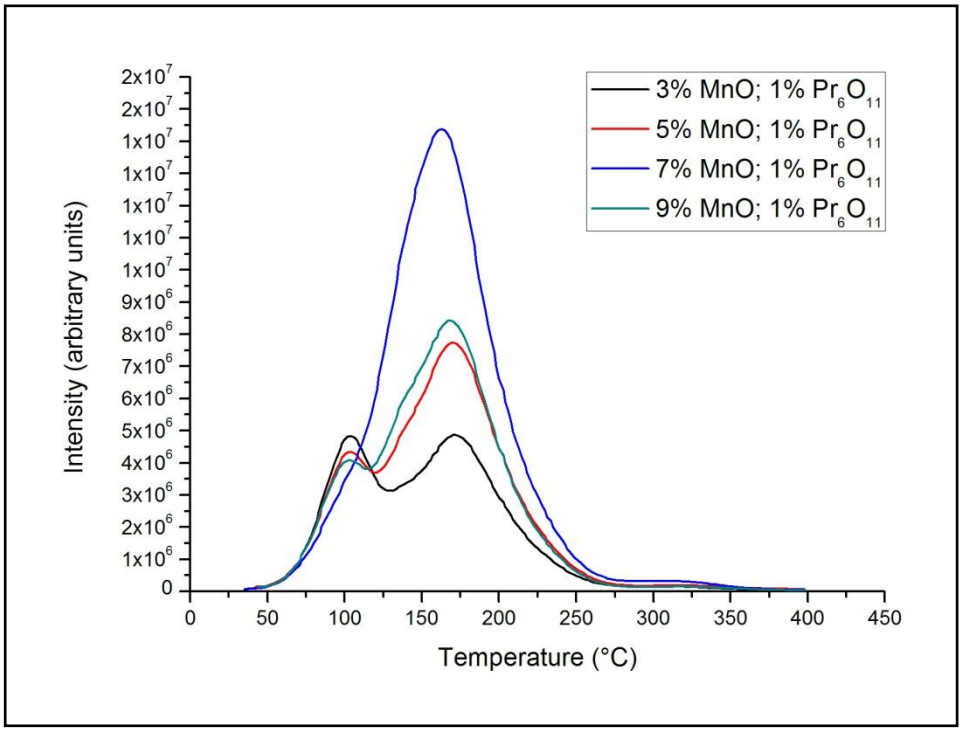

Figure 4.35 Glow curves of $Sr_2P_2O_7$ doped with 1% Pr_6O_{11} and 3-5% MnO

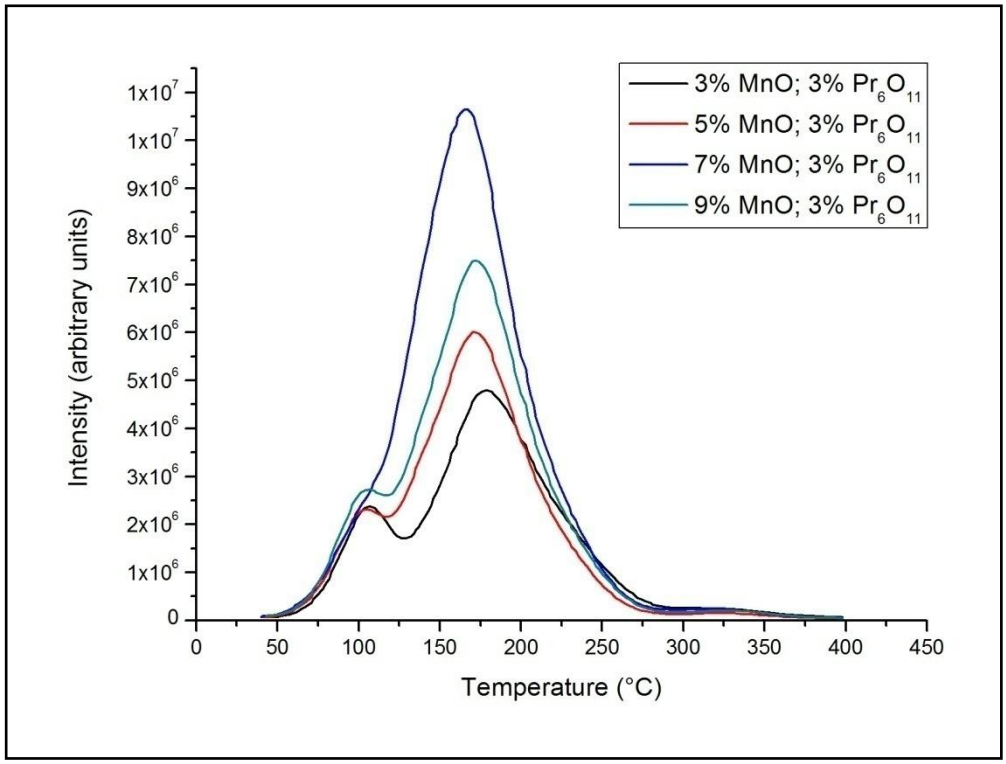

Figure 4.36 Glow curves of $Sr_2P_2O_7$ doped with 3% Pr_6O_{11} and 3-5% MnO

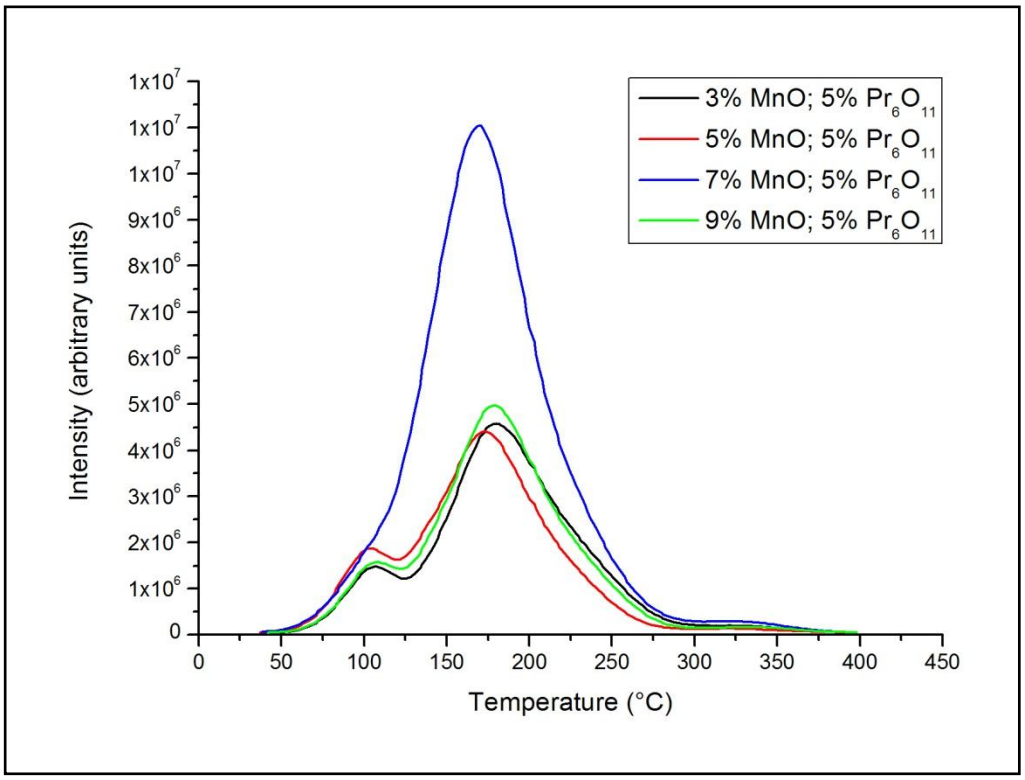

Figure 4.37 Glow curves of $Sr_2P_2O_7$ doped with 5% Pr_6O_{11} and 3-5% MnO

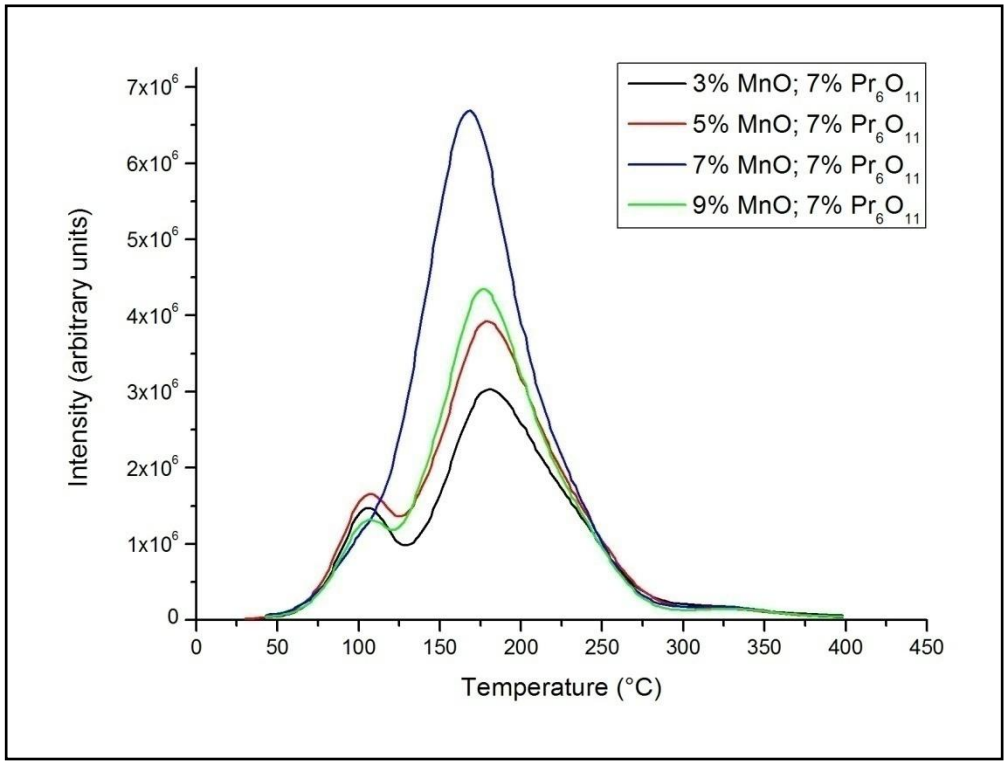

Figure 4.38 Glow curves of $Sr_2P_2O_7$ doped with 7% Pr_6O_{11} and 3-5% MnO

CHAPTER 5

CONCLUSION AND RECOMMENDATIONS

The aim of this study was to synthesize, to characterize and to investigate thermoluminescence properties of strontium pyrophosphate doped with metal oxides. The conclusions derived from the investigations and experiments conducted are as follows:

1. Strontium pyrophosphate was synthesized with solid-state synthesis method by exposing the reactants strontium carbonate and ammonium dihydrogen phosphate to final heating at 900°C for 14.5 hours. The produced material was doped with different amounts and combinations of metal dopants such as, copper-indium, copper-silver and manganese-praseodymium ions. According to the X-ray Diffraction results, the production of strontium pyrophosphate was successful. Increase in the amount of all metal oxide dopants lowered the two significant peaks of strontium pyrophosphate at 2θ values around 26 and 45 degrees; and increased the peak around 30 degrees with 310 hkl value.

2. FTIR results proved the presence of pyrophosphate within the structure; and records indicated that addition of the activators Cu, In, Ag, Mn and Pr caused no noticeable change in vibrational modes; which means that the anionic part of matrix compound that is strontium pyrophosphate had structural stability.

3. The results of DTA analysis showed that the compounds were thermally stable. By SEM the morphologies of the doped and undoped strontium pyrophosphate showed that the particle size distributions were not homogeneous and particles had smooth surfaces.

4. Thermoluminescence analyses were conducted on strontium pyrophosphate doped with different amounts of dopants. Glow curves showed that intensities were affected by different amounts of dopants. It can be concluded from the thermoluminescence analysis that strontium pyrophosphate doped with 7% MnO and 1% Pr_6O_{11} had the most powerful peak intensity around 160°C.

5. It is recommended to investigate the thermoluminescence properties of strontium pyrophosphate doped with other metal oxides.

REFERENCES

1. Pagonis, V., Kitis, G., Furetta, C.: Numerical and Practical Exercises in Thermoluminescence. Springer Science+Business Media, Inc., New York (2006)

2. Seyyidoğlu, S.: Synthesis and Characterization of Novel Rare Earth Phosphates and Rietveld Structuıral Analysis of Rare Earth Orthoborates. PhD Thesis, METU, Ankara (2009)

3. Seyyidoğlu, S., Özenbaş, M., Yazıcı, N., Yılmaz, A.: Investigation of solid solution of ZrP_2O_7-$Sr_2P_2O_7$. Journal of Material Science 42, 6453-6463 (April 2007)

4. Corbridge, D.: The structural chemistry of phosphorus. Elsevier Scientific Pub. Co., Amsterdam ; New York (1974)

5. Wazer, J.: Phosphorus and its compounds. Interscience Publishers, New York (1958-1961)

6. Weber, M.: Phosphor Handbook: Second Edition. CRC Press, Boca Raton; London; New York (2007)

7. Natarajan, V., Bhide, M. K., Dhobale, A. R., Godboleb, S. V., Seshagirib, T. K., Pageb, A. G., Lua, C.-H.: Photoluminescence, thermally stimulated luminescence and electron paramagnetic resonance of europium-ion doped strontium pyrophosphate. Materials Research Bulletin(39), 2065-2075 (July 2004)

8. Ye, S., Liu, Z.-S., Wang, J.-G., Jing, X.-P.: Luminescent properties of $Sr_2P_2O_7$:Eu,Mn phosphor under near UV excitation. Materials Research Bulletin(43), 1057–1065 (August 2008)

9. Guler, H., Kurtulus, F.: A microwave-assisted route for the solid-state synthesis of lead pyrophosphate, $Pb_2P_2O_7$. Journal of Material Science 40(24), 6565-6569 (October 2005)

10. Khay, N., Ennaciri, A., Harcharras, M.: Vibrational spectra of double diphosphates $RbLnP_2O_7$ (Ln = Dy, Ho, Y, Er, Tm, Yb). Vibrational Spectroscopy 27(2), 119-126 (December 2001)

11. Khay, N., Ennaciri, A.: Vibrational spectra of double diphosphates $CsLnP_2O_7$ (Ln=Gd, Tb, Dy, Ho, Y, Er, Tm, Yb). Journal of Alloys and Compounds 323-324, 800-805 (July 2001)

12. McKeever, S., Moscovitch, M., Townsend, P.: Thermoluminescence Dosimetry Materials: Properties and Uses. Nuclear Technology Publishing, England (1995)

13. Harvey, E.: A History of Luminescence: From the Earliest Times Until 1900. Dover Phoenix Editions, USA (2005)

14. Chen, R., McKeever, S.: Theory of Thermoluminescence and Related Phenomena. World Scientific Publishing Co. Pte. Ltd., Singapore (1997)

15. Furetta, C.: Handbook of Thermoluminescence. World Scientific Publishing Co. Pte. Ltd., Singapore (2003)

16. Pekpak, E.: Synthesis and Characterization of Lithium Tetraborate Doped with Metals. MS Thesis, METU, Ankara (2009)

17. Schauer, D., Brodsky, A., Sayeg, J.: Handbook of Radioactivity Analysis, Second Edition. Academic Press, Great Britan (2003)

18. McKeever, S. W. S.: Thermoluminescence of solids. Cambridge University Press, Cambridge (1983)

19. Kortov, V.: Materials for thermoluminescent dosimetry: Current status and future

needs. Radiation Measurements(42), 576-581 (2007)

20. Özdemir, Z., Özbayoğlu, G., Yılmaz, A.: Investigation of thermoluminescence properties of metal oxide. Journal of Material Sciences(42), 8501-8508 (2007)

21. Özdemir, Z.: Synthesis and Characterization of Metal Doped Lithium Triborate as a Thermoluminescent Material. PhD Thesis, METU, Ankara (2005)

22. Ardıçoğlu, B., Özbayoğlu, G., Özdemir, Z., Yılmaz, A.: Production and identification of rare-earth doped lithium borate. Journal of Alloys and Compounds(418), 77-79 (2006)

23. Ardıçoğlu, B.: Synthesis of rare-earth doped lithium triborate. Thesis, METU, Ankara (2009)

24. Depci, T., Özbayoğlu, G., A. Yılmaz, N.: The thermoluminescent properties of lithium triborate activated by aluminum. Nuclear Instruments and Methods in Physics Research(266), 755-762 (2008)

25. Kayhan, M.: Effects of Synthesis and Doping Methods on Therluminescence Glow Curves of Manganese Doped Lithium Tetraborate. MS Thesis, METU, Ankara (2009)

26. Ferid, M., Horchani-Naifer, K.: Synthesis, crystal structure and vibrational spectra of a new form of diphosphate $NaLaP_2O_7$. Materials Research Bulletin 39, 2209-2217 (2004)

27. Ferid, M., Horchani, K., Amami, J.: Preparation, structure and infrared spectrum of $NaEuP_2O_7$. Materials Research Bulletin(39), 1949-1955 (2004)

28. Hamady, A., Zid, M., Jouini, T.: Crystal structure of KYP_2O_7. Journal of Solid State Chemistry(113), 120 (1994)

29. Trunov, K., Oboznenko, V., Sirotinkin, P., Tskhelashvili, B.: Crystal Structure Refinement of $K_2SrP_2O_7$. Inorganic materials 27, 1993 (1991)

30. Trunov, V., Oboznenko, Y., Sirotinkin, S., Tskhelashvili, N.: Crystal Structures of the Double Diphosphates $Rb_2SrP_2O_7$ and $Cs_2SrP_2O_7$. Inorganic Materials 27, 2026-2029 (1991)

31. Ledain, S., Leclaire, A., Borel, M., Raveau, B.: $LiMoP_2O_7$. Acta Crystallographica(C52), 1593-1594 (1996)

32. Boutfessi, A., Boukhari, A., Holt, E. M.: Lead(II) Diiron(III) Pyrophosphate and Barium Diiron(III) Pyrophosphate. Acta Cryst.(C52), 1594-1597 (1996)

33. Boutfessi, A., Boukhari, A., Holt, E.: Copper(II) Diiron(III) Pyrophosphate. Acta Cryst.(C52), 1597-1599 (1996)

34. Serghini Idrissi, M., Rghioui, L., Nejjar, R., Benarafa, L., Saidi Idrissi, M., Lorriaux, A., Wallart, F.: Vibrational spectra of monoclinic diphosphate of the formula AMP_2O_7. Spectrochimica Acta, Part A: Molecular and Biomolecular Spectroscopy(60A), 2043-2052 (2004)

35. Stock, N., Ferey, G., Cheetham, A.: Hydrothermal synthesis and characterization of a chromium(II) pyrophosphate, $Na_2CrP_2O_7.0.5H_2O$. Solid State Sciences (2), 307-312 (2000)

36. Assaaoudi, H., Butler, I., Kozinski, J., Belanger-Gariepy, F.: Crystal structure, vibrational spectra and thermal decomposition study of a new, dicationic, acidic pyrophosphate: $KHMgP_2O_7.2H_2O$. Journal of Chemical Crystallography(35), 809-820 (2005)

37. Varga, T., Wilkinson, A., Haluska, M., Payzant, E.: Preparation and thermal expansion of $(M_{III05}M_{V0.5})P_2O_7$ with the cubic ZrP_2O_7 structure. Journal of Solid State Chemistry(178), 3541-3546 (2005)

38. Chernaya, V., Mitiaev, S., Chizhov, S., Dikarev, E., Shpanchenko, R., Antipov, E., Korolenko, M., Fabritchnyi, P.: Synthesis and Investigation of Tin(II) Pyrophosphate ($Sn_2P_2O_7$). Chemistry of Materials(17), 284-290 (2005)

39. Gover, R., Withers, N., Allen, S., Withers, R., Evans, J.: Structure and phase transitions of SnP_2O_7. Journal of Solid State Chemistry(166), 42-48 (2002)

40. Withers, R., Tabira, Y., Evans, J., King, I., Sleight, A.: A New Three-Dimensional Incommensurately Modulated Cubic Phase (in ZrP_2O_7) and Its Symmetry Characterization via Temperature-Dependent Electron Diffraction. Journal of Solid State Chemistry(157), 186-192 (2001)

41. Lisnyak, V., Stus, V., S. Slobodyanik, M., Markiv, V.: Crystal structure of a novel cubic pyrophosphate WP_2O_7. Journal of Alloys and Compounds(309), 83-87 (2000)

42. Shao-Long, T., Yuan-Ying, L., Yan-Sheng, Y.: Structure and vibration spectra of new pseudo-pyrophosphate $NaDyP_2O_7$. Journal of Physics and Chemistry of Solids(58), 957-961 (1997)

43. I. Marcu, J.: Semiconductive and redox properties of Ti and Zr pyrophosphate catalysts (TiP_2O_7 and ZrP_2O_7). Catalysis Letters(78), 273 (2002)

44. Kim, C., Yim, H.: The effect of tetravalent metal on dielectric property in ZrP_2O_7 and TiP_2O_7. Solid State Communications(110), 137-142 (1999)

45. Amezawa, K., Tomii, Y., Yamamoto, N.: High temperature protonic conduction in $Sr_2P_2O_7$–$LaPO_4$ system. Solid State Ionics 176, 143-048 (2005)

46. Doat, A., Pellé, F., Lebugle, A.: Europium-doped calcium pyrophosphates: Allotropic forms and photoluminescent properties. Journal of Solid State Chemistry 178(7), 2354-2362 (2005)

47. Schipper, J., J. Piet, J., Blasse, G.: On the luminescence of hafnium compounds. Materials Research Bulletin 29(1), 23-30 (1994)

48. Assaaoudi, H., Butler, S., Kozinski, A.: Crystal structure and vibrational and luminescence spectra of a new erbium potassium pyrophosphate dihydrate. Solid State Sciences 8(11), 1353-1360 (November 2006)

49. Li, M., Liu, W., Chen, H., Yang, X., Wei, B., Cao, H., Gu, M., Zhao, T.: Low-Temperature Flux Synthesis, Crystal Structure and Ce-Doped Luminescence of the First Lutetium Diphosphate $NH_4LuP_2O_7$. European Journal of Inorganic Chemistry(23), 4693-4696 (2005)

50. Pang, R., Li, C., Shi, L., Su, Q.: A novel blue-emitting long-lasting proyphosphate phosphor $Sr_2P_2O_7$:Eu^{2+}, Y^{3+}. Journal of Physics and Chemistry of Solids(70), 303-306 (2009)

51. R., P., Li, C., Jiang, L., Su, Q.: Blue long lasting phosphorescence of Tm^{3+} in zinc pyrophosphate phosphor. Journal of Alloys and Compounds(471), 364-367 (2009)

52. Pang, R., Li, C., Zhang, S., Su, Q.: Luminescent properties of a new blue long-lasting phosphor $Ca_2P_2O_7$:Eu^{2+}, Y^{3+}. Materials Chemistry and Physics(113), 215-218 (2009)

53. Miyoshi, H., Yoshino, T.: Radiation induced thermoluminescence of calcium pyrophosphate powders prepared from thulium nitrate aqueous solution. Radiation Physics and Chemistry 48(3), 315-318 (September 1996)

54. Kundua, H., Massanda, P., Marathea, P., Venkatamarana, G.: Sodium pyrophosphate - A new thermoluminescent detector. Nuclear Instruments and Methods 15(2-3), 363-367 (September 1980)

55. Powder Diffraction File Card No: 24-1011. Joint Committee on Powder Diffraction Standards, Swathmore, PA

56. Wall, B., Driscoll, C., Strong, J., Fisher, E.: The Suitability of Different Preparations of Thermoluminescent Lithium Borate for Medical Dosimetry. Physical Medical biology, 1023-1034 (1982)

57. Powder Diffraction File Card No: 80-1917. Joint Committee on Powder Diffraction Standards, Swathmore, PA

58. Powder Diffraction File Card No: 88-2160. Joint Committee on Powder Diffraction Standards, Swathmore, PA

59. Powder Diffraction File Card No: 84-1108. Joint Committee on Powder Diffraction Standards, Swathmore, PA

60. Powder Diffraction File Card No: 42-1121. Joint Committee on Powder Diffraction Standards, Swathmore, PA

61. Powder Diffraction File Card No: 78-0424. Joint Committee on Powder Diffraction Standards, Swathmore, PA

62. Harcharras, M., Ennaciri, A., Assaaoudi, H., Mattei, G., D'Orazio, V., Moliterni, A. G. G., Capitellid, F.: Crystal structure and vibrational spectra of tetrasodium dimagnesium dihydrogen diphosphate octahydrate $Na_4Mg_2(H_2P_2O_7)_4.8H_2O$. Journal of Solid State Chemistry(172), 160-165 (November 2003)

63. Boonchom, B., Phuvongpha, N.: Synthesis of new binary cobalt iron pyrophosphate $CoFeP_2O_7$. Materials Letters(63), 1709-1711 (May 2009)

APPENDIX A

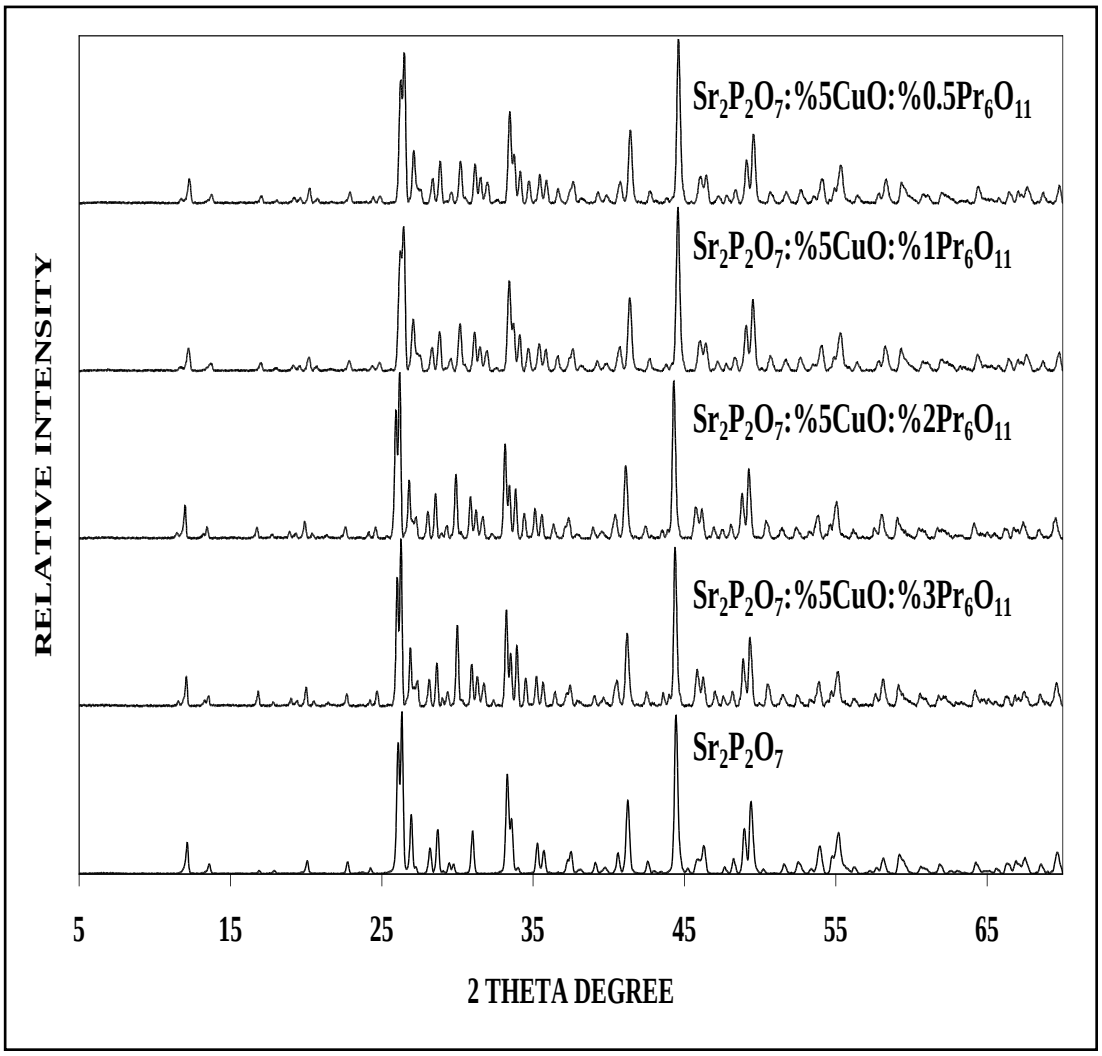

Figure A.1 X-ray powder diffraction pattern of strontium pyrophosphate doped with 5% CuO and 0.5-3% Pr_6O_{11} [2]

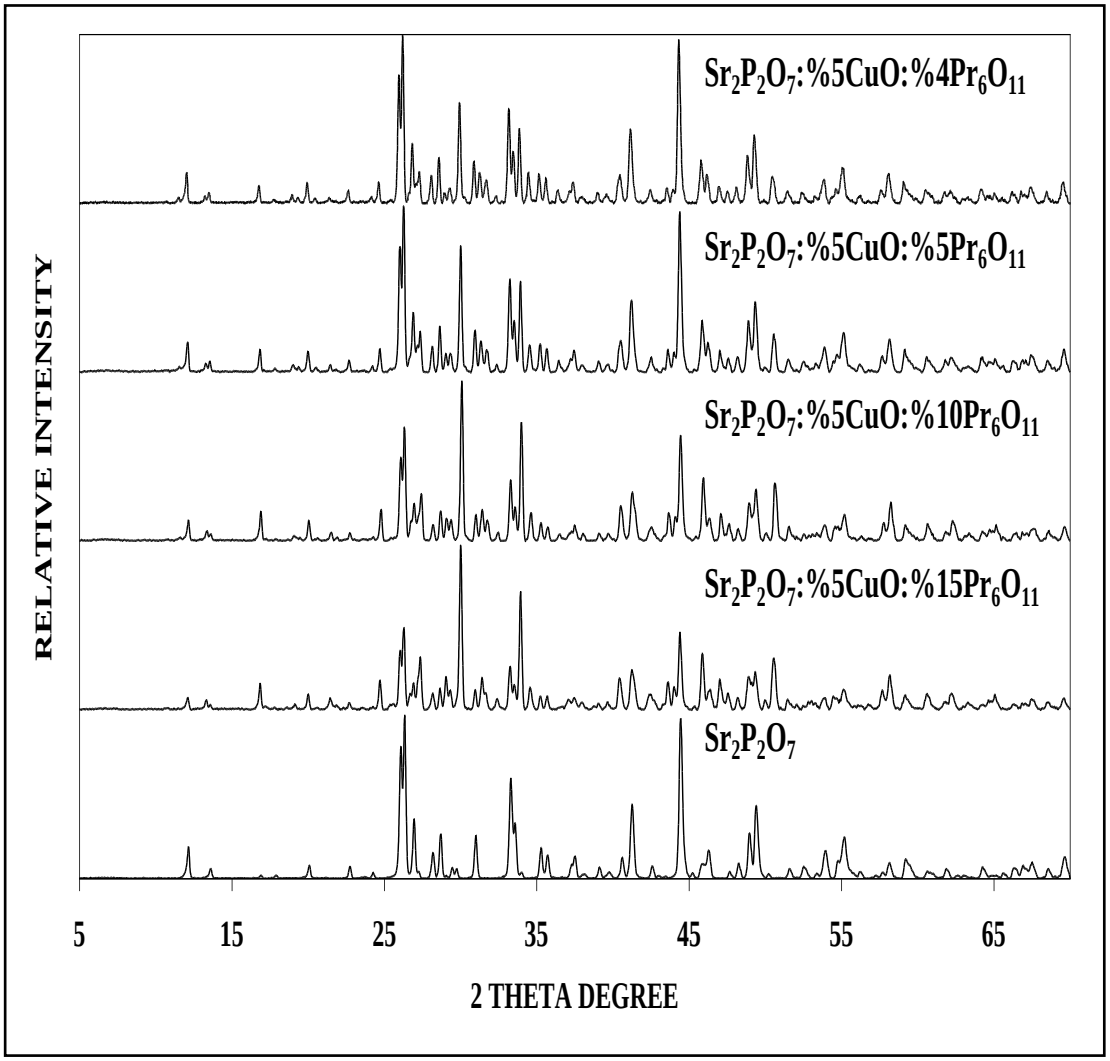

Figure A.2 X-ray powder diffraction pattern of strontium pyrophosphate doped with 5% CuO and 4-15% Pr_6O_{11} [2]

APPENDIX B

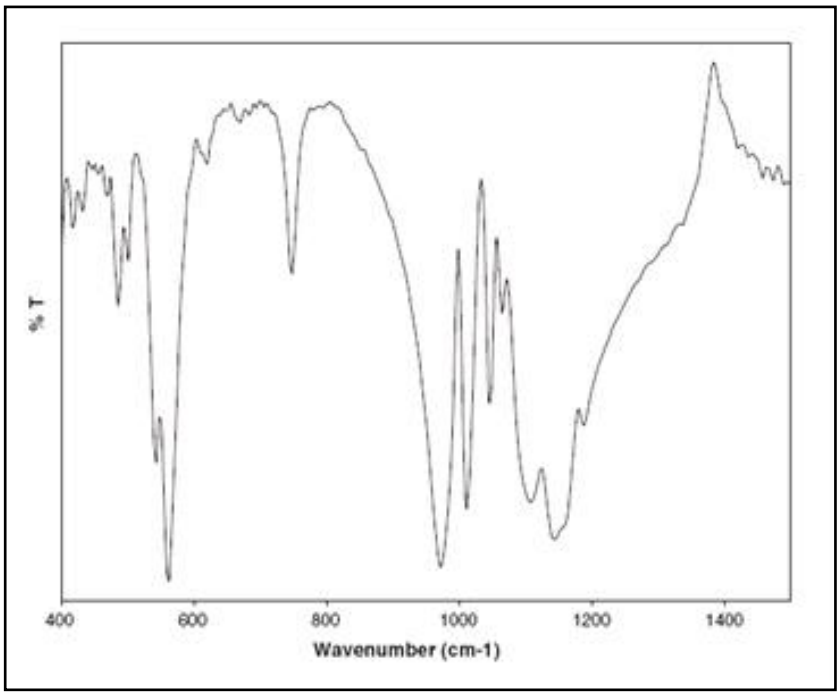

Figure A.3 FTIR spectra of orthorhombic strontium pyrophosphate [3]

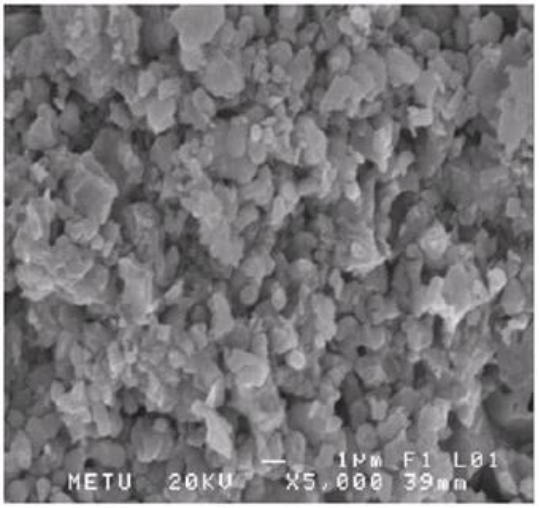

Figure A.4 SEM micrographs of strontium pyrophosphate [3]

APPENDIX C

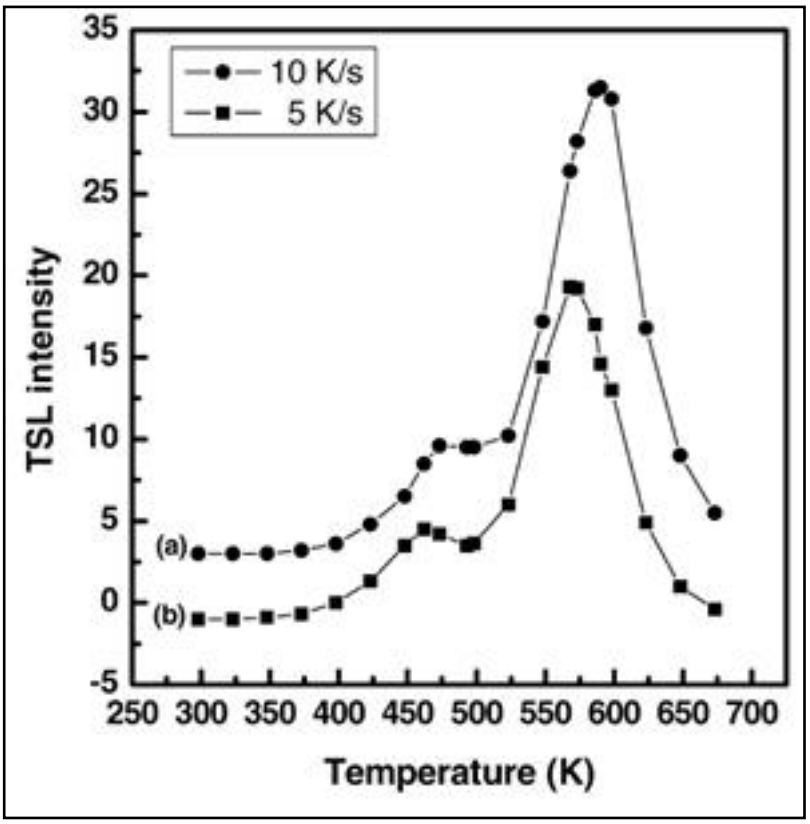

Figure A.5 Thermoluminescence glow curves of europium doped strontium pyrophosphate [7]

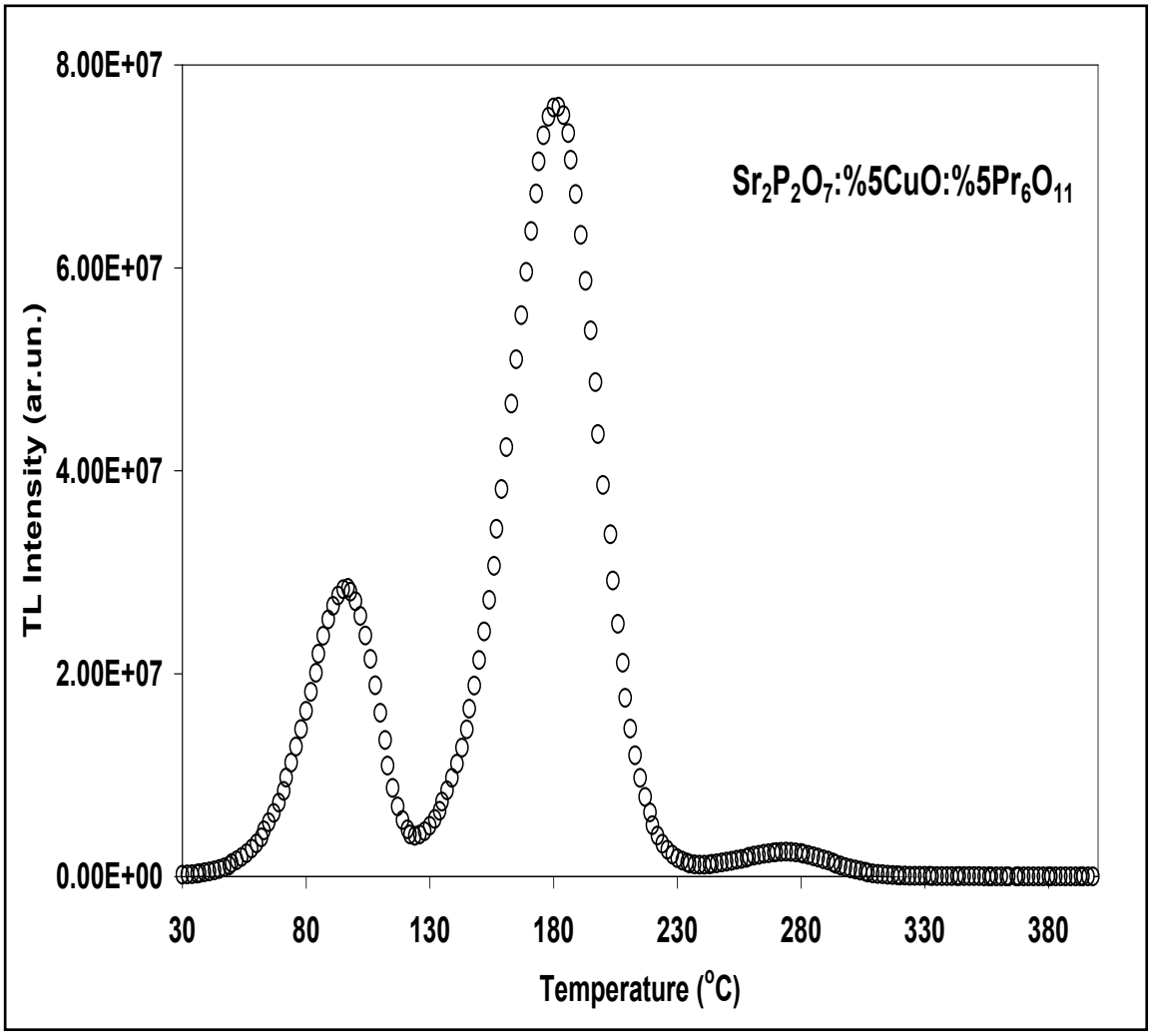

Figure A.6 Thermoluminescence glow curves of 5% CuO and 5% Pr_6O_{11} doped strontium pyrophosphate [2]

APPENDIX D

Table A.1 X-ray Powder Diffraction data of Undoped $Sr_2P_2O_7$ Synthesized for Mn-Pr Group (First one)

	$2\theta_{observed}$	$2\theta_{JCPDS[24-1011]}$	I	h k l
1	12.400	11.949	**15**	1 1 0
2	20.350	19.881	**8**	2 0 0
3	23.000	22.547	**7**	1 3 0
4	24.600	24.071	**7**	2 2 0
5	26.350	25.885	**77**	2 0 1
6	26.600	26.140	**100**	0 3 1
7	27.250	26.773	**32**	2 1 1
8	28.400	28.017	**36**	1 3 1
9	28.950	28.511	**25**	2 3 0
10	30.000	29.275	**19**	2 2 1
11	31.250	30.806	**26**	3 1 0
12	33.550	33.151	**57**	0 0 2
13	33.850	33.406	**30**	1 4 1
14	34.100	33.821	**7**	2 4 0
15	35.550	35.106	**18**	3 1 1
16	35.950	35.522	**13**	1 5 0
17	37.550	37.087	**10**	3 2 1
18	37.800	37.342	**13**	1 2 2
19	39.400	38.956	**6**	2 0 2
20	40.900	40.413	**13**	4 0 0
21	41.500	41.086	**48**	0 6 0
22	44.700	44.276	**94**	2 3 2
23	45.050	45.616	**9**	4 3 0
24	46.550	46.131	**19**	4 2 1
25	47.950	47.487	**7**	3 2 2
26	48.550	48.074	**10**	2 4 2
27	49.200	48.759	**28**	4 3 1
28	49.650	49.209	**43**	2 6 1
29	51.900	51.405	**7**	0 7 1
30	52.750	52.322	**12**	4 4 1
31	54.250	53.781	**18**	0 6 2
32	55.050	54.578	**10**	5 1 1
33	55.400	54.968	**19**	2 0 3
34	55.550	55.112	**18**	0 3 3
35	58.350	57.939	**12**	3 7 0
36	59.450	58.996	**14**	4 6 0
37	60.850	60.468	**8**	3 1 3
38	62.200	61.676	**8**	4 6 1

APPENDIX E

Table A.2 X-ray Powder Diffraction data of Undoped $Sr_2P_2O_7$ Synthesized for Mn-Pr Group (Second one)

	$2\theta_{observed}$	$2\theta_{JCPDS[24-1011]}$	I	h k l
1	12.400	11.949	**15**	1 1 0
2	20.350	19.881	**8**	2 0 0
3	23.000	22.547	**7**	1 3 0
4	24.600	24.071	**7**	2 2 0
5	26.350	25.885	**77**	2 0 1
6	26.600	26.140	**100**	0 3 1
7	27.250	26.773	**32**	2 1 1
8	28.400	28.017	**36**	1 3 1
9	28.950	28.511	**25**	2 3 0
10	30.000	29.275	**19**	2 2 1
11	31.250	30.806	**26**	3 1 0
12	33.550	33.151	**57**	0 0 2
13	33.850	33.406	**30**	1 4 1
14	34.100	33.821	**7**	2 4 0
15	35.550	35.106	**18**	3 1 1
16	35.950	35.522	**13**	1 5 0
17	37.550	37.087	**10**	3 2 1
18	37.800	37.342	**13**	1 2 2
19	39.400	38.956	**6**	2 0 2
20	40.900	40.413	**13**	4 0 0
21	41.500	41.086	**48**	0 6 0
22	44.700	44.276	**94**	2 3 2
23	45.050	45.616	**9**	4 3 0
24	46.550	46.131	**19**	4 2 1
25	47.950	47.487	**7**	3 2 2
26	48.550	48.074	**10**	2 4 2
27	49.200	48.759	**28**	4 3 1
28	49.650	49.209	**43**	2 6 1
29	51.900	51.405	**7**	0 7 1
30	52.750	52.322	**12**	4 4 1
31	54.250	53.781	**18**	0 6 2
32	55.050	54.578	**10**	5 1 1
33	55.400	54.968	**19**	2 0 3
34	55.550	55.112	**18**	0 3 3
35	58.350	57.939	**12**	3 7 0
36	59.450	58.996	**14**	4 6 0
37	60.850	60.468	**8**	3 1 3
38	62.200	61.676	**8**	4 6 1

APPENDIX F

Table A.3 X-ray Powder Diffraction data of Undoped $Sr_2P_2O_7$ Synthesized for Cu-Ag Group

	$2\theta_{observed}$	$2\theta_{JCPDS[24-1011]}$	I	h k l
1	12.250	11.949	**19**	1 1 0
2	13.750	13.404	**7**	0 2 0
3	20.200	19.881	**8**	2 0 0
4	22.850	22.547	**9**	1 3 0
5	24.400	24.071	**5**	2 2 0
6	26.200	25.885	**76**	2 0 1
7	26.450	26.140	**100**	0 3 1
8	27.050	26.773	**34**	2 1 1
9	28.250	28.017	**25**	1 3 1
10	28.800	28.511	**28**	2 3 0
11	29.550	29.275	**8**	2 2 1
12	31.100	30.806	**26**	3 1 0
13	33.400	33.151	**55**	0 0 2
14	33.700	33.406	**31**	1 4 1
15	35.400	35.106	**18**	3 1 1
16	35.850	35.522	**14**	1 5 0
17	37.400	37.087	**9**	3 2 1
18	37.650	37.342	**12**	1 2 2
19	39.200	38.956	**6**	2 0 2
20	39.650	39.598	**4**	2 1 2
21	40.700	40.413	**12**	4 0 0
22	41.350	41.086	**43**	0 6 0
23	42.650	42.358	**8**	1 6 0
24	44.550	44.276	**95**	2 3 2
25	46.050	45.738	**9**	1 6 1
26	46.400	46.131	**17**	4 2 1
27	47.750	47.487	**6**	3 2 2
28	48.350	48.074	**10**	2 4 2
29	49.050	48.759	**26**	4 3 1
30	49.500	49.209	**43**	2 6 1
31	52.600	52.322	**9**	4 4 1
32	53.550	53.141	**4**	5 2 0
33	54.000	53.781	**14**	0 6 2
34	54.850	54.578	**9**	5 1 1
35	55.300	54.968	**21**	2 0 3
36	57.750	57.519	**4**	4 3 2
37	58.200	57.939	**9**	3 7 0
38	59.300	58.996	**13**	4 6 0
39	60.750	60.468	**6**	3 1 3
40	61.950	61.676	**7**	4 6 1

APPENDIX G

Table A.4 X-ray Powder Diffraction data of Undoped $Sr_2P_2O_7$ Synthesized for Cu-In Group

	$2\theta_{observed}$	$2\theta_{JCPDS[24-1011]}$	I	h k l
1	12.200	11.949	**18**	1 1 0
2	13.650	13.404	**7**	0 2 0
3	20.150	19.881	**8**	2 0 0
4	22.800	22.547	**7**	1 3 0
5	26.100	25.885	**73**	2 0 1
6	26.350	26.140	**99**	0 3 1
7	27.000	26.773	**34**	2 1 1
8	28.700	28.511	**28**	2 3 0
9	29.500	29.275	**8**	2 2 1
10	31.050	30.806	**27**	3 1 0
11	33.350	33.151	**56**	0 0 2
12	33.600	33.406	**33**	1 4 1
13	35.300	35.106	**21**	3 1 1
14	35.750	35.522	**13**	1 5 0
15	37.300	37.087	**9**	3 2 1
16	37.550	37.342	**14**	1 2 2
17	39.150	38.956	**7**	2 0 2
18	40.650	40.413	**14**	4 0 0
19	41.300	41.086	**43**	0 6 0
20	42.600	42.358	**8**	1 6 0
21	44.450	44.276	**100**	2 3 2
22	46.350	46.131	**16**	4 2 1
23	47.650	47.487	**10**	3 2 2
24	48.300	48.074	**9**	2 4 2
25	49.000	48.759	**30**	4 3 1
26	49.450	49.209	**46**	2 6 1
27	51 .600	51.405	**7**	0 7 1
28	52.500	52.322	**15**	4 4 1
29	54.000	53.781	**16**	0 6 2
30	54.800	54.578	**9**	5 1 1
31	55.150	54.968	**19**	2 0 3
32	55.250	55.112	**19**	0 3 3
33	55.850	55.619	**9**	2 7 1
34	58.150	57.939	**12**	3 7 0
35	59.200	58.996	**15**	4 6 0
36	59.600	59.367	**9**	1 4 3
37	60.600	60.468	**11**	3 1 3
38	61.950	61.676	**8**	4 6 1

APPENDIX H

Table A.5 X-ray Powder Diffraction data of $Sr_2P_2O_7$ Doped with 7% CuO and 15% In_2O_3

	$2\theta_{observed}$	$2\theta_{JCPDS[24-1011]}$	I	h k l
1	17.000	16.713	10	1 2 0
2	20.100	19.881	10	2 0 0
3	26.200	25.885	16	2 0 1
4	26.500	26.140	22	0 3 1
5	27.100	26.773	8	2 1 1
6	27.450	27.071	28	0 4 0
7	30.050	29.275	100	2 2 1
8	33.500	33.151	15	0 0 2
9	34.050	33.406	65	1 4 1
10	34.650	33.821	14	2 4 0
11	35.800	35.522	10	1 5 0
12	39.650	39.598	7	2 1 2
13	40.450	40.413	10	4 0 0
14	41.350	41.086	17	0 6 0
15	43.650	43.251	20	2 5 1
16	44.550	44.276	23	2 3 2
17	46.400	46.131	9	4 2 1
18	49.100	48.759	11	4 3 1
19	55.200	54.968	7	2 0 3
20	58.200	57.939	22	3 7 0
21	60.950	60.468	9	3 1 3
22	62.050	61.676	17	4 6 1

APPENDIX I

Table A.6 X-ray Powder Diffraction data of $Sr_2P_2O_7$ Doped with 7% CuO and 15 % $AgNO_3$

	$2\theta_{observed}$	$2\theta_{JCPDS[24-1011]}$	I	h k l
1	12.200	11.949	**9**	1 1 0
2	26.100	25.885	**57**	2 0 1
3	26.350	26.140	**63**	0 3 1
4	27.000	26.773	**21**	2 1 1
5	27.300	27.071	**32**	0 4 0
6	28.700	28.511	**18**	2 3 0
7	29.150	28.898	**8**	1 4 0
8	30.150	29.275	**100**	2 2 1
9	31.000	30.806	**16**	3 1 0
10	33.350	33.151	**41**	0 0 2
11	33.750	33.406	**93**	1 4 1
12	35.300	35.106	**16**	3 1 1
13	35.750	35.522	**11**	1 5 0
14	37.550	37.342	**8**	1 2 2
15	40.500	40.243	**26**	3 3 1
16	41.300	41.086	**25**	0 6 0
17	44.500	44.276	**63**	2 3 2
18	45.800	45.616	**45**	4 3 0
19	46.350	46.131	**10**	4 2 1
20	49.000	48.759	**27**	4 3 1
21	49.400	49.209	**22**	2 6 1
22	51.550	51.405	**12**	0 7 1
23	53.950	53.781	**15**	0 6 2
24	55.200	55.112	**22**	0 3 3
25	56.350	56.018	**8**	5 2 1
26	57.700	57.519	**15**	4 3 2
27	58.150	57.939	**12**	3 7 0
28	61.850	61.676	**11**	4 6 1

APPENDIX J

Table A.7 X-ray Powder Diffraction data of $Sr_2P_2O_7$ Doped with 9% MnO and 7% Pr_6O_{11}

	$2\theta_{observed}$	$2\theta_{JCPDS[24-1011]}$	I	h k l
1	12.350	11.949	**13**	1 1 0
2	22.950	22.547	**9**	1 3 0
3	26.250	25.885	**61**	2 0 1
4	26.550	26.140	**86**	0 3 1
5	27.150	26.773	**29**	2 1 1
6	27.500	27.071	**14**	0 4 0
7	28.400	28.017	**14**	1 3 1
8	28.900	28.511	**23**	2 3 0
9	29.300	28.898	**13**	1 4 0
10	29.950	29.275	**63**	2 2 1
11	31.200	30.806	**22**	3 1 0
12	33.500	33.151	**65**	0 0 2
13	34.050	33.821	**10**	2 4 0
14	35.500	35.106	**18**	3 1 1
15	35.900	35.522	**13**	1 5 0
16	37.450	37.087	**9**	3 2 1
17	37.700	37.342	**13**	1 2 2
18	39.300	38.956	**8**	2 0 2
19	40.000	39.598	**8**	2 1 2
20	40.850	40.413	**10**	4 0 0
21	41.450	41.086	**48**	0 6 0
22	42.750	42.358	**11**	1 6 0
23	43.700	43.251	**11**	2 5 1
24	44.650	44.276	**100**	2 3 2
25	45.950	45.616	**10**	4 3 0
26	46.500	46.131	**17**	4 2 1
27	48.450	48.074	**12**	2 4 2
28	49.150	48.759	**32**	4 3 1
29	49.550	49.209	**43**	2 6 1
30	52.700	52.322	**7**	4 4 1
31	54.100	53.781	**25**	0 6 2
32	54.950	54.578	**10**	5 1 1
33	55.350	54.968	**19**	2 0 3
34	58.250	57.939	**12**	3 7 0
35	59.400	58.996	**14**	4 6 0
36	59.800	59.367	**13**	1 4 3
37	61.750	61.676	**10**	4 6 1

APPENDIX K

Table A.8 X-ray Powder Diffraction data of $Sr_2P_2O_7$ Doped with 7% MnO and 1% Pr_6O_{11}

	$2\theta_{observed}$	$2\theta_{JCPDS[24-1011]}$	I	h k l
1	12.250	11.949	**18**	1 1 0
2	13.700	13.404	**7**	0 2 0
3	20.150	19.881	**8**	2 0 0
4	26.150	25.885	**70**	2 0 1
5	26.450	26.140	**84**	0 3 1
6	27.050	26.773	**33**	2 1 1
7	28.300	28.017	**15**	1 3 1
8	28.800	28.511	**24**	2 3 0
9	29.600	28.898	**6**	1 4 0
10	30.100	29.275	**28**	2 2 1
11	31.100	30.806	**25**	3 1 0
12	33.400	33.151	**60**	0 0 2
13	33.700	33.406	**27**	1 4 1
14	35.400	35.106	**16**	3 1 1
15	35.800	35.522	**13**	1 5 0
16	37.600	37.342	**14**	1 2 2
17	39.200	38.956	**8**	2 0 2
18	40.700	40.413	**12**	4 0 0
19	41.350	41.086	**44**	0 6 0
20	42.650	42.358	**10**	1 6 0
21	43.600	43.251	**8**	2 5 1
22	44.550	44.276	**100**	2 3 2
23	45.850	45.616	**16**	4 3 0
24	46.400	46.131	**16**	4 2 1
25	48.350	48.074	**9**	2 4 2
26	49.050	48.759	**31**	4 3 1
27	49.500	49.209	**43**	2 6 1
28	52.600	52.322	**7**	4 4 1
29	54.850	54.578	**11**	5 1 1
30	55.200	54.968	**21**	2 0 3
31	55.350	55.112	**16**	0 3 3
32	56.300	56.018	**7**	5 2 1
33	58.200	57.939	**13**	3 7 0
34	59.300	58.996	**12**	4 6 0
35	59.600	59.367	**11**	1 4 3
36	62.000	61.676	**8**	4 6 1
37	12.250	11.949	**18**	1 1 0

APPENDIX L

Table A.9 JCPDS Card 80-1917 [57]

CuO				
	2θ	**d value**	**Intensity**	**h k l**
1	32.496	2.753	8	1 1 0
2	35.502	2.526	95	0 0 2
3	35.502	2.526	95	-1 1 1
4	38.733	2.323	100	1 1 1
5	38.930	2.311	30	2 0 0
6	46.208	1.963	2	-1 1 2
7	48.658	1.870	29	-2 0 2
8	51.392	1.776	2	1 1 2
9	53.429	1.713	10	0 2 0
10	56.670_	1.623	1	0 2 1
11	58.369	1.580	14	2 0 2
12	61.492	1.507	19	-1 1 3
13	65.770	1.419	14	0 2 2
14	66.175	1.411	14	-3 1 1
15	67.963	1.378	10	1 1 3
16	68.054	1.376	14	2 2 0
17	68.813	1.363	1	-2 2 1
18	71.584	1.317	1	-3 1 2
19	72.430	1.304	6	3 1 1
20	72.941	1.296	1	2 2 1
21	75.029	1.265	6	0 0 4
22	75.145	1.263	7	-2 2 2
23	79.710	1.202	1	0 2 3
24	80.075	1.197	2	-2 0 4
25	82.230	1.171	4	-3 1 3
26	83.093	1.161	4	2 2 2
27	83.589	1.156	4	4 0 0
28	83.589	1.156	4	3 1 2
29	86.425	1.125	2	-4 0 2
30	86.640	1.123	1	-2 2 3
31	88.068	1.108	1	1 1 4
32	88.068	1.108	1	1 3 0
33	89.672	1.092	5	-1 3 1

Table A.10 JCPDS Card 84-1108 [59]

AgO				
	2θ	**d value**	**Intensity**	**h k l**
1	16.118	5.494	1	1 0 1
2	25.866	3.441	1	2 0 0
3	26.764	3.328	1	1 1 2
4	30.626	2.917	2	1 2 1
5	32.565	2.747	100	2 0 2
6	36.905	2.434	50	2 2 0
7	39.480	2.280	20	0 0 4
8	40.507	2.225	1	3 0 1
9	41.718	2.163	1	2 1 3
10	42.047	2.147	1	2 2 2
11	43.801	2.065	1	1 1 4
12	46.172	1.964	1	1 3 2
13	47.805	1.901	1	2 0 4
14	48.689	1.869	1	3 2 1
15	49.741	1.831	1	3 0 3
16	51.796	1.763	1	1 0 5
17	53.183	1.721	13	4 0 0
18	55.147	1.664	23	2 2 4
19	55.947	1.642	1	1 4 1
20	56.903	1.617	1	3 2 3
21	57.165	1.610	1	4 0 2
22	58.575	1.575	1	3 1 4
23	58.783	1.569	1	1 2 5
24	60.061	1.539	1	4 2 0
25	63.766	1.458	24	2 4 2
26	65.286	1.428	1	3 0 5
27	67.265	1.391	10	2 0 6
28	68.216	1.374	10	4 0 4
29	68.925	1.361	1	4 3 1
30	71.275	1.322	1	3 3 4
31	71.464	1.319	1	3 2 5
32	73.036	1.294	1	5 1 2
33	73.364	1.289	1	2 2 6
34	73.965	1.280	1	1 0 7
35	74.281	1.276	1	4 2 4
36	74.965	1.266	1	2 5 1
37	75.788	1.254	1	4 3 3
38	76.338	1.246	1	1 3 6
39	77.425	1.232	1	4 1 5
40	78.549	1.217	3	4 4 0
41	79.861	1.200	1	2 1 7
42	81.643	1.178	1	2 5 3
43	81.866	1.176	1	4 4 2
44	83.071	1.162	1	1 5 4
45	84.356	1.147	1	6 0 0
46	84.988	1.140	1	0 0 8
47	85.650	1.133	1	3 0 7
48	86.615	1.123	1	6 1 1
49	87.632	1.113	4	6 0 2
50	87.863	1.110	2	3 3 6
51	87.863	1.110	2	1 1 8
52	89.005	1.099	1	5 0 5

Table A.11 JCPDS Card 88-2160 [58]

In_2O_3				
	2θ	**d value**	**Intensity**	**h k l**
1	17.517	5.058	1	2 0 0
2	21.496	4.130	13	2 1 1
3	24.871	3.577	1	2 2 0
4	30.584	2.921	100	2 2 2
5	33.102	2.704	2	3 2 1
6	35.461	2.529	29	4 0 0
7	37.690	2.385	5	4 1 1
8	39.813	2.262	2	4 2 0
9	41.845	2.157	5	3 3 2
10	43.799	2.065	1	4 2 2
11	45.686	1.984	8	4 3 1
12	49.291	1.847	3	5 2 1
13	51.021	1.788	31	4 4 0
14	52.710	1.735	2	4 3 3
15	54.362	1.686	1	6 0 0
16	55.981	1.641	4	6 1 1
17	57.569	1.600	1	0 2 6
18	59.129	1.561	4	5 4 1
19	60.665	1.525	21	6 2 2
20	62.178	1.492	5	6 3 1
21	63.670	1.460	4	4 4 4
22	65.143	1.431	2	5 4 3
23	66.598	1.403	1	0 4 6
24	68.038	1.377	3	6 3 3
25	69.464	1.352	2	6 4 2
26	73.666	1.285	2	1 5 6
27	75.045	1.265	3	8 0 0
28	76.416	1.245	3	8 1 1
29	77.779	1.227	2	8 2 0
30	79.135	1.209	2	3 5 6
31	80.484	1.192	1	8 2 2
32	81.829	1.176	2	8 3 1
33	83.169	1.161	5	6 6 2
34	84.505	1.146	1	7 5 2
35	85.839	1.131	3	0 4 8
36	87.169	1.117	1	8 3 3
37	88.498	1.104	1	2 4 8
38	89.828	1.091	2	6 5 5

Table A.12 JCPDS Card 78-0424 [61]

MnO				
	2θ	**d value**	**Intensity**	**h k l**
1	34.956	2.565	65	1 1 1
2	40.584	2.221	100	2 0 0
3	58.741	1.570	47	2 2 0
4	70.215	1.339	17	3 1 1
5	73.838	1.282	12	2 2 2
6	87.833	1.110	5	4 0 0

Table A.13 JCPDS Card 42-1121 [60]

Pr_6O_{11}				
	2θ	**d value**	**Intensity**	**h k l**
1	28.248	3.157	100	1 1 1
2	32.738	2.733	28	2 0 0
3	46.991	1.932	30	2 2 0
4	55.704	1.649	24	3 1 1
5	58.422	1.578	4	2 2 2
6	68.585	1.367	3	4 0 0
7	75.729	1.255	5	3 3 1
8	78.079	1.223	4	4 2 0
9	87.261	1.116	4	4 2 2
10	94.115	1.052	4	5 1 1
11	105.617	0.967	1	4 4 0
12	112.885	0.924	3	5 3 1
13	115.411	0.911	2	6 0 0